Computational Intelligence and Neuroscience

Cognitive-Based EEG BCIs and Human Brain-Robot Interactions

Lead Guest Editor: Wei Li
Guest Editors: Jing Jin and Feng Duan

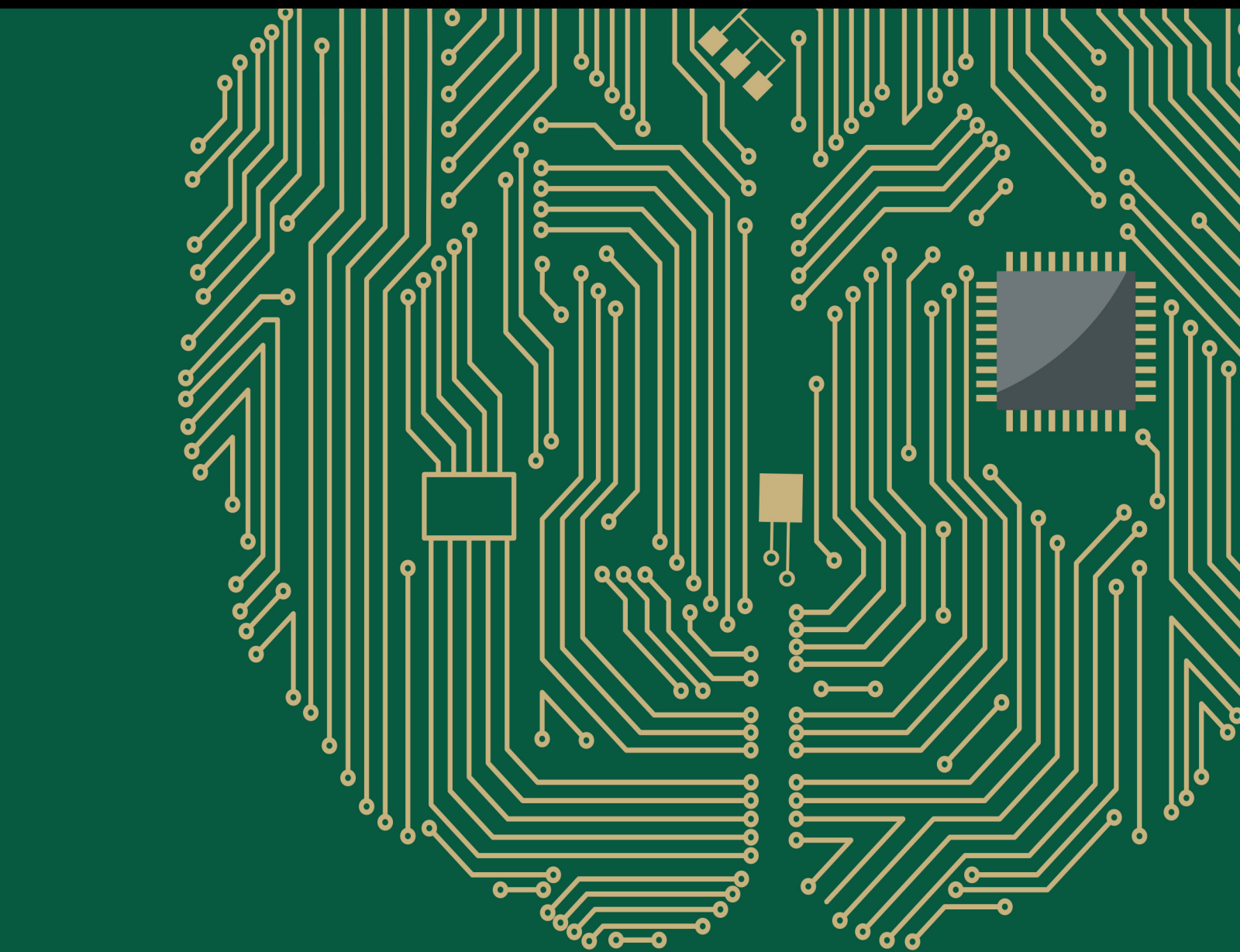

Cognitive-Based EEG BCIs and Human Brain-Robot Interactions

Computational Intelligence and Neuroscience

Cognitive-Based EEG BCIs and Human Brain-Robot Interactions

Lead Guest Editor: Wei Li
Guest Editors: Jing Jin and Feng Duan

Editorial Board

Contents

Hindawi
Computational Intelligence and Neuroscience
Volume 2017, Article ID 9471841, 2 pages
https://doi.org/10.1155/2017/9471841

Editorial

Cognitive-Based EEG BCIs and Human Brain-Robot Interactions

Wei Li,[1] Jing Jin,[2] and Feng Duan[3]

[1]*Department of Computer & Electrical Engineering and Computer Science, California State University, Bakersfield, CA 93311, USA*
[2]*Key Laboratory of Advanced Control and Optimization for Chemical Processes, Ministry of Education, East China University of Science and Technology, Shanghai 200237, China*
[3]*Department of Automation and Intelligence Science, College of Computer and Control Engineering, Nankai University, Tianjin 300071, China*

Correspondence should be addressed to Wei Li; wli@csub.edu

Received 18 June 2017; Accepted 18 June 2017; Published 28 August 2017

Brain computer interface (BCI) technology has been used to assist disabled patients in their daily life, via controlling external devices with brain activities. Noninvasive BCI systems typically rely on the scalp-recorded electroencephalogram (EEG). Many BCIs require the user to perform specific voluntary tasks to produce distinct EEG patterns, such as paying attention to a stimulus or performing some other mental tasks (e.g., motor imagery), related to human cognitive control. BCI has been used to control intelligent peripherals in brain-robot interaction (BRI), but a number of the issues, such as individual differences among subjects, accuracies, and information transfer rate, still need to be addressed. In addition, developing shared control approaches by combining human intelligence and machine intelligence (e.g., computer vision) is important to improve the performance of BRI systems.

In this context, a variety of evoking mechanisms have been put forward, such as SSVEP (steady-state visual evoked potential), ERP (event-related potential), and MI (motor imagery). The corresponding control intelligent peripherals include wheelchair, manipulator, drone, and humanoid robot. With subsequent problems, the interaction between human brain and the intelligent peripherals has to be taken into consideration. Therefore, the theme of cognitive-based EEG BCIs and human brain-robot interactions refers to many research fields of medicine, engineering, psychology, and robotics. It must be one of the hottest emerging topics in the 21st century.

To summarize the current research status, problems to be solved, and challenges in the field, a review article by X. Mao et al. gave a comprehensive report in this special session. They first briefly introduced the background and development of mind-controlled robot technologies. Second, they discussed the EEG-based brain signal models with respect to generating principles, evoking mechanisms, and experimental paradigms. Subsequently, they reviewed in detail commonly used methods for decoding brain signals, namely, preprocessing, feature extraction, and feature classification, and summarize several typical application examples. Next, they described a few BRI applications, including wheelchairs, manipulators, drones, and humanoid robots with respect to synchronous and asynchronous BCI-based techniques. Finally, they addressed some existing problems and challenges with future BRI techniques. This article provides a useful reference for not only beginners but also experienced researchers to do further exploration in this field.

Following the review article, some research articles covering the current developing trend contribute to the special session. For example, aiming at the evoking mechanisms, many researchers are engaged in developing new stimulus patterns to enhance the response potentials in the human brain so that higher classification accuracy can be achieved. J. Cheng et al. compared the performance of P300-based BCI between the semitransparent face pattern (STF-P) (the subject could see the target character when the stimuli were flashed) and the traditional face pattern (F-P) (the subject could not see the target character when the stimuli were flashed). They presented the two patterns in 6×6 matrix displayed on the monitor for the subjects to analyze the

difference between the two event-related potentials. As a result, they validated that the two paradigms had similar vertex positive potential (VPP) over frontal and central areas. However, a few differences were found in N200 and P300 over parietal and occipital sites. STF-P had relatively higher peak values across N200 and P300 than those of F-P over parietal and occipital sites. Due to the larger components, the STF-P could improve the classification accuracy and bit rate of the BCI system compared with the F-P. Although the research studied two paradigms only (semitransparency and nontransparency) and focused less on the different transparent degrees based on the state of being transparent, it provides a new insight into the studies of face stimuli and demonstrates that other distinct components could strongly affect the BCI performance.

Despite the evoking mechanisms, many classic and improved algorithms are applied to recognize different EEG-based paradigms. For instance, the common spatial pattern (CSP) and other spatiospectral feature extraction methods have become the most effective and successful approaches to solve the problem of MI pattern recognition. However, these methods need a lot of preprocessing and postprocessing, which influence the classification accuracy easily. Therefore, W. Zhang et al. put forward low-rank linear dynamical systems (LR-LDSs) for MI EEG to overcome these problems, by extracting both spatial and temporal features simultaneously, to improve the classification performance. They validated the systems on two MI datasets and the proposed LR-LDSs methods which performed better than CSP and common spatial-spectral pattern (CSSP).

Additionally, some hybrid BCIs have been proposed to improve the detection performance through combining different types of EEG-based paradigms. J. Long et al. designed an efficient framework for EEG analysis with applications for hybrid brain computer interfaces based on MI and P300. Traditional methods optimize two modalities separately. The proposed method optimized them together by concatenating the features of MI and P300 in a block diagonal form. Under this framework, the hybrid features of MI and P300 can be learned, selected, and combined together directly. They tested the method on the dataset of hybrid BCI based on MI and P300. The classification accuracies using their method are more stable and better than that with other methods. Furthermore, better performance can be obtained using their method for a shorter time. In fact, there are also many other hybrid BCIs raised to increase the classification accuracy or diversity of control commands.

T. Li et al. developed a novel motor imagery control technique and applied it in a 3D Tetris and an analogous 2D game playing environment. Their hybrid BCI recognized both EEG and blink electrooculogram (EOG) signals. To enhance player's BCI control ability, the article focused on feature extraction from EEG and control strategy supporting game-BCI system operation. Then, they compared numerical differences between spatial features extracted with CSP and their proposed multifeature extraction. The result showed the multifeature extraction produced more prominent numerical differences between spatial features extracted from different motor imagery signals. Therefore, it suggested that the immersive and rich-control environment for MI would improve the associated mental imagery and enhance MI-based BCI skills.

Not only can the BCIs be used to interact with intelligent peripherals, but also they fuse with other computational intelligence algorithms to understand human brain activities. For example, X. Mao et al. contributed a research article to this session about the fusion of a P300 paradigm and fuzzy-based image processing algorithm to extract an object representing a human intention. They proposed a P300-based IFCE (improved fuzzy color extractor) to extract an object in cluttered environment, which combined a P300-based BCI with a computational algorithm. The P300 paradigm was used to select a seed pixel representing an object that the human was interested in, and the IFCE extracted the corresponding object in a cluttered environment. They tested their system in the NAO humanoid robot using its camera. Since the system fused the computer vision with the BCI, NAO will execute more behaviors via fewer commands. This will definitely decrease the workload of a human brain.

The emerging of BCIs aims at helping people with severe motor disabilities or the elders, but now they have the possibility of assisting people who are unable to use both hands in some circumstances. Researchers are committed to increasing the classification accuracies and information transfer rate, by designing novel EEG evoking patterns and some adaptive EEG decoding methods. Combining computer intelligence with BCI is able to improve the efficiency of BRI, so more and more computational algorithms are added to a BRI system. Indeed, there are also many problems to be addressed, like the individual differences among people, the portability of EEG devices, and so on. With the emergence of the combination of EEG and other brain signal detecting methods (e.g., fMRI and fNIRS), this technique will be particularly useful in the design of BCI devices and BRI systems. In the future, the BCI will certainly play an important role as an advanced detecting means in BRI systems to provide humans with advanced intelligent devices.

Wei Li
Jing Jin
Feng Duan

Hindawi
Computational Intelligence and Neuroscience
Volume 2017, Article ID 5468208, 12 pages
https://doi.org/10.1155/2017/5468208

Research Article

Object Extraction in Cluttered Environments via a P300-Based IFCE

Xiaoqian Mao,[1] Wei Li,[2,3] Huidong He,[1] Bin Xian,[1] Ming Zeng,[1] Huihui Zhou,[4] Linwei Niu,[5] and Genshe Chen[6]

[1]*School of Electrical Engineering and Automation, Tianjin University, Tianjin 300072, China*
[2]*Department of Computer & Electrical Engineering and Computer Science, California State University, Bakersfield, CA 93311, USA*
[3]*State Key Laboratory of Robotics, Shenyang Institute of Automation, Shenyang, Liaoning 110016, China*
[4]*Shenzhen Institutes of Advanced Technology, Chinese Academy of Sciences, Shenzhen 518055, Guangdong, China*
[5]*Department of Math and Computer Science, West Virginia State University, 5000 Fairlawn Ave, Institute, WV 25112, USA*
[6]*Intelligent Fusion Technology, Inc., Germantown, MD 20876, USA*

Correspondence should be addressed to Wei Li; wli@csub.edu

Received 14 December 2016; Revised 3 April 2017; Accepted 24 May 2017; Published 27 June 2017

Academic Editor: Hasan Ayaz

One of the fundamental issues for robot navigation is to extract an object of interest from an image. The biggest challenges for extracting objects of interest are how to use a machine to model the objects in which a human is interested and extract them quickly and reliably under varying illumination conditions. This article develops a novel method for segmenting an object of interest in a cluttered environment by combining a P300-based brain computer interface (BCI) and an improved fuzzy color extractor (IFCE). The induced P300 potential identifies the corresponding region of interest and obtains the target of interest for the IFCE. The classification results not only represent the human mind but also deliver the associated seed pixel and fuzzy parameters to extract the specific objects in which the human is interested. Then, the IFCE is used to extract the corresponding objects. The results show that the IFCE delivers better performance than the BP network or the traditional FCE. The use of a P300-based IFCE provides a reliable solution for assisting a computer in identifying an object of interest within images taken under varying illumination intensities.

1. Introduction

One of the primary color segmentation tasks is to extract objects (regions) of interest from an image, since a variety of vision-based applications rely on the quality of the extracted objects. Over the past years, many researchers have used color segmentation algorithms to extract regions of interest, but the low robustness of the existing algorithms to illumination variation in cluttered environments is still problematic. For example, Felzenszwalb and Huttenlocher defined a predicate for measuring the evidence for a boundary between two regions using a graph-based representation of the color image. The developed algorithm constructs the boundary of the graph by comparing the difference between two components and their internal differences, respectively, computed by minimum spanning tree (MST) and the edge weights based on the absolute intensity difference or all three (red, green, and blue) of the color plane segmentations for color images [1]. Dony and Wesolkowski introduced an edge detection approach for color images, which was based on the calculation of the vector angle between two adjacent pixels. The method detected only chromatic differences so that it was suitable for applications where differences in illumination were irrelevant [2]. Shi and Malik treated color image segmentation as a graph-partitioning problem and proposed a global criterion, that is, the normalized cut, for segmenting the graph. The normalized-cut criterion measures the total dissimilarity between the different groups as well as the total similarity within the groups. Then, they optimized this criterion using a computational approach based on the generalized-eigenvalue

technique [3]. Malik et al. used contour and texture analysis for color image segmentation. They provided an algorithm for partitioning greyscale images into disjoint regions of coherent brightness and texture. The cues of contour and texture differences were exploited simultaneously. Then, they introduced a gating operator based on the texturedness of the neighborhood of a pixel that facilitates cue combination. Finally, the spectral-graph theoretical framework of normalized cuts was used to find partitions of the image in regions of coherent texture and brightness [4]. Albalooshi and Asari proposed a self-organizing lattice Boltzmann active-contour (SOLBAC) approach for segmentation while preserving the precise details of the object's region of interest. Even though the approach improved the computational time cost, the computer could not effectively identify the object of interest [5]. In terms of the psychology of object and pattern recognition, Brewer and Williams think that the pattern or object recognition is the process by which the brain recognizes light, shapes, and colors as particular objects or patterns. It is the process of "assigning meaning to the visual input by identifying the objects in the visual field." This ability combines perception, attention, and memory [6]. Therefore, it is too difficult to identify an arbitrary object depending only on machine understanding, even if it seems simple for humans, since the recognition process is so sophisticated.

General segmentation algorithms usually process the entire image instead of the regions of interest [7]. However, these segmentation algorithms suffer from a computational time that is too long to satisfy the real-time requirements because a number of segments that are not of interest have to be processed when the algorithms are applied to vision-based robot-tracking systems. For robot operations, the segmentation of only regions of interest to fulfill robot tasks in real time should be a priority. For example, the objects of interest are goals, robots, doors, and so forth, in RoboCup [8]. For a match between two robot teams, the use of fast and robust algorithms for extracting these objects is the key step to winning the match. The popular algorithms proposed for this goal were mostly the color-based segmentation and geometrical image-processing methods [9]. Among them, the most commonly used color space is HSV [10] and the most commonly used geometrical image-processing tool is the Hough transform for circle detection [11, 12]. Moreover, Kaufmann et al. proposed the visual robot-detection technique by training the vertical and horizontal color histograms and other features using two BP networks and combining the output of the two neural networks to make the final classification decision [13]. For extracting an object of interest in cluttered environments under diverse and varying light illumination for robot navigation or operations, the robustness and fast processing time of the algorithms are critical.

In this paper, we present a method of segmenting regions (objects) of interest with color similarity via the P300-based IFCE. First, we design a 3X3 P300 paradigm to stimulate the targets, that is, the interesting-object candidates, including their corresponding fuzzy parameters and seed pixels. An object of interest to which a subject pays attention is identified while the P300 stimuli are flashing. Second, to extract an object of interest reliably, the IFCE proposed herein processes each detected pixel based on the angle between two vectors from the detected pixel to the seed pixel in RGB space coordinates. The vector length corresponds to the pixel illumination intensity and the direction corresponds to the color. The IFCE is much more robust than other color-extraction algorithms because the pixel illumination intensity and the color are separately represented. This algorithm extracts an object of interest quickly since the corresponding seed pixel and fuzzy parameters are predetermined in the training process. Last, we conducted comparative studies of the proposed algorithm with a BP network and the traditional FCE. The results show that the proposed P300-IFCE method is very robust for segmenting regions of interest. This study not only benefits people with severe motor disabilities, but also works as an auxiliary means of assisting the nondisabled man when both of his hands are busy, for example, our current project on control of an underwater manipulator via brainwaves [14]. In this application, the operator uses a P300 paradigm to control the underwater manipulator, while both the operator's hands are used to operate the underwater vehicle movement.

The motivations of this study are trying to address the following issues: First, effectively extracting an object of interest in a cluttered environment usually suffers from the following: how to use a computer to model the object like human understanding in mind and how to extract the object of interest from the cluttered environment under varying illumination conditions. In order to solve these two issues, we propose the method for object extraction via the P300-based IFCE. The P300 paradigm is used to identify an object of interest for robot navigation to simplify the complex process of identifying the object using a computer. Although the P300 paradigm could not directly represent the operator's mind, it indirectly maps the operator mental activities into his/her intention to identify the object which the machine should extract, while the IFCE operator is used to deal with the varying light conditions to improve the quality of the object of interest to be extracted. Second, the trend to developing an intelligent robot system is trying to combine human and machine intelligence. The study in this paper would be an attempt to fuse brainwaves, which indirectly or directly represent the human intentions, and the fuzzy logic-based IFCE operator, which is a typical computational algorithm, to enhance the performance of the object extraction in a cluttered environment. Mental activities through brain signals in psychology may not need a complex computational process, but currently it is very difficult for engineers to use the conclusions from psychology studies to implement the process without knowing the inside principles. Finally, this study would especially benefit people with severe motor disabilities; they cannot express their mind through a keypad, a mouse, or even speaking a word. In this circumstance, the P300 paradigm, as an auxiliary tool, establishes argumentative communication for them to select an object of interest in order to express their mental activities. By analysing the P300 components from their brain signals, the machine can identify which objects of

interest should be extracted with help of the IFCE algorithm.

Up to now, most of the BRI approaches have focused on low level control of a robot system via brain signals [15–21]. For example, the works [22, 23] used four or six visual stimuli designed in the SSVEP or ERP model to control a humanoid robot's walking behaviors. On the contrary, the study in this article applies the P300 paradigm into a BRI system at a high level to assist the computer to express an object of interest that a human understands. Following the introduction, Section 2 describes the IFCE in detail and how to use it to extract an object. Section 3 gives an introduction to the P300-based seed-pixel selection, which includes establishing a P300 model, acquiring data and analysing signals, and guaranteeing that the seed pixels represent objects of interest. Section 4 presents some experiments in cluttered environments and compares the P300-based IFCE with two other algorithms to validate the robustness and efficiency of the proposed P300-based IFCE method. In addition, the last section draws some conclusions and puts forward some ideas for future work.

2. Improved Fuzzy Color Extractor

The fuzzy color extractor (FCE) was first proposed as an Iterative Fuzzy-Segmentation (IFS) algorithm by Li [24]. He applied IFS to extract color components of a chemical plume and its odour source for visual confirmation of the identified odour source [25]. The fuzzy color extractor can directly extract the chemical plume and its source by defining their color patterns. However, the color patterns are defined in the RGB space and the components of R, G, and B vary due to changes in illumination intensity. Once the illumination intensity changes, the color patterns are supposed to be recalibrated. In this paper, the traditional FCE is modified by defining a new color pattern to improve its robustness under different illumination intensities. Herein, the new color pattern is defined by the angle between the vectors of two pixels in RGB space coordinates and then replaces the R, G, and B values as the input of the traditional FCE. Based on the newly defined color pattern, a pixel is classified as belonging or not belonging to the target after fuzzification and defuzzification. The IFCE will be explained in detail as follows.

2.1. Color Pattern Definition. Traditionally, the colors of an image are described in the RGB space, where colors are represented by their red, green, and blue components in an orthogonal Cartesian space, as shown in Figure 1. The color of each pixel $p(m,n)$, denoted by $(m,n)_{\mathrm{RGB}}$, is processed to separate its red, green, and blue components $(p(m,n)_{\mathrm{R}}, p(m,n)_{\mathrm{G}}, p(m,n)_{\mathrm{B}})$ [7]. To distinguish between two different pixels, for example, $p(m,n)$ and $q(s,t)$, three variables must be calculated, as presented in (1). In this paper, a new color pattern is put forward that compresses these three variables into a single variable. First, each pixel in RGB space is regarded as a three-dimensional vector from the original point to this pixel, as shown by points p and q in Figure 1. The length of the vector represents the illumination intensity while the direction of the vector represents the color. Thus, the illumination intensity and the color of a pixel are decomposed so that the representation method is able to adapt to variations in illumination conditions. The compressed single variable is described as (2), where $d(p,q)$ represents the difference between the two pixels p and q. In the new color pattern, the angle between two vectors replaces the three distances of RGB values, which reduces the influence of illumination-intensity variations:

$$\begin{aligned}
\mathrm{dif}(p,q)_{\mathrm{R}} &= p(m,n)_{\mathrm{R}} - q(s,t)_{\mathrm{R}},\\
\mathrm{dif}(p,q)_{\mathrm{G}} &= p(m,n)_{\mathrm{G}} - q(s,t)_{\mathrm{G}},\\
\mathrm{dif}(p,q)_{\mathrm{B}} &= p(m,n)_{\mathrm{B}} - q(s,t)_{\mathrm{B}},
\end{aligned} \tag{1}$$

$$d(p,q) = \arccos \frac{p(m,n)_{\mathrm{R}} \cdot q(s,t)_{\mathrm{R}} + p(m,n)_{\mathrm{G}} \cdot q(s,t)_{\mathrm{G}} + p(m,n)_{\mathrm{B}} \cdot q(s,t)_{\mathrm{B}}}{\sqrt{p(m,n)_{\mathrm{R}}^2 + p(m,n)_{\mathrm{G}}^2 + p(m,n)_{\mathrm{B}}^2} \cdot \sqrt{q(s,t)_{\mathrm{R}}^2 + q(s,t)_{\mathrm{G}}^2 + q(s,t)_{\mathrm{B}}^2}}, \tag{2}$$

where $0 \leqslant m, s \leqslant M$, $0 \leqslant n, t \leqslant N$, and M and N indicate the size of the array containing the image.

2.2. Fuzzy Rules. Here, we apply the following fuzzy rules to process the input $d(p,q)$:

If $d(p,q)$ is zero,
then $p(m,n)$ and $q(s,t)$ are matched.
If $d(p,q)$ is negative or positive,
then $p(m,n)$ and $q(s,t)$ are unmatched.

In fact, $q(s,t)$ often corresponds to a seed pixel, which can represent an object to be extracted. Thus, "matched" means that $p(m,n)$ is matched with the seed pixel. Both rules indicate that the pixel $p(m,n)$ belongs to the object to be extracted if the angle between $p(m,n)$ and the seed pixel in the RGB coordinate system is small enough; otherwise, $p(m,n)$ does not belong to the object.

2.3. Fuzzification and Defuzzification. When we obtain the angle $d(p,q)$, the membership can be calculated. Figure 2(a)

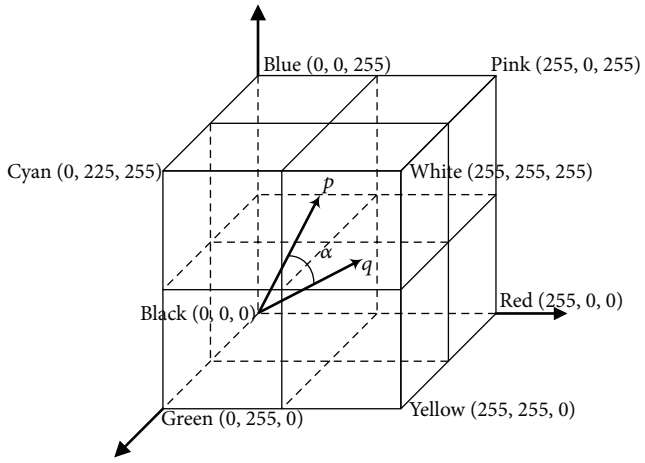

Figure 1: RGB space coordinate system.

shows the membership functions $(\mu_N(x), \mu_Z(x), \mu_P(x))$ for the input fuzzy variables (negative, zero, and positive) that are defined by

$$\mu_N(x) = \begin{cases} 1 & -\frac{pi}{2} \le x < -\alpha_2 \\ \frac{x+\alpha_1}{\alpha_1-\alpha_2} & -\alpha_2 \le x < -\alpha_1 \\ 0 & -\alpha_1 \le x \le \frac{pi}{2}, \end{cases}$$

$$\mu_Z(x) = \begin{cases} 0 & -\frac{pi}{2} \le x < -\alpha_2 \\ \frac{x+\alpha_2}{\alpha_2-\alpha_1} & -\alpha_2 \le x < -\alpha_1 \\ 1 & -\alpha_1 \le x < \alpha_1 \\ \frac{\alpha_2-x}{\alpha_2-\alpha_1} & \alpha_1 \le x < \alpha_2 \\ 0 & \alpha_2 \le x < \frac{pi}{2}, \end{cases} \quad (3)$$

$$\mu_P(x) = \begin{cases} 0 & -\frac{pi}{2} \le x < -\alpha_1 \\ \frac{x-\alpha_1}{\alpha_2-\alpha_1} & \alpha_1 \le x < \alpha_2 \\ 1 & \alpha_2 \le x < \frac{pi}{2}. \end{cases}$$

Figure 2(b) shows the membership functions $(\mu_M(x), \mu_U(x))$ for the output fuzzy variables (matched, unmatched), which are defined by

$$\mu_M(x) = \begin{cases} \frac{\rho_U - x}{\rho_U} & 0 \le x < \rho_U \\ 0 & \rho_U \le x \le \frac{pi}{2}, \end{cases}$$

$$\mu_U(x) = \begin{cases} 0 & 0 \le x < \rho_M \\ \frac{x-\rho_M}{pi/2-\rho_M} & \rho_M \le x \le \frac{pi}{2}, \end{cases} \quad (4)$$

where $\rho_M + \rho_U = pi/2$. Based on the membership functions for angles $d(p,q)$, the fuzzy rules produce the matched weight ω_m and unmatched weight ω_u according to

$$\omega_m = \mu_Z(d(p,q)),$$
$$\omega_u = \max\{\mu_N(d(p,q)), \mu_P(d(p,q))\}. \quad (5)$$

Figure 2(b) shows the produced areas in the output domain for the case in which ω_m and ω_u cut $\mu_M(x)$ and $\mu_U(x)$. A crisp output value, $\Delta\rho_F$, is calculated by the centroid-defuzzification method, as shown in

$$\Delta\rho_F = \frac{\int \mu_{\text{out}}(x)\, x\, dx}{\int \mu_{\text{out}}(x)\, dx}, \quad (6)$$

where $\mu_{\text{out}}(x)$ represents the envelope function of the areas cut by ω_m and ω_u in the fuzzy output domain. If $\Delta\rho_F < \sigma$, where σ is a threshold, $p(m,n)$ is extracted; otherwise, $p(m,n)$ is not extracted. The IFCE can be understood as a mapping operator between angle $d(p,q)$ in the RGB space and a difference $\Delta\rho_F$ in the intensity space under a fuzzy metric.

2.4. Subregion Generation and Object Extraction. Given a seed pixel, similar pixels that are "matched" in one image are extracted. However, the extracted pixels may include some discrete points. Not only the object itself but also some noise is extracted. Usually, the noise is distributed discretely and randomly, so some measures must be taken to ignore it. Meanwhile, the pixels belonging to some subregions need to be merged together in order to extract the entire object.

Here, we use a technique that is different from the traditional region-growing based method [26] to generate subregions. The subregion generation, as shown in Figure 3, occurs together with the "matching" process. First, the first seed pixel representing the object is obtained from the stimulus target induced by the P300 potential. Second, the angles between the seed pixel and every other pixel in the image are calculated and the minimal angle is selected as the starting pixel. Third, we use the IFCE to determine the "matched" pixels in one subimage based on the pattern, as shown in Figure 3(c). When all the "matched" pixels based on the seed pixel are determined in a subregion, the subregion extraction is complete. Then, a new pixel is selected with the minimal angle from the remaining pixels and the process described above is repeated to extract the next subregion. The extraction process continues until (7) is not satisfied or there is no "matched" pixel adjacent to the subregion:

$$d(p,q) = \sum_i \left[p(m,n)_i - q(s,t)_i\right]^2 < r, \quad (7)$$

where i represents the R, G, and B values and r is the threshold that was preset based on experience. $d(p,q)$ calculates the distance between one pixel and the seed pixel in RGB space. The equation guarantees that the pixel to be extracted is near to the seed pixel in order to extract the pixel whose color

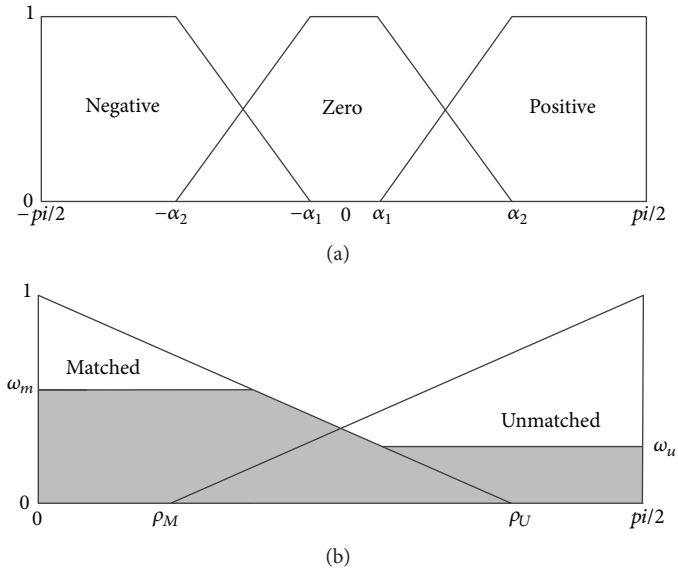

Figure 2: (a) Membership functions for angles. (b) Membership functions for defuzzification.

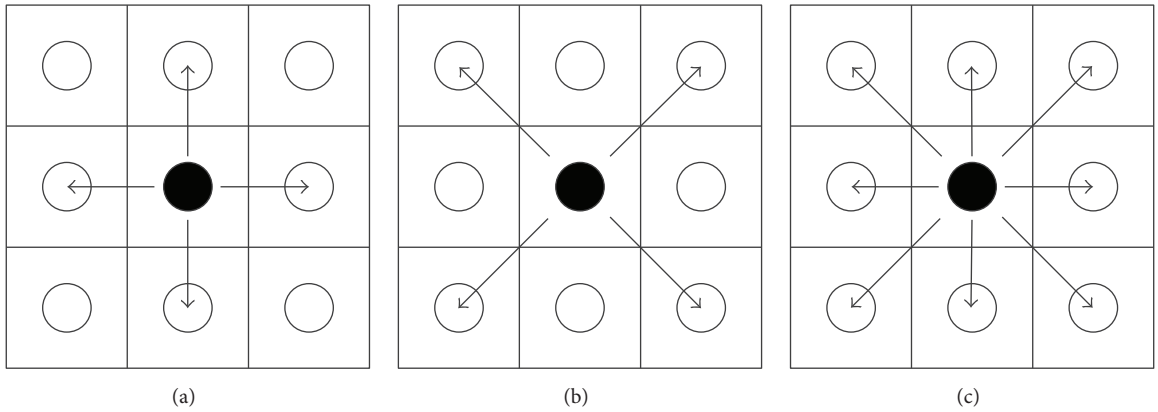

Figure 3: The subregion growing towards (a) its 4 adjacent neighbors, (b) its 4 diagonal neighbors, and (c) its 8 surrounding neighbors.

is similar to the seed pixel. Still, this threshold may change based on different colors, but not the image. The threshold remains the same for objects with similar colors.

Lastly, several subregions are obtained. In this paper, it is assumed that the subregion with the largest number of pixels is the object. During the process of pixel extraction, there might be some bad pixels belonging to the object that are not extracted to the subregion because of the reflection of light. Therefore, we fill in the pixels missing in the object. When the number of unextracted pixels between two extracted pixels is smaller than a given threshold, the unextracted pixels should be regarded as part of the object and be extracted. This process is executed in every row and column. As a result, only the subregion representing the object is extracted.

3. Seed Pixels and Fuzzy Parameters

This paper proposes a method for object extraction from a cluttered image, which combines the P300 paradigm and IFCE. Just as with the most object recognition methods [27, 28], the proposed method consists of offline and online phases. The offline phase is to establish a dataset of the parameters of objects in a cluttered image for the IFCE, including seed pixels and fuzzy parameters, while the online phase is to use the P300 paradigm to select an object of interest, that is, to select its corresponding parameters from the dataset for the IFCE-based object extraction process.

Figure 4 shows the selection process of P300-based object parameters. During this process, the subject first focuses on an object of interest represented by the P300 visual stimuli. Then, his/her brain signals acquired by the EEG device are analysed and classified to choose the parameters of the object of interest from the dataset. Last, the corresponding parameters are delivered to IFCE to extract the object on which the subject is focusing. The detailed explanation of the process is addressed in the following paragraphs.

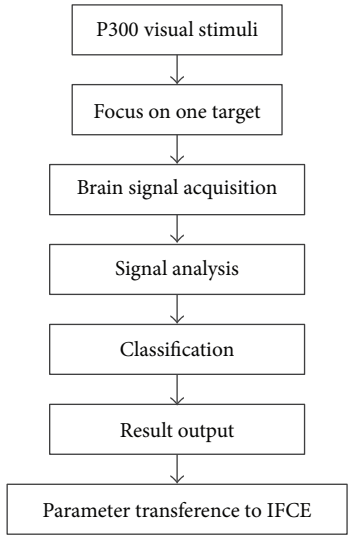

Figure 4: The process of P300-based seed-pixel selection.

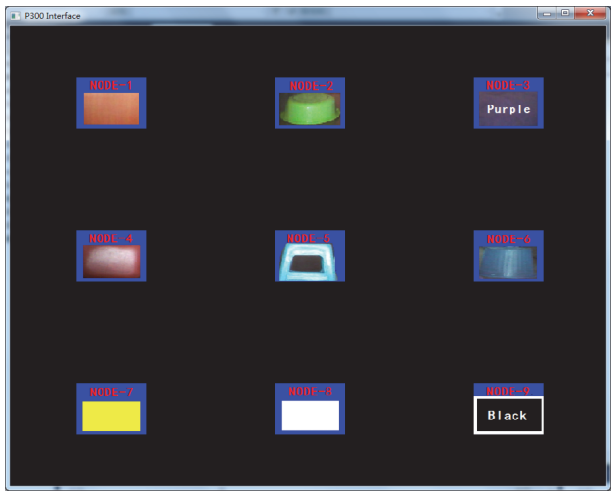

Figure 5: 3 × 3 P300 speller user interface.

3.1. P300 Paradigm. Among various EEG models, P300 has the advantages of having multiple targets, high accuracy, and short training time. Therefore, we designed a 3 × 3 P300 speller as the user interface, as shown in Figure 5, to represent an object of interest that contains the RGB-value information of the seed pixel and the fuzzy parameters. Once the target, that is, the object of interest, is selected, the corresponding parameters are delivered to the IFCE to extract the object in an image. Therefore, the accuracy and real-time performance of the P300 model can directly influence the performance of the IFCE. In this article, we need 7 targets and reserve 2 additional targets to expand the number of seed pixels when needed.

The P300 experiment consists of offline training and an online experiment. The offline training is used to train a classifier for the online experiment. During a P300 experiment, one repetition consists of flashing each of the six rows and columns one by one in a random order. The presentation time of a row or a column is 200 ms and the interstimulus interval (ISI) [29] is 300 ms; thus one display cycle (one repetition) is 1.8 s. A single repetition flashes every row and every column once, and every target flashes twice. A number of repetitions constitute a trial, in which the subject is asked to focus on only one target. Each target consists of 6 repetitions in the offline training process and 3 repetitions in the online experiment. In this article, each target flashes 6 times (namely, 3 trials) before the P300 model outputs a result. The subject is suggested to count the times where the target is presented [30]. Figure 6 shows the time sequence of the offline trial, online trial, one repetition, and one flash.

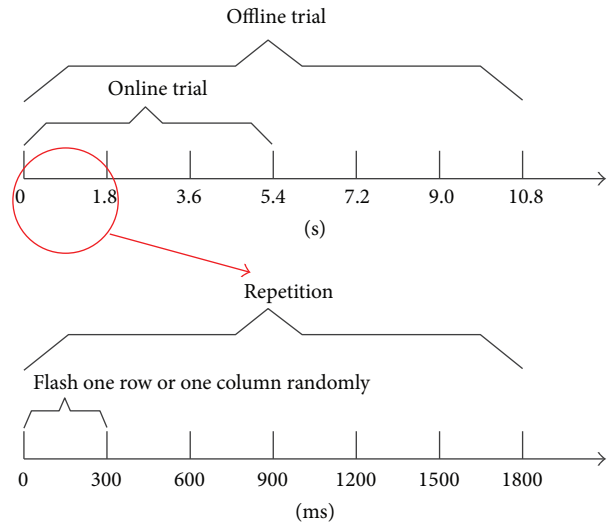

Figure 6: The time sequence of the offline trial, online trial, one repetition, and one flash.

EEG signals were recorded from 8 subjects who participated in 6 sessions of the P300-model testing, including 3 offline and 3 online experiments. The acquired neural signals are amplified, preprocessed by an analog low-pass filter of 50 Hz, and digitalized with a sampling frequency of 1000 Hz. The standard EEG cap with 30 channels is used to acquire the EEG signals.

3.2. Signal Analysis. Signal analysis consists of preprocessing, feature extraction, and classification. In preprocessing, a digital band-pass filter with a bandwidth of 0.1 to 30 Hz filtered the data segment lasting 800 ms from a stimulus appearance. Then, we selected data from 50 ms to 800 ms to remove the average component. Lastly, data after 50-fold frequency reduction were used to form the feature vectors. In feature extraction, the data of 30 channels were connected together head to tail. Thus, the feature vectors of the target and nontarget were obtained. For classification, we used a Fisher Linear Discriminant Analysis (FLDA) as our classifier. The two classes of target and nontarget were marked with Labels 1 and −1, respectively. The FLDA classifier in the online experiment used the classifier trained by offline data.

Table 1: Seed-pixel dataset (partial).

Object	RGB	α_1	α_2	ρ_M	σ
O1	186,69,34	.2	.3	.2	.5
O2	104,140,53	.2	.3	.2	.5
O3	130,100,142	.1	.2	.3	.6
O4	141,47,48	.1	.4	.3	.6
O5	87,133,166	.1	.3	.3	.6
O6	134,147,181	.15	.25	.8	.5
O7	176,134,36	.2	.3	.4	.4

3.3. Seed-Pixel and Fuzzy-Parameter Selection. A seed-pixel dataset consists of the RGB values of every pixel and the corresponding fuzzy parameters, as shown in Table 1. O1 to O7 represent seven objects in cluttered environments, corresponding to the first seven stimuli in the P300 model. The RGB value is obtained from the original image shot by a camera. For each group of R, G, and B values, a pixel belonging to the object is randomly extracted, except for some reflective pixels. The remaining parameters in Table 1 are obtained according to the results of the fuzzy training process based on experience. Once one target of the seven is selected, the corresponding parameters will be delivered to the IFCE and the object of interest is to be extracted.

Thus, the subject can select a seed pixel from a predefined set of pixels to directly identify different targets. Not only the seed pixel but also the fuzzy parameters are optimized choices because they are all pretrained before the experiment. Since the seed-pixel selection is straightforward, the computation time of seed-pixel determination is greatly reduced and the real-time performance of the system is improved.

4. Experiments and Results

4.1. Evaluation of the P300-Based Model. The evaluation of the P300-based model consists of two parts: offline training and online experiment. In the offline training process, the acquired data that are processed and classified as described in the previous section are used to train the FLDA classifiers of different subjects. In the online experiments, we applied the FLDA classifiers to recognize the target and provide feedback to the subjects in real time.

Eight subjects (seven right-handed, one left-handed) with normal vision volunteered to undergo the experiments. The collected neural signals are divided into the training and testing data for the FLDA classifier. To evaluate the P300-based model objectively, the acquired data are randomly chosen to train the FLDA classifier, and then the remaining data are used as test data for testing the FLDA classifier. The evaluation process repeats the procedure for training and testing the FLDA classifier 6 times. Table 2 lists the accuracy rates of the classification results for every time and every subject.

After the offline training, in the online experiment, the FLDA classifier with the highest accuracy from 6 evaluations of every subject were chosen. However, in the online experiment, we finalized a classification result after voting based on 3 repetitions. The target that has more than two votes will be selected as the final target. Similarly, Table 3 lists the accuracy rates of the classification results for every time and every subject in the online experiment. We conducted the online experiment 3 times and each experiment includes 9 targets for 2 cycles. Then, the accuracy rates are summarized for every experiment.

Table 2: Classification accuracy rates of the offline training.

Subject	Acc. 1	2	3	4	5	6	Average
S1	94.44	100	100	100	94.44	100	98.15
S2	100	100	100	100	100	100	100
S3	100	100	100	100	100	100	100
S4	94.44	100	100	100	100	100	99.07
S5	100	100	100	100	94.44	100	99.07
S6	100	100	91.67	100	91.67	100	94.44
S7	100	100	88.89	100	88.89	100	96.30
S8	83.33	100	91.67	100	100	100	95.83

Table 3: Classification accuracy rates of the online experiment.

Subject	Acc. 1	2	3	Average
S1	100	100	100	100
S2	100	100	100	100
S3	100	100	100	100
S4	94.44	100	100	98.15
S5	100	100	100	100
S6	100	100	100	100
S7	100	94.44	94.44	96.29
S8	100	100	100	100

By analysing the evaluation results, we find that the accuracy rates of the offline and online experiments are higher than 95%. Furthermore, some subjects, despite having no experience with the P300-based model, can achieve an accuracy rate of 100%. The results demonstrate that the P300-based model is very suitable for seed-pixel selection.

4.2. Segmentation of Objects of Interest. To demonstrate the advantages of the IFCE, we contrast the segmentation results obtained using a BP network, the traditional FCE, and the IFCE. The object recognition results will be demonstrated in the following part.

Figures 7(a) and 7(b) show two original images taken by a NAO robot [31] whose camera is set to a resolution of 320×240 pixels. The objects shown in the image are all based on the material from the camera itself. However, the image is not dependent on the property of the camera so any camera that can take color pictures should work. The images reveal an ordinary scene in daily life and the illumination intensity varies from early in the morning with sunlight to late in the evening with the lights on. The color threshold methods [32] cannot be used to segment the objects from the image because there are too many colors in the image. Therefore,

(a) (b)

Figure 7: The original images. (a) Early in the morning with sunlight. (b) Late in the evening with the lights on.

this paper uses a BP network [13] and the traditional FCE to segment the images in order to contrast the results with those of the IFCE. Figures 8 and 9 show the segmentation results of 7 objects obtained using a BP network, the FCE and the IFCE. Additionally, the BP network and FCE also used the subregion-generation method in the process of segmentation.

When the illumination condition is early in the morning with sunlight, the results shown in Figures 8(a), 8(d), and 8(g) indicate that the BP network and FCE worked with the bright colors and achieved good performance. For some dark colors, Figures 8(b) and 8(e) show that the BP network and the FCE basically extracted the objects, but the details of the objects were not revealed well and some noise pixels were also extracted along with the objects. Furthermore, in Figures 8(c) and 8(f), the objects of interest were totally submerged in the noise. However, the proposed IFCE was able to successfully extract all 7 of the objects of interest. When the illumination intensity changes late in the evening with the lights on, the results in Figure 9 show the strong robustness of the IFCE, in contrast with the BP network and FCE. As is shown in Figures 9(a), 9(b), 9(c), 9(e), and 9(g), the objects of interest were extracted, but the two methods performed badly in terms of presentation of the details and noise elimination. Figures 9(d) and 9(f) show that the wrong regions were extracted as the objects of interest. Note that Figures 8 and 9 share the same parameters even though the illumination intensities are different. Thus, the IFCE was more robust than the BP network and FCE. For Figures 8(f) and 9(f), the two parameters of the IFCE are changed to obtain the segmentation result. In total, the IFCE is able to adapt to illumination-intensity variations without recalibrating the parameters, but the BP network possibly needs to be retrained when the illumination intensity changes. In our experiment, we used the IFCE to segment the image and acquire the objects of interest.

4.3. Discussion. To illustrate the illumination-intensity variations, we compare the saturation and the lightness between the 7 objects in the two images. Table 4 lists the variation rates of the same pixel under different illumination intensities. As the table shows, the IFCE is able to segment the regions of interest for saturation-variation rates ranging from 9.1% to 57.2% and lightness-variation rates ranging from 4.4% to 33.3%. Therefore, the IFCE is adaptive to a wide range of illumination-intensity variations. For the object in Figures 8(f) and 9(f), the difficulty in segmenting is caused not only by a relatively large illumination-intensity variation but also by its small areas; thus, a recalibration process is still needed to obtain the object.

Table 4: Variations in the saturation and lightness at different illumination intensities.

Object	Saturation		Variation rate (%)	Lightness		Variation rate (%)
O1	140	163	16.4	120	103	14.2
O2	102	92	9.8	121	96	20.7
O3	44	40	9.1	90	120	33.3
O4	144	128	11.1	96	88	8.3
O5	173	74	57.2	145	118	18.6
O6	32	16	50.0	114	109	4.4
O7	240	157	34.6	150	101	32.7

Furthermore, the training processes of the parameters of the BP network and IFCE (similar to the traditional FCE) are different from each other. The BP network often needs a variety of samples to obtain a good model, while the IFCE only needs one pixel belonging to the object to train the fuzzy parameters. Therefore, the BP network needs to extract as many pixels belonging to the object as possible in order to obtain enough training samples. An interest region covering a small area may be not enough to train a BP network. For any region of interest, a single seed pixel is able to train the fuzzy parameters for segmentation. Thus, the IFCE has more potential to reduce the burden of humans and computers.

In terms of seed-pixel selection, it is the first key step for image segmentation. In this paper, the first very initial seed pixel is manually selected by using a mouse to click a pixel on the object of interest and the corresponding fuzzy parameters are preset. During the offline phase of the setting

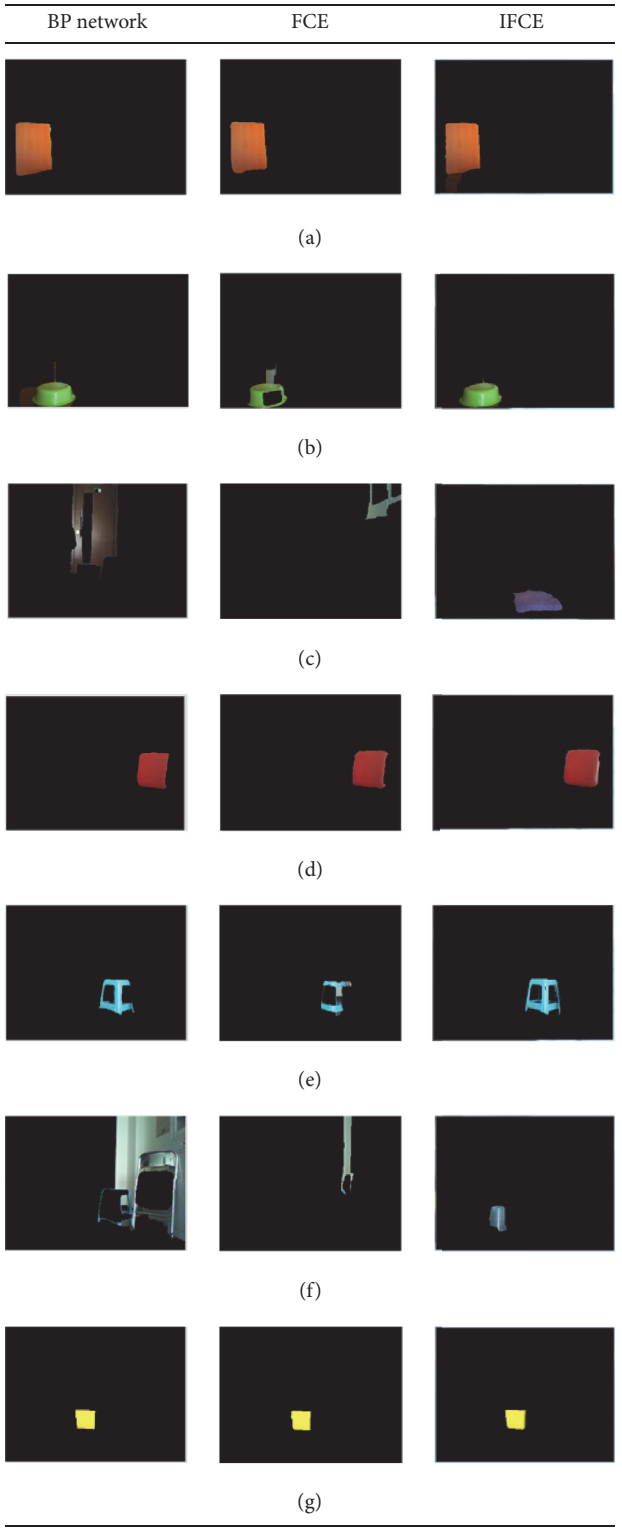

Figure 8: Comparison of the results obtained using a BP network, FCE, and IFCE (early in the morning with sunlight).

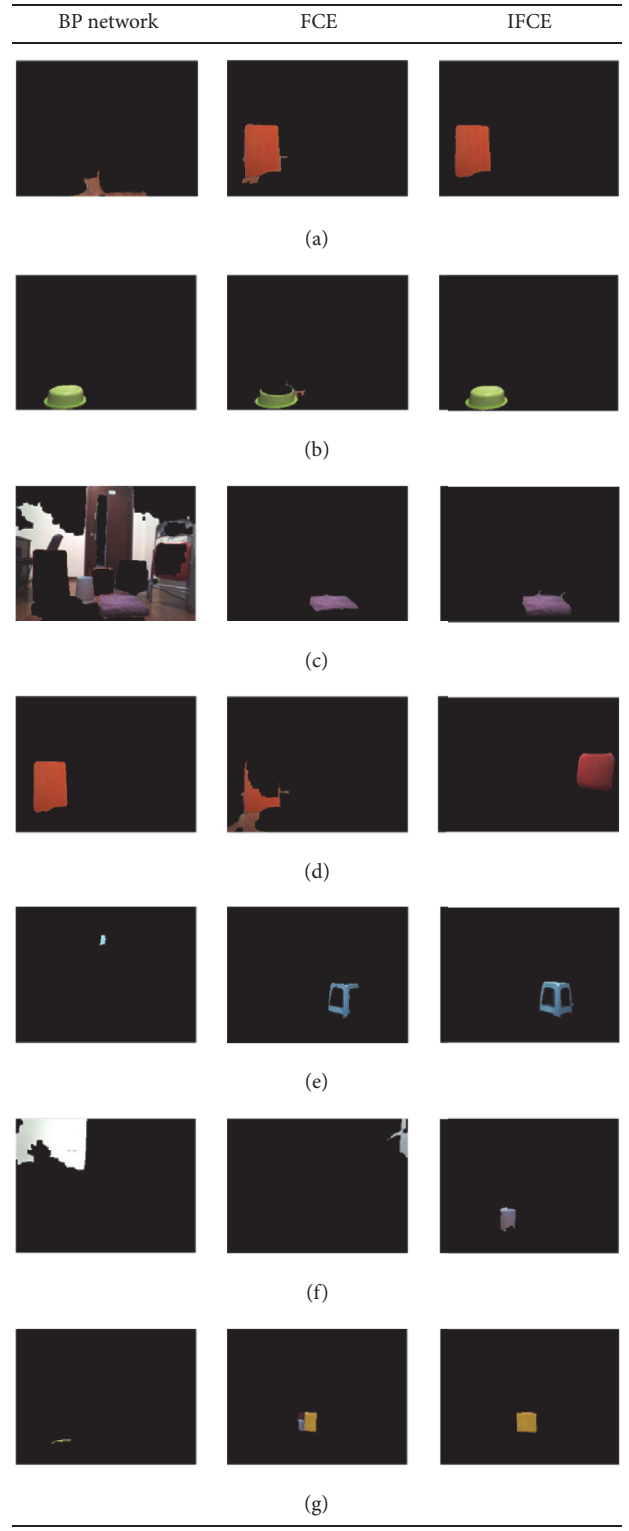

Figure 9: Comparison of the results obtained using a BP network, FCE, and IFCE (late in the evening with the lights on).

process, the remaining seed pixels for extracting this object are automatically determined based on (7). The criterion for evaluating good performance is defined by observing object contours as whole as possible and redundant pixels as few as possible. This strategy for the seed-pixel selection process combining the manual selection of the initial seed pixel and

automatic determination of the remaining seed pixels delivers better performance than only using manual selection of all the seed pixels. The P300-based model directly selects a seed pixel and its corresponding fuzzy parameters from a preestablished dataset that has no accidental error with the help of the P300-based model. In addition, the introduction of brain signals provides an effective means to assist the computer in recognizing the objects that are of interest to humans.

For any given experimental environments, we analyse those objects in an image needed for specific operation tasks to establish a dataset for the P300 paradigm. In this paper, we usually choose the objects that are commonly used for robot navigation tasks, so the proposed method works as long as the objects exist in the environment since each object has the same parameters even under different conditions. The dataset grows when more objects in an unknown environment needed to be extracted.

The reasons for applying the P300 paradigm into object recognition in the BRI area are as follows: First, it is an unsolved problem: how to use a machine to effectively represent objects of interest that a human understands. Like controlling robot motion via brainwaves, applying the P300 paradigm is indirectly incorporating human intentions to identify the object of interest for robot navigation, which is able to provide abundant visual stimuli to expand objects of interest in complex environments and to achieve high recognition accuracy because they represent human intentions correctly. Second, the visual stimuli are directly presented in the form of objects of interest, instead of simple words or squares, because the objects of interest might provide subjects with more instinctive information to understand the visual stimuli meaning and help subjects concentrate on their mental activities [33], which elite the high quality P300 potentials. Finally, the P300-based IFCE would be the first attempt to combine the BCI technologies with machine vision, which may lead to fusing human knowledge and machine intelligence.

5. Conclusions

In this article, we integrate the EEG-based P300 model into the object extraction process. The extraction of an object is a complex process from the aspect of psychology, so it is very difficult for a computer to understand an object of interest without human involvement. Therefore, this article draws support from the P300-based model to assist the computer in extracting an object of interest. Herein, the P300-based paradigm was used to induce a stimulus target representing an object of interest including its seed pixel in the image. Once the seed pixel was obtained via P300 brain signals, the segmentation method uses the IFCE to process the image to generate the subregions of interest that form the object of interest from the image.

To validate the feasibility of the system, we conducted some experiments and compared the results obtained using the proposed segmentation method with those obtained using other methods. Eight subjects participated in the P300 offline and online experiments and the average accuracy rates reached higher than 95%. Each target of the P300 interface represented a seed pixel containing the corresponding RGB values and fuzzy parameters of the object. After the target was locked by the subject, the data would be transferred to the IFCE for segmentation. At last, the IFCE was tested on two images taken in a daily life environment with different illumination intensities. The results showed that the IFCE had a better performance than the BP network and the traditional FCE, especially for some objects with dark colors. Moreover, there is no need to recalibrate the fuzzy parameters of the IFCE even when the illumination intensity changes. Therefore, even if the image changes as a whole, the method is still effective as long as the objects in the original image appear in a new image. If a new object appears in the image, the corresponding parameters are obtained to update the dataset by a short time training process which then can be used to extract the object.

Due to the robustness and precision of interesting-object extraction, the exact color and shape information can be revealed vividly, which provides an effective means for automatically identifying an object of interest by matching a property with the object via P300 brain signals. Once an object of interest is identified, the NAO is able to find a path to approach the object and to conduct the operation [34]. Nevertheless, the current IFCE algorithm aims at extracting an object with "single" similar color. As for a very complex object, we can consider combining the color information with others, such as object shapes and textures, to represent the object. In addition, we try to set multiple seed pixels representing an object with "multiple" similar colors to extract them via IFCE. Then, these multiple similar colors near to each other will merge together to form the object. Generally, each object may have its specific colors different from the others, so using these specific colors may be the very convenient way to solve the problem.

Our future work will focus on applying the P300 paradigm into robot vision because processing images acquired from the camera of a robot provides a variety of applications in daily life. Combining the P300-based paradigm with the IFCE will make robot operations more effective and efficient to serve in complex environments and especially provide an auxiliary means for people who are unable to use both hands in some circumstances. Furthermore, this is our first attempt to combine the brain signal with the objects extraction algorithm. In the future, first we will develop algorithms to automatically update the dataset when any untrained object appears, and second we will apply an optimization algorithm, such as a generic algorithm (GA), to determine the initial seed pixel and fuzzy sets instead of manual adjusting.

Conflicts of Interest

The authors declare that there are no conflicts of interest regarding the publication of this paper.

Acknowledgments

This research work was funded by the National Natural Science Foundation of China under Grant no. 61473207.

Huihui Zhou is supported by CAS Hundred Talent Program, Shenzhen, Grant nos. JCYJ20151030140325151 and KQTD20140630180249366.

References

[1] P. F. Felzenszwalb and D. P. Huttenlocher, "Efficient graph-based image segmentation," *International Journal of Computer Vision*, vol. 59, no. 2, pp. 167–181, 2004.

[2] R. Dony and S. Wesolkowski, "Edge detection on color images using RGB vector angles," in *Proceedings of the Engineering Solutions for the Next Millennium, 1999 IEEE Canadian Conference on Electrical and Computer Engineering*, pp. 687–692, Edmonton, Alberta, Canada.

[3] J. Shi and J. Malik, "Normalized cuts and image segmentation," *IEEE Transactions on Pattern Analysis and Machine Intelligence*, vol. 22, no. 8, pp. 888–905, 2000.

[4] J. Malik, S. Belongie, T. Leung, and J. Shi, "Contour and texture analysis for image segmentation," *International Journal of Computer Vision*, vol. 43, no. 1, pp. 7–27, 2001.

[5] F. A. Albalooshi and V. K. Asari, "A self-organizing lattice Boltzmann active contour (SOLBAC) approach for fast and robust object region segmentation," in *Proceedings of the IEEE International Conference on Image Processing (ICIP '15)*, pp. 1329–1333, Quebec City, QC, Canada, September 2015.

[6] K. Brewer and E. Williams, "The Psychology of Object and Pattern Recognition: A Brief Introduction," ISBN: 978-1-904542-16-2, 2004.

[7] G. Zhao, Y. Li, G. Chen et al., "A fuzzy-logic based approach to color segmentation," in *The International Society for Optical Engineering*, vol. 8739 of *Proceedings of SPIE Defense, Security, and Sensing*, Baltimore, Md, USA, 2013.

[8] H. Kitano, M. Asada, Y. Kuniyoshi, I. Noda, E. Osawa, and H. Matsubara, "Robocup: a challenge problem for AI and robotics," *AI Magazine*, vol. 18, no. 1, pp. 73–85, 1997.

[9] J. M. Cañas, D. Puig, E. Perdices et al., "Visual Goal Detection for the RoboCup Standard Platform League," *Combinatorics Probability & Computing*, vol. 24, no. 2, pp. 1344–1349, 2015.

[10] Y. Takemura, Y. Sato, K. Azeura et al., "SOM based color constancy algorithm for RoboCup robots," in *Proceedings of the 2008 Symposium on Cryptography and Information Security (SCIS 2008)*, vol. 2008, pp. 1495–1500, Miyazaki, Japan.

[11] X. Liang Y, L. I. Yong-Xin, J. Zhang et al., "Application of hough transform in robocup vision system," *Machinery Design & Manufacture*, 2008.

[12] C. Gönner, M. Rous, and K.-F. Kraiss, "Real-time adaptive colour segmentation for the RoboCup middle size league," in *RoboCup 2004: Robot Soccer World Cup VIII*, pp. 402–409, 2004.

[13] U. Kaufmann, G. Mayer, G. Kraetzschmar, and G. Palm, "Visual robot detection in RoboCup using neural networks," in *RoboCup 2004: Robot Soccer World Cup VIII*, pp. 262–273, 2005.

[14] J. Zhang, W. Li, J. Yu, X. Mao, M. Li, and G. Chen, "Operating an underwater manipulator via P300 brainwaves," in *Proceedings of the 2016 23rd International Conference on Mechatronics and Machine Vision in Practice (M2VIP)*, pp. 1–5, Nanjing, China, November 2016.

[15] C. J. Bell, P. Shenoy, R. Chalodhorn, and R. P. N. Rao, "Control of a humanoid robot by a noninvasive brain-computer interface in humans," *Journal of Neural Engineering*, vol. 5, no. 2, pp. 214–220, 2008.

[16] J. Zhao, Q. Meng, W. Li, M. Li, F. Sun, and G. Chen, "An OpenViBE-based brainwave control system for Cerebot," in *Proceedings of the 2013 IEEE International Conference on Robotics and Biomimetics (ROBIO '13)*, pp. 1169–1174, Shenzhen, China, December 2013.

[17] K. Bouyarmane, J. Vaillant, N. Sugimoto, F. Keith, J.-I. Furukawa, and J. Morimoto, "Brain-machine interfacing control of whole-body humanoid motion," *Frontiers in Systems Neuroscience*, vol. 8, article 138, 2014.

[18] B. J. Choi and S. H. Jo, "A low-cost EEG system-based hybrid brain-computer interface for humanoid robot navigation and recognition," *PLoS ONE*, vol. 8, no. 9, Article ID e74583, 2013.

[19] E. Tidoni, P. Gergondet, A. Kheddar, and S. M. Aglioti, "Audio-visual feedback improves the BCI performance in the navigational control of a humanoid robot," *Frontiers in Neurorobotics*, vol. 8, article 20, 2014.

[20] P. Stawicki, F. Gembler, and I. Volosyak, "Driving a semiautonomous mobile robotic car controlled by an SSVEP-based BCI," *Computational Intelligence and Neuroscience*, vol. 2016, Article ID 4909685, 14 pages, 2016.

[21] X. Mao, M. Li, W. Li et al., "Progress in EEG-based brain robot interaction systems," *Computational Intelligence and Neuroscience*, vol. 2017, Article ID 1742862, 25 pages, 2017.

[22] M. Li, W. Li, J. Zhao, Q. Meng, M. Zeng, and G. Chen, "A p300 model for cerebot—a mind-controlled humanoid robot," in *Robot Intelligence Technology and Applications 2*, vol. 274 of *Advances in Intelligent Systems and Computing*, pp. 495–502, 2014.

[23] J. Zhao, W. Li, and M. Li, "Comparative study of SSVEP- and P300-based models for the telepresence control of humanoid robots," *PLoS ONE*, vol. 10, no. 11, Article ID e0142168, 2015.

[24] W. Li, "An iterative fuzzy segmentation algorithm for recognizing an odor source in near shore ocean environments," in *Proceedings of the 2007 IEEE International Symposium on Computational Intelligence in Robotics and Automation (CIRA '07)*, pp. 101–106, Jacksonville, Fla, USA, June 2007.

[25] Y. Tian, X. Kang, Y. Li et al., "Identifying rhodamine dye plume sources in near-shore oceanic environments by integration of chemical and visual sensors," *Sensors*, vol. 13, no. 3, pp. 3776–3798, 2013.

[26] N. A. Mat-Isa, M. Y. Mashor, and N. H. Othman, "Seeded region growing features extraction algorithm; its potential use in improving screening for cervical cancer," *International Journal of the Computer the Internet & Management*, vol. 13, 2005.

[27] P. F. Felzenszwalb and D. P. Huttenlocher, "Pictorial structures for object recognition," *International Journal of Computer Vision*, vol. 61, no. 1, pp. 55–79, 2005.

[28] C.-F. Juang and L.-T. Chen, "Moving object recognition by a shape-based neural fuzzy network," *Neurocomputing*, vol. 71, no. 13-15, pp. 2937–2949, 2008.

[29] C. J. Gonsalvez and J. Polich, "P300 amplitude is determined by target-to-target interval," *Psychophysiology*, vol. 39, no. 3, pp. 388–396, 2002.

[30] M. Li, W. Li, J. Zhao, Q. Meng, M. Zeng, and G. Chen, "A p300 model for cerebot—a mind-controlled humanoid robot," in *Robot Intelligence Technology and Applications 2*, vol. 274 of *Advances in Intelligent Systems and Computing*, pp. 495–502, Springer International Publishing, 2014.

[31] J. Kulk and J. S. Welsh, "Evaluation of walk optimisation techniques for the NAO robot," *PLOS ONE*, vol. 7, no. 6, pp. 306–311, 2011.

[32] M. Cheriet, J. N. Said, and C. Y. Suen, "A recursive thresholding technique for image segmentation," *IEEE Transactions on Image Processing*, vol. 7, no. 6, pp. 918–921, 1998.

[33] M. Li, W. Li, and H. Zhou, "Increasing N200 potentials via visual stimulus depicting humanoid robot behavior," *International Journal of Neural Systems*, vol. 26, no. 1, Article ID 1550039, 2015.

[34] X. Mao, H. He, and W. Li, "Path finding for a NAO humanoid robot by fusing visual and proximity sensors," in *Proceedings of the 12th World Congress on Intelligent Control and Automation (WCICA '16)*, pp. 2574–2579, Guilin, China, June 2016.

Hindawi
Computational Intelligence and Neuroscience
Volume 2017, Article ID 5863512, 16 pages
https://doi.org/10.1155/2017/5863512

Research Article

Development of a Novel Motor Imagery Control Technique and Application in a Gaming Environment

Ting Li,[1] Jinhua Zhang,[2] Tao Xue,[1] and Baozeng Wang[2]

[1]*School of Computer Science, Xi'an Polytechnic University, Xi'an, China*
[2]*State Key Laboratory for Manufacturing Systems Engineering, School of Mechanical Engineering, Xi'an Jiaotong University, Xi'an, China*

Correspondence should be addressed to Ting Li; cangtianhaoxue@sina.com

Received 18 October 2016; Revised 5 December 2016; Accepted 30 January 2017; Published 9 May 2017

Academic Editor: Jing Jin

We present a methodology for a hybrid brain-computer interface (BCI) system, with the recognition of motor imagery (MI) based on EEG and blink EOG signals. We tested the BCI system in a 3D Tetris and an analogous 2D game playing environment. To enhance player's BCI control ability, the study focused on feature extraction from EEG and control strategy supporting Game-BCI system operation. We compared the numerical differences between spatial features extracted with common spatial pattern (CSP) and the proposed multifeature extraction. To demonstrate the effectiveness of 3D game environment at enhancing player's event-related desynchronization (ERD) and event-related synchronization (ERS) production ability, we set the 2D Screen Game as the comparison experiment. According to a series of statistical results, the group performing MI in the 3D Tetris environment showed more significant improvements in generating MI-associated ERD/ERS. Analysis results of game-score indicated that the players' scores presented an obvious uptrend in 3D Tetris environment but did not show an obvious downward trend in 2D Screen Game. It suggested that the immersive and rich-control environment for MI would improve the associated mental imagery and enhance MI-based BCI skills.

1. Introduction

Gamification is the application of game-design elements and game principles in nongame contexts [1, 2] in attempts to improve user engagement [3, 4], organizational productivity [5], physical exercise [6], and traffic violations [7], among others [8]. With the development of gamification, video game has been playing important roles in a variety of environments, from marketing [9–11] to inspiration [12] to health [13] and education [14–16]. Moreover, many areas of neuroscience (supported by Open Fund of Key Laboratory of Electronic Equipment Structure Design (Ministry of Education) in Xidian University (EESD-OF-201401)) have used video games as tools to study the effectiveness of electroencephalography in measuring visual fatigue, Internet game addiction, and remedies for motion sickness [17–22], which makes video game studies span a wide range of areas and clinical applications. Video game environment involves human interaction with a user interface to generate visual feedback on a video device or commands to control a robot. The feedback expresses user's motion, emotional and some other intentions. Those feedbacks to the nervous system close the control loop of the man-machine system [23]. In some applications, control of devices by means of neural processes (e.g., via EEG signals) can replace or enhance motor control. A particularly important application is rehabilitation, particularly with individuals who may have mobility restrictions.

Brain-computer interface (BCI) is a direct communication pathway between an enhanced or wired brain and an external device [17]. As a particular class of human-machine interface, BCI has spurred a surge of research interest. This technology serves the demands of activities from rehabilitation to assistive technology to daily civil field. Noninvasive EEG-based technologies and interfaces have been used for a much broader variety of applications. As the most discussed BCI control method, motor imagery (MI)

offers an essential basis for the development of BCIs [18]. Researchers have set up demonstrations on the feasibility of motor imagery brain-computer interface (MI-BCI) for different applications, especially in rehabilitation. From the perspectives of temporal regularities, neural encoding rules, and biomechanical constraints, researchers have uncovered many significant properties of motor imagery [18]. However, current MI-based BCIs are limited in imagination of only four movements: left hand, right hand, feet, and tongue [19]. It is still challenging to design an effective and flexible BCI system for complex controls in practical applications since the number of control commands in the BCI system is strictly limited [20]. Although EEG-based interfaces are easy to wear and do not require surgery, they have relatively poor spatial resolution and cannot effectively use higher-frequency signals. Most MI-BCI systems rely on temporal, spectral, and spatial features to distinguish different MI patterns. Another substantial barrier to using EEG as a BCI was the extensive training required before users can work the technology [21, 22, 24].

One of important factors improving the efficiency of MI-based BCI is the experiment paradigm, because the motivational experiment paradigms for MI provide more enlightenment and guidance for users to study neural control of movement. Allison et al. [25] proposed that if BCI methods are effective, gamers will be the most active testers. Van Erp and colleagues [26] predicted that, beyond rehabilitation uses, video game and entertainment would be the most promising application of BCIs. In the near future, games seem likely to be a very potent direction for application of BCI technology [27]. Video display has been a primary and important experimental tool in the BCI field, such as imaging hands or other parts of body moving according to certain static cue shown on the computer screen. "Static cue" is the original instruction pattern appearing in MI research. The thinking about this pattern is to simplify environmental stimuli, so that the participants can concentrate on mental tasks. This kind of experiment paradigm suits users without too much experience to gain MI skills, but lack of interestingness and inspiration for extensive training. People live in complicated and dense environments. They pay attention to objects which are important or interesting to them. Intuitively, it would seem that combining MI and BCI should provide more flexible environments, leading to enhancement of users' sense of stimuli. Current 3D video games provide abundant and rich information (stimulus and feedback) to immerse players in the game scenarios. The interaction patterns of these games include powerful move-enabled control and accurate feedback of players' operations. So we deduce that MI-BCI with game environment can connect the player to the action in the game in a more realistic and involving way.

How can a BCI experimental paradigm be more attractive? Though games can provide strong motivation for practicing and achieving better control for users within a rehabilitation system, the amount of information interaction during gaming should be adjusted to a proper range. The idealized experimental environments would not only be attractive to players (to reduce distraction) but also enhance the performing efficiency of motor imagery and help inexperienced users. So experimental objectives should be the core design principles of experimental design; meanwhile, content and forms should be vivid and rich. Marshall et al. designed a system to encourage rapid generation of mental commands and enhance the user's experience in motor imagery-based BCI [28]. Lalor et al. [29] refitted a game paradigm by introducing traditional steady-state visual evoked potential (SSVEP) BCI to improve user's concentration. That form of BCI used the SSVEP generated in response to phase-reversing checkerboard patterns to achieve binary control in a visually elaborate immersive 3D Mind Balance game [30]. The software converted brain signals relevant to two classes of motor imagery (left and right hand movement) to pinball game commands for control of left and right paddles [31]. In addition, studies have demonstrated examples of BCI applications developed in other game environments, such as Pacman [32], Tetris [33], and World of Warcraft [34]. The systems mentioned above mainly provided binary control, and players had a low level of operation, which would weaken the entertainment and immersion of BCI system. To resolve this problem, we must enable Game-BCI systems to provide more training functions. In order to make video game program in which BCI control is feasible, researchers need to simplify the original program to achieve the application with game-design elements and game principles in nongame contexts [1, 2].

Based on the reasons mentioned above, we conjectured that an immersive 3D game environment could promote characteristic brain state generation in the context of motor imagery. We implemented in a Game-BCI system for 3D Tetris game playing, which was a hybrid brain-computer interface (BCI) system, with the recognition of motor imagery based on EEG and blink EOG signals. A hybrid BCI system usually contained two or more types of BCI systems. And BCI system also could be combined with another system which is not BCI-based, for example, combining a BCI system with an electromyogram- (EMG-) based system. The research on hybrid BCI has been a mainstream research direction in BCI field. Many works [35–38] with great academic value stated the important ideas for the development of hybrid BCI.

The main content of paper can be divided into five parts. In Sections 2.4.2 and 3.2, the method of multifeature extraction for extracting features of MI EEG was developed and tested separately. The mechanism in translation from classification results of MI to the control commands in 3D Tetris game was explained in Section 2.5. Then in the work reported in this paper, to help demonstrate the effectiveness of the system, and as a point of comparison with the 3D environment, we also applied the new system in a 2D game scenario. Through all this work we expected to prove the effectiveness of gamification strategy for enhancing players' BCI control abilities.

2. Materials and Methods

2.1. Participants. Ten players (3 females and 7 males) without previous BCI experience participated in the experiment voluntarily. All these players were right-handed, and their mean age was 24.6 years with a standard deviation of 3.3

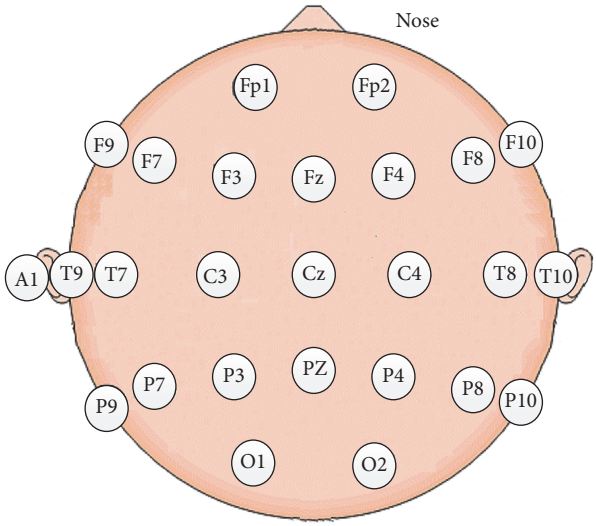

Figure 1: Positions of 25-channel EEG electrodes on players' scalps.

years. All these players were conducted in accordance with the highest ethical standards of Xi'an Jiaotong University and signed the declaration file to declare they volunteered for the research experiment.

2.2. Apparatus. We used the 40-channel NuAmps system (America, Neuroscan Co.) to acquire EEG and EOG data. The system collected and transformed data using the TCP/IP (Transmission Control Protocol/Internet Protocol) protocol. The sampling rate was 1000 Hz. EEG data was recorded from 25 scalp electrodes, placed as shown in Figure 1. The reference electrode was on the left ear (Electrode A1). For all electrodes, the impedance was $<5\,\text{k}\Omega$. Four additional electrodes were used to record horizontal and vertical EOG. Scan 4.5 performed online EOG artifact rejection. A 50 Hz notch filter suppressed line noise.

2.3. Procedures

2.3.1. Motor Imagery Training. Before 3D Tetris game playing, all players went through a process of MI training. We familiarized them with the feeling of performing of four kinds of motor imagery. In the MI training phase, the participant sat in a comfortable armchair in front of a computer screen (Dell S2316 M LED monitor, maximum resolution: 1920×1080) for sixty centimeters. We instructed participants to imagine right hand, left hand, foot, and tongue movements corresponding to visual cues showed on the computer screen. Each trial began with a 2 sec interval in which the screen was blank. Then players took 4 secs to do motor imagery. The screen then was again blanked to begin the next trial. The flow of one single trial for MI training was showed in Figure 2. We collected data for each participant in two sessions over two days. Each session contained two runs, in each of which the four types of cue were displayed 15 times in a randomized order, giving a total of 240 trials for each participant. Each session lasted approximately sixteen minutes.

2.3.2. 3D Tetris Game Playing. In the 3D Tetris experiment, we divided the 10 players into two equal groups: One group experienced the traditional asynchronous BCI paradigm and the other group experienced the 3D Tetris paradigm. The 3D Tetris procedure was a puzzle game that used a three-dimensional playing field, as opposed to the traditional two dimensional pattern mentioned in literature [39]. In the 3D Tetris displays, three-dimensional block groups constructed of small single cubic blocks arranged in different shapes keep falling into a 3D space from the top of the screen. The player adjusted the position and moving direction of these block groups such that they fell into a pattern forming a larger complete shape with no gaps. The 3D space was a cuboid with an open top and closed bottom (see Figure 3). The bottom plane appeared as a white grid. The four standing planes displayed as a red grid, green grid, yellow grid, and blue grid. Here, we used names associated with the semantic meanings of MI cues appearing in MI training phase to label the four standing planes, namely, Foot Plane, Left Plane, Tongue Plane, and Right Plane (see Figure 3).

During game playing, we used the names of standing planes to label the direction of motion of the block groups. In coordinates of block group, Foot Plane represents y-axis positive direction. Left Plane represents x-axis positive direction. Tongue Plane represents y-axis negative direction. Right Plane represents x-axis negative direction. "Moving to Foot Plane" meant that if the Game-BCI system produced an identification result of the player's mental state as "MI of foot motion," then the block group would move one unit length in the direction of the Foot Plane. The unit length of a block group move was determined by the original 3D Tetris program and was not changed in this research. This 3D space contained 20 vertical layers. When players filled one layer with falling block groups, that layer disappeared, and the player earned one score unit. If blocks stacked over a given layer, but gaps remained in the layer, the number of layers went down by one. The game was over when the final layer was lost. In our experimental paradigm, players used four kinds of MI commands to control the movement direction of block groups and used two kinds of blink EOG commands to rotate the block groups. With the control commands translated from EOG, the falling three-dimensional block groups could be rotated about any of the three coordinate axes. As a block fell, its shadow appeared at the bottom of the 3D space; the shadow indicated where the block would land, if it continued to fall without the player's intervention. The BCI control details are explained in Section 2.5.

2.4. Data Handling Procedures. In this research, the data processing showed in Figure 4 contained two sections: offline data analysis and algorithm training and online control. The processing of online control would use the characteristic component filter, ICA demixing matrix, CSP spatial filter, and Small World Neural Network Classifier, which were obtained from the processing of offline data analysis and algorithm training.

In both offline calculation and online control, preprocessing steps included power frequency filtering, EOG extraction, and baseline correction of EEG. We used all EEG data

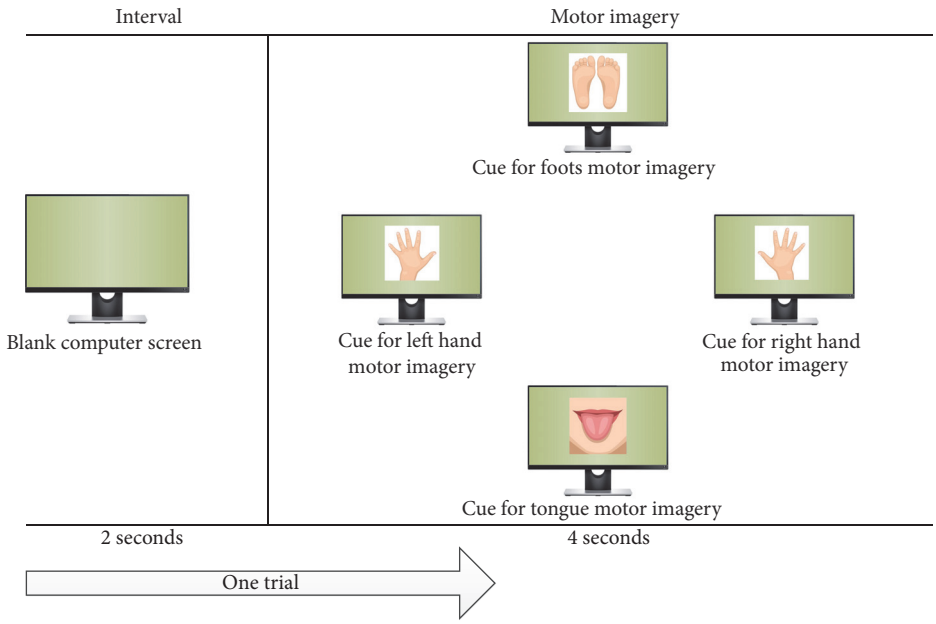

Figure 2: The flow of one single trial for MI training.

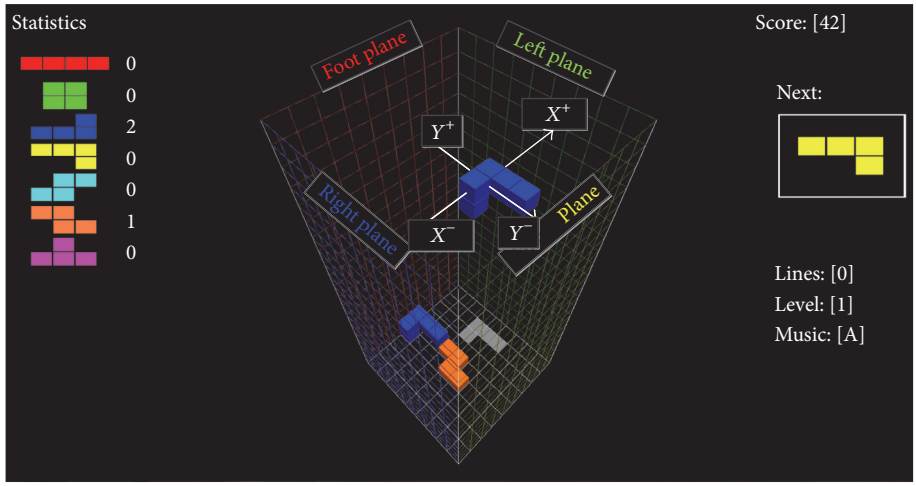

Figure 3: 3D Tetris Scene.

collected in the MI training phrase in feature component extraction and algorithm training (classification and feature extraction). Trial data striping and feature component extraction only occurred in offline calculation.

2.4.1. Characteristic Component. Ten players participated in the MI training phrase. For each player, we collected 240 trials of EEG data, giving 60 trials for each kind of motor imagery. For each kind of motor imagery, we averagely separated the data of each player into 6 parts. Each part contained 10 trials EEG data related to given kind of motor imagery. For each trial of EEG data, we applied CAR spatial filtering to each of the 25 data channels firstly and then selected the data recorded after 4 seconds of the MI cue presentation. Chebyshev I Bandpass filters of order 10 were used for extracting multiband data, with the range from 0 Hz to 60 Hz and frequency band 2 Hz wide. Subsequently, the filtered data was separated into components labeled by frequency band and electrode.

We calculated the spectral power for each selected component and the average R-squared values of components, which were labeled by the same frequency band and electrode, but by different MI categories. R-squared values provide a measure for the amount to which a particular EEG feature is influenced by the subject's task (e.g., hand versus foot imagery) [40]. It is an evaluation index used to determine which brain signal feature differ the most between two particular tasks. Then it is necessary to verify whether

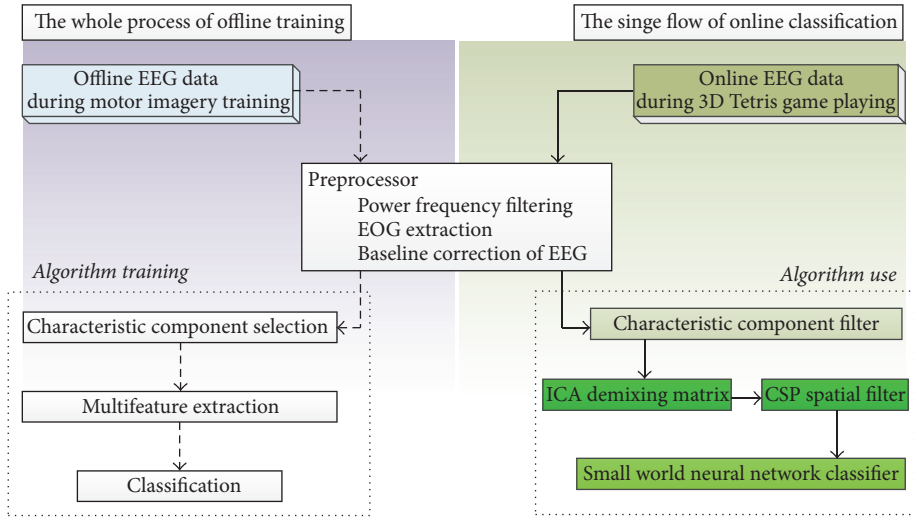

Figure 4: The illustration of data handling procedures.

the feature in question is consistent with the sensorimotor rhythm's known properties to avoid misconfiguration due to EEG artifacts, other noises, or random effects [40]. According to the R-squared values among the four kinds of motor imagery, we noted frequencies and electrodes of the components with the top 10 largest R-squared values. Depending on the R-squared values, the most significant components were found. Then according to the properties of ERD and ERS patterns appearing in the process of MI [41], we screened all selected components and picked up the most suitable ones for the classification of motor imagery. All selected components were used to train the algorithms for feature extraction and classification.

2.4.2. Multifeature Extraction. In this investigation, we proposed a method of multifeature extraction. That procedure combined independent component analysis and common spatial patterns in a renovated mode.

(1) Independent Component Analysis Keeping Temporal Structure of EEG Signals. The first step was to conduct an independent component analysis (ICA), keeping the temporal structure of the EEG signal. EEG is a kind of mixed signal, generated by underlying components of brain activity in many different regions and recorded from a number of locations on the scalp. To find the original components of brain activity and define the brain states, our task was to reveal the underlying brain activity by separating the mixed signal into components associated with their independent sources. The traditional ICA algorithm identifies temporally independent sources in multichannel EEG data. However, on account of the strong noise and the ignorance of the temporal structure of EEG signals, the algorithm fails to remove EEG noise from EEG waveforms. Therefore, we formulated a new method for independent sources extraction, which could pass on the time pattern from the original signals to the statistically independent components. This computational method adopted multivariable autoregression to represent the original temporal structures. All regression coefficients were estimated by least square methods. Concerning the measure of the independence, we analyzed the residuals in the autoregression model, instead of estimating source signals, by minimizing the mutual information between them, and modified the unmixing matrix by the natural gradient algorithm.

In this method, we described the time pattern of the sources by a stationary autoregression model

$$S_t = \sum_{K=1}^{P} A_K S_{t-K} + \Phi_t \tag{1}$$

in which $S_t = [S_t^1, S_t^2, \ldots, S_t^M]^T$ is a vector including M source signals, A_K stands for the regression coefficients, and $\Phi_t = [e_1(t), e_2(t), \ldots, e_M(t)]^T$ is the residual vector. Considering the course of regression coefficients estimation, (1) could be rewritten as

$$V_t = AU_t + E_t, \quad t = 1, \ldots, N, \tag{2}$$

where $A = (A_1, A_2, \ldots, A_p) \in R^{M \times M \times P}$ is the coefficient matrix. And $U_t = (S_{t-1}, \ldots, S_{t-p})^T \in R^{M \times P}$, $V_t = S_t$. Then (2) approximates a multilinear regression model. That meant that we could take P values in the source signals before t time point as a time-sampling to be an independent variable of the linear system and the value at t time point as a predicted value to the dependent variable accordingly.

The assumption which was important to the least squares estimation method used in linear regression analysis required residuals to have the statistic characteristics $e \sim N_M(O_{M \times 1}, \sigma^2{}_{M \times M})$. When e_i kept statistical independence from others, the linear system had normal random

Table 1: The correspondence between motor imagery, object control command, and game effect.

Motor imagery	Control command	3D Tetris coordinate
Foot motion	Moving to Foot Plane	Positive y-axis
Tongue motion	Moving to Tongue Plane	Negative y-axis
Left hand motion	Moving to Left Plane	Positive x-axis
Right hand motion	Moving to Right Plane	Negative x-axis

distribution. So there was no serial correlation between all independent variables, expressed as

$$E(e_i) = 0,$$
$$\operatorname{cov}(e_i, e_j) = \begin{cases} \sigma^2, & i = j \\ 0, & i \neq j, \end{cases} \quad (3)$$
$$i, j = 1, 2, \ldots, M.$$

Based on this equivalence relationship, the correlation among all independent components in the temporal model was measured with minimization of mutual information.

(2) One-versus-Rest CSP. The next step is common spatial pattern (CSP) extraction. The procedure discussed above explains our approach to temporal feature extraction. We aimed to find an algorithm for spatial feature discovery, which could use ICA components as inputs. The main trick in the binary case is that the CSP algorithm yields a simultaneous diagonalization of both covariance matrices whose eigenvalues sum to one. We adopted a CSP method termed one-versus-rest (OVR), which enabled the CSP in the ordinary sense to handle a multiclassification problem. In this algorithm, each model corresponding to one kind of MI would produce a spatial filter versus other models. The details of the CSP algorithm are in Appendix.

In order to compare the multifeature extraction to traditional CSP, we define two computation processes. First, we let the feature components be the processing objects of the CSP spatial filter directly. The spatial features obtained in this way are called cspW_Data. Second, we let the feature components go through the independent component analysis and then used CSP spatial filtering to process those independent components. The spatial features obtained with the method of multifeature extraction were called cspW_IC. By comparing the quantitative differences between spatial feature cspW_Data and cspW_IC, we tried to demonstrate the effectiveness of the method of multifeature extraction.

2.4.3. Classification. In this work, we used the small world neural network (SWNN), discussed in previous research [42], as the classifier. The SWNN was constructed based on a multilayered feedforward perception model, with the weight adjustment mechanism involving both backpropagation and cutting and rewiring connections. The SWNN included one input layer, one output layer, and 10 hidden layers with eight neurons in each hidden layer. The dimension of a given CSP feature determined the number of neurons in the input layer. The output layer contained four neurons. We assigned the hard-limit transfer function [43] to the output layer, which made the SWNN output a 4-bit gray code (right hand motor imagery: 0001, light hand motor imagery: 0010, foots motor imagery: 0100, and tongue motor imagery: 1000).

During classifier training, we defined four 4-bit gray codes to stand for the four kinds of motor imagery. If the SWNN produced a 4-bit gray code different from the four desired ones, we defined this brain state as idle. There was no "idle" data collected in the MI training phase, but players would exhibit idle states during game playing. The features extracted from idle state data would not produce a 4-bit gray code to be one of the four predefined ones.

2.5. Control Strategy. In the original 3D Tetris game, the coordinate system of the 3D space and the local coordinate system of the block group were predefined. So the BCI system just took advantage of the original definition of the coordinate systems to adjust the movement and rotation of the block groups. In the proposed control strategy, the BCI system recognized the player's mental states (four kinds of motor imagery) and translated them into control commands. The correspondence between MI and control command was determined in the procedure of secondary development of 3D Tetris (Table 1).

In addition, two kinds of blink detected from EOG recordings yielded rotation commands for block group control. The block group could be rotated about the x-axis, y-axis, and z-axis in block group coordinate. We used a double blink to alternate the rotation axis in an X-Y-Z loop, and used a single blink to rotate the block group about a given axis. We adopted the theory of behavior-based control to construct the interactive logic. The part of movement and speed control was described as a finite-state automaton (FSA). We interpreted the FSA as a 5-tuple:

$$M = (Q, \Sigma, \delta, q, F), \quad (4)$$

where Q was a set of states, q was a set of initial (or starting) states, F was a set of final states, Σ was the input alphabet (a finite, nonempty set of symbols), and δ was a partial mapping $\delta(q_t, P(t, T_i)) \rightarrow q_{t+1}$ denoting transitions (Table 2).

The block group descended at a constant speed in the 3D game space. Players used mentally generated control to move and rotate the block groups in two dimensions. During the BCI game, V_c meant the current speed of block group, which was the vector sum of x-axis and y-axis velocities, ΔV^X was the unit increment of speed about x-axis, $V_c + \Delta V^X$ meant that the speed of the block group increased in direction of the x-axis, $V_c - \Delta V^X$ meant the speed of the block group decreased

Table 2: State transition for movement and speed control.

Input	Current state					
	Start/$V_c = 0$	$V_c + \Delta V^x$	$V_c - \Delta V^x$	$V_c + \Delta V^Y$	$V_c - \Delta V^Y$	N_B
Left	$V_c + \Delta V^x$		$V_c + \Delta V^x$	$V_c + \Delta V^x$	$V_c + \Delta V^x$	
Right	$V_c - \Delta V^x$	$V_c - \Delta V^x$		$V_c - \Delta V^x$	$V_c - \Delta V^x$	
Tongue	$V_c - \Delta V^Y$	$V_c - \Delta V^Y$	$V_c - \Delta V^Y$	$V_c - \Delta V^Y$		
Foot	$V_c + \Delta V^Y$	$V_c + \Delta V^Y$	$V_c + \Delta V^Y$		$V_c + \Delta V^Y$	
$P_=$		$V_c + \Delta V^x$	$V_c - \Delta V^x$	$V_c + \Delta V^Y$	$V_c - \Delta V^Y$	
P_+		$V_c + \Delta V^x$	$V_c - \Delta V^x$	$V_c + \Delta V^Y$	$V_c - \Delta V^Y$	
P_- && $V_c > 0$		$V_c + \Delta V^x$	$V_c - \Delta V^x$	$V_c + \Delta V^Y$	$V_c - \Delta V^Y$	
Touch	$V_c = 0$	$V_c = 0$	$V_c = 0$	$V_c = 0$	$V_c = 0$	$V_c = 0$
Fallen		N_B	N_B	N_B	N_B	
Cross	Reset	Reset	Reset	Reset	Reset	Reset
Null						$V_c = 0$

in direction of the x-axis, and ΔV^Y had the same function in speed adjustment with respect to the y-axis. Start was the initial state of all control. Once a new block group appeared at the top of 3D space, the FSA turned to the state N_B (New Block group). So the set of states was $\{V_c + \Delta V^X, V_c - \Delta V^X, V_c + \Delta V^Y, V_c - \Delta V^Y, V_c = 0$, Start, N_B, Reset$\}$.

We defined the alphabet Σ as $\{P_=, P_+, P_-\&\&V_c > 0$, Cross, Fallen, Touch, Null, ton, foot, left, right$\}$. Definitions of these symbols are as follows: $P_=$ meant that the number of a given MI category detected from the EEG within one second (unit time) did not change; P_+ meant that the number increased; P_- && $V_c > 0$ meant that the number decreased and the current speed was more than zero. There were 20 vertical layers in 3D space. Event outcomes were coded as follows: if the block groups overflowed from 3D space, the Cross outcome turned the FSA to Reset. The code, ton, meant that the FSA received the recognition result, "MI of tongue motion," as a signal for a state transition. The code, foot, corresponded to "MI of foot motion." Respectively, left corresponded to "MI of left hand motion" and right corresponded to "MI of right hand motion." There were four outcome codes: the Touch code meant the Block group touched one of the four standing planes of the 3D game space, while Fallen meant the Block group touched the bottom plane of the 3D space. Cross denoted that the block groups filled the 3D space; then the FSA turned to Reset. NULL meant that the FSA did not receive any directional control commands.

3. Results

3.1. Characteristic Components. Through the preprocessing of motor imagery training data, we picked up the most suitable characteristic components for the classification of motor imagery described in Table 3. Take Player 1, for example, the characteristic components came from electrode Cz in the 8–12 Hz frequency band, electrode C3 in the 12–16 Hz frequency band, electrode Fz in the 14–16 Hz frequency band, electrode F4 in the 20–22 Hz frequency band, and electrode T7 in the 24–26 Hz frequency band. After gaining all players characteristic components, we carried out filtering operation as Table 3 for preprocessed EEG data. The selected characteristic components would be used in offline algorithm training.

3.2. Multifeature Extraction. We took Player 1 as example to interpret the output of the verification program (Figure 5), and illustrate how the proposed ICA (retaining the temporal structure of EEG signals) impacted common spatial features positively.

The CSP spatial filters trained from two kinds of components were called cspW_Data and cspW_IC, respectively. The lower left part of Figure 5 illustrates the quantitative difference between the first and last feature components extracted from cspW_Data. The mean quantitative difference relevant to the motor imagery of foot was 0.78×10^{-18}, and it was 1.26×10^{-18} relevant to the motor imagery of left hand. The lower right part illustrates the difference between the first and last feature components extracted from cspW_IC. The mean quantitative difference relevant to the motor imagery of foot was 0.51×10^{-12}, and it was 1.97×10^{-12} relevant to the motor imagery of left hand. For Player 1, compared from the angle of order of magnitude, cspW_IC produced more prominent quantitative differences between spatial features extracted from two kinds of motor imagery signals.

3.3. Pattern Discrimination. To verify the effectiveness of EEG features extracted by multifeature extraction, we compared the performances on EEG data for each player among SWNN, RBF neural network, BP neural network, and least squares support vector machines (LS-SVM) techniques. The average accuracy or error rate was over 10 runs of the 10×10-fold cross-validation procedure. We implemented the LS-SVM multiclass with one versus one decomposition strategy, using MATLAB (ver. 7.7, R2009b) using the LS-SVMlab toolbox (Version 1.8). The details about parameter setting for these three algorithms and algorithm toolboxes using are in the literature (Table 4) [44].

3.4. Control Task. In the control task, ten players were divided into two equal sized groups. One group (Group S) experienced the traditional asynchronous BCI paradigm. The other group (Group 3D) experienced the 3D Tetris paradigm.

Table 3: The frequencies and electrodes of all feature components.

Player	Electrode	Frequency	[R^2: mean ± var]
Player 1	Cz	8–12 Hz	[0.49 ± 0.024]
	C3	12–16 Hz	[0.48 ± 0.032]
	Fz	14–16 Hz	[0.35 ± 0.03]
	F4	20–22 Hz	[0.26 ± 0.022]
	T7	24–26 Hz	[0.23 ± 0.032]
Player 2	C4	16–20 Hz	[0.49 ± 0.03]
	Cz	20–24 Hz	[0.38 ± 0.025]
	C3	24–26 Hz	[0.32 ± 0.031]
	F4	10–12 Hz	[0.30 ± 0.042]
	T3	24–28 Hz	[0.22 ± 0.02]
Player 3	C4	16–18 Hz	[0.43 ± 0.024]
	Cz	20–24 Hz	[0.42 ± 0.04]
	C3	26–28 Hz	[0.40 ± 0.048]
	P3	18–22 Hz	[0.37 ± 0.01]
	Pz	10–18 Hz	[0.32 ± 0.024]
Player 4	C4	20–16 Hz	[0.49 ± 0.024]
	F3	12–10 Hz	[0.37 ± 0.01]
	C3	20–22 Hz	[0.32 ± 0.01]
	T3	22–26 Hz	[0.32 ± 0.022]
	Cz	14–16 Hz	[0.26 ± 0.024]
Player 5	Cz	10–14 Hz	[0.58 ± 0.062]
	F3	18–22 Hz	[0.37 ± 0.050]
	C4	20–24 Hz	[0.37 ± 0.075]
	T7	8–14 Hz	[0.34 ± 0.700]
	C3	10–14 Hz	[0.21 ± 0.062]
Player 6	C4	12–16 Hz	[0.47 ± 0.022]
	Cz	20–24 Hz	[0.36 ± 0.032]
	Fz	24–26 Hz	[0.36 ± 0.059]
	C3	8–16 Hz	[0.35 ± 0.03]
	F7	22–24 Hz	[0.3 ± 0.042]
Player 7	Cz	10–12 Hz	[0.52 ± 0.062]
	Pz	20–26 Hz	[0.44 ± 0.070]
	C4	22–24 Hz	[0.33 ± 0.055]
	C3	10–14 Hz	[0.31 ± 0.700]
	T8	10–12 Hz	[0.28 ± 0.062]
Player 8	C4	16–22 Hz	[0.49 ± 0.03]
	Cz	20–24 Hz	[0.48 ± 0.042]
	Pz	20–24 Hz	[0.44 ± 0.032]
	Fz	16–22 Hz	[0.44 ± 0.031]
	F4	10–18 Hz	[0.37 ± 0.05]
Player 9	C4	18–24 Hz	[0.55 ± 0.03]
	Cz	22–28 Hz	[0.52 ± 0.01]
	C3	24–28 Hz	[0.38 ± 0.032]
	Pz	18–22 Hz	[0.42 ± 0.03]
	P3	22–26 Hz	[0.33 ± 0.01]
Player 10	Fz	10–18 Hz	[0.43 ± 0.024]
	C3	18–22 Hz	[0.42 ± 0.04]
	T4	24–28 Hz	[0.41 ± 0.048]
	C4	26–28 Hz	[0.32 ± 0.01]
	F3	10–14 Hz	[0.32 ± 0.024]

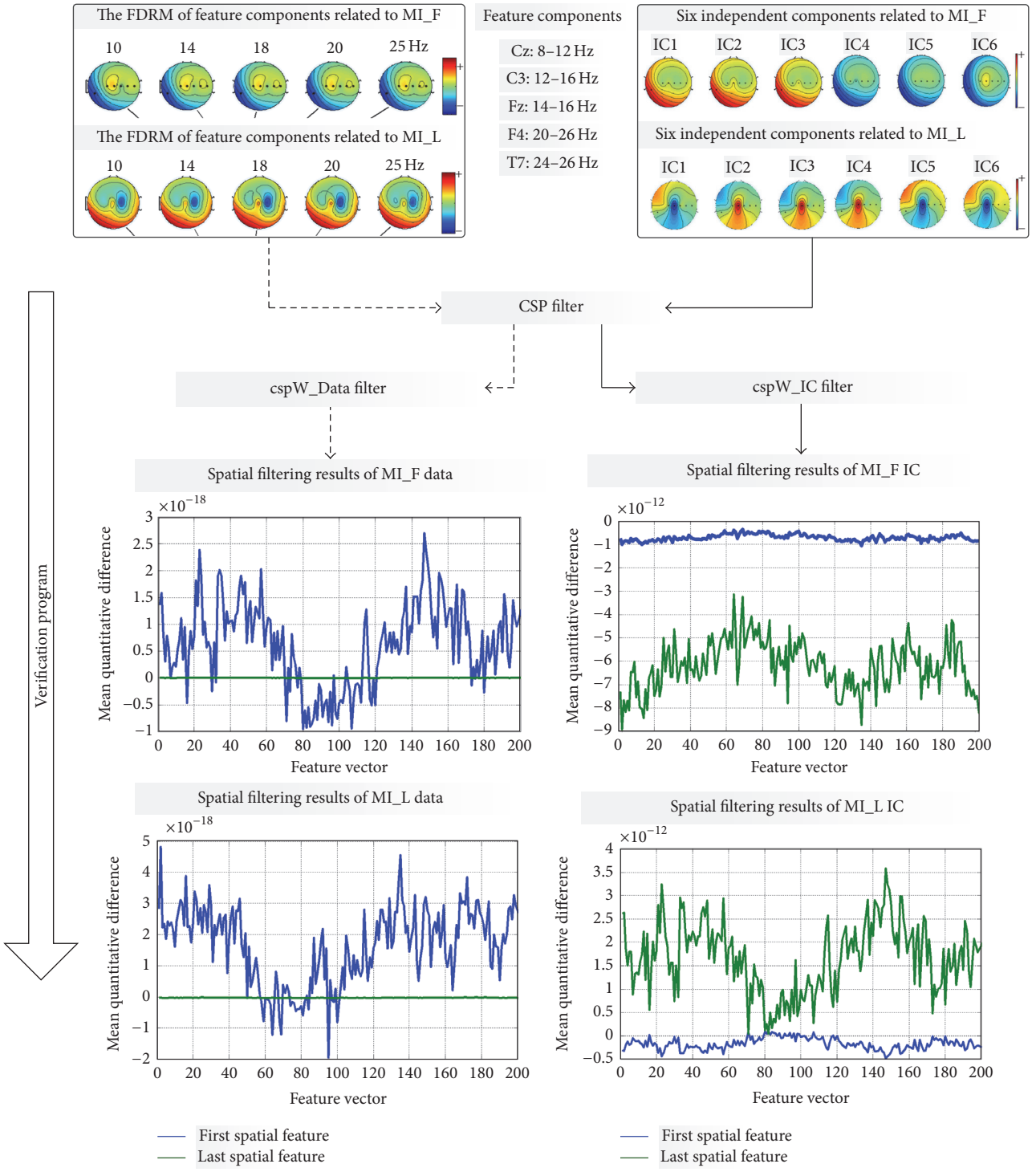

FIGURE 5: Comparisons of results from cspW_Data and cspW_IC. The upper left part is the frequency domain relief topographic map (FDRM) of feature components relevant to the motor imagery of foot (MI_F) and left hand (MI_L). The upper right part is the frequency domain relief map of independent components relevant to the motor imagery of foot and left hand.

Group S contained Player 1 (S1), Player 2 (S2), Player 3 (S3), Player 4 (S4), and Player 5 (S5). Group 3D contained Player 6 (3D_1), Player 7 (3D_2), Player 8 (3D_3), Player 9 (3D_4), and Player 10 (3D_5). All players went through the given paradigm for 10 runs in one day. The control task lasted ten days.

For Game-BCI 3D Tetris, the rules and mechanisms were described in Sections 2.3.2 and 2.5. A single run in this pattern

Table 4: The mean accuracy of classification from four classifiers based *on two kinds* of feature extraction.

	SWNN (mean)		RBF (mean)		BP (mean)		LS-SVM (mean)	
	cspW_Data	cspW_IC	cspW_Data	cspW_IC	cspW_Data	cspW_IC	cspW_Data	cspW_IC
Player 1	87.10	86.6	78.61	85.2	82.74	80.6	68.37	72.0
Player 2	79.66	82.9	72.11	74.72	75.90	77.5	71.64	68.0
Player 3	65.29	74.0	83.67	76.1	62.37	72.8	67.20	72.2
Player 4	76.40	76.4	66.81	67.51	59.31	71.2	71.59	70.4
Player 5	60.80	63.6	59.72	53.92	61.54	63.3	58.20	59.4
Player 6	74.60	78.5	66.27	77.2	54.87	74.6	62.81	67.5
Player 7	56.30	76.3	49.52	74.97	72.10	69.6	52.61	60.1
Player 8	66.94	81.3	49.83	79.30	53.30	72.8	57.22	62.0
Player 9	72.13	77.45	65.81	73.62	65.26	77.3	63.70	68.95
Player 10	71.16	83.6	50.6	82.0	57.0	75.1	59.77	74.7
Mean	71.03	***78.7***	64.3	***74.5***	64.4	***73.5***	63.3	***67.5***
P value	**0.008**		**0.042**		**0.038**		**0.019**	

The classification results from four classifiers indicated that cspW_IC produced more quality features than cspW_Data. To investigate the statistical significance of the accuracies, we performed an analysis of variance (ANOVA) on each player's result based on all classification accuracies (10 runs of the 10 × 10-fold cross-validation procedure). The *P*-value from SWNN was 0.008, 0.042 from RBF neural network, 0.038 from BP neural network, and 0.019 from LS-SVM. These *P*-values were less than 0.05 for all players, which indicated that the difference was significant.

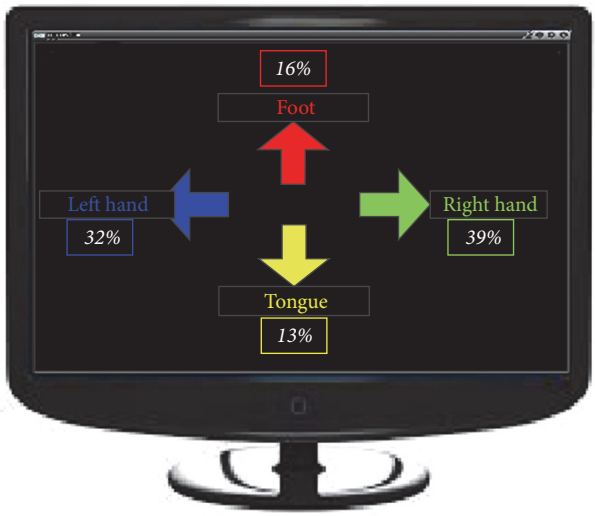

Figure 6: Screen Game Scene.

started from player's Start command by pressing the button "Game Start." Once the state of Cross occurred, the single run ended. If, during a given run, the player made one layer of Block-heap disappear, the player scored one point. The player's final score for a given test day was the average score over 10 runs. We used the daily scores as the evaluation criterion of the player's spontaneous ERD production ability.

The traditional asynchronous BCI paradigm used as contrast experiment in this paper was called the Screen Game; it ran in a 2D environment (Figure 6). We collected EEG recordings as described in Section 2.2. The calculation flow of EEG signal processing started from preprocessing steps mentioned in Section 2.4. With multifeature extraction, CSP spatial filtering used the independent components as inputs. The classifier was SWNN. Here, no control strategy functioned in the game. The feedback of one kind of motor imagery was shown on the screen as a percentage number, which was the ratio of its frequency of occurrence to the total number of times during certain time period (the average amount of time taken to complete 3D Tetris single run). The objective of this game was for players to produce ERD features to balance four percentage numbers relevant to different motor imagery categories. The standard deviation of these four percentage numbers was the evaluation criterion. Decreasing standard deviations across days indicated improvement.

3.4.1. Significance Analysis of ERD/ERS. Just as prior knowledge of the physiological processes underlying motor imagery does, hand motor imagery will stimulate the electroactivities focusing on contralateral regions over the motor cortex area containing Mu or Beta event-related desynchronization (ERD) and ipsilateral event-related synchronization (ERS) activity. Both ERD and ERS patterns localizing in the midcentral or parietal area are significant for the foot motor imagery. Otherwise, only ERS activity in this area is sufficiently dominant for tongue motor imagery [44]. With two different experimental paradigms and EEG calculating processes, we extracted ERD/ERS features related to MI. Using the EEG power spectrum in the idle state as the benchmark, we compared the mean quantitative differences between idle state and MI (Figure 7).

In Figure 7, each line represents a single player: left column, Screen Game (2D) environment; right column, 3D Tetris environment. Each point is the mean performance on a given day and each line represents the overall trend of the mean numerical differences over 10 training days.

We performed a 2 (groups: Group S, Group 3D) × 10 (test days) two-way ANOVA, with repeated measures over day, on

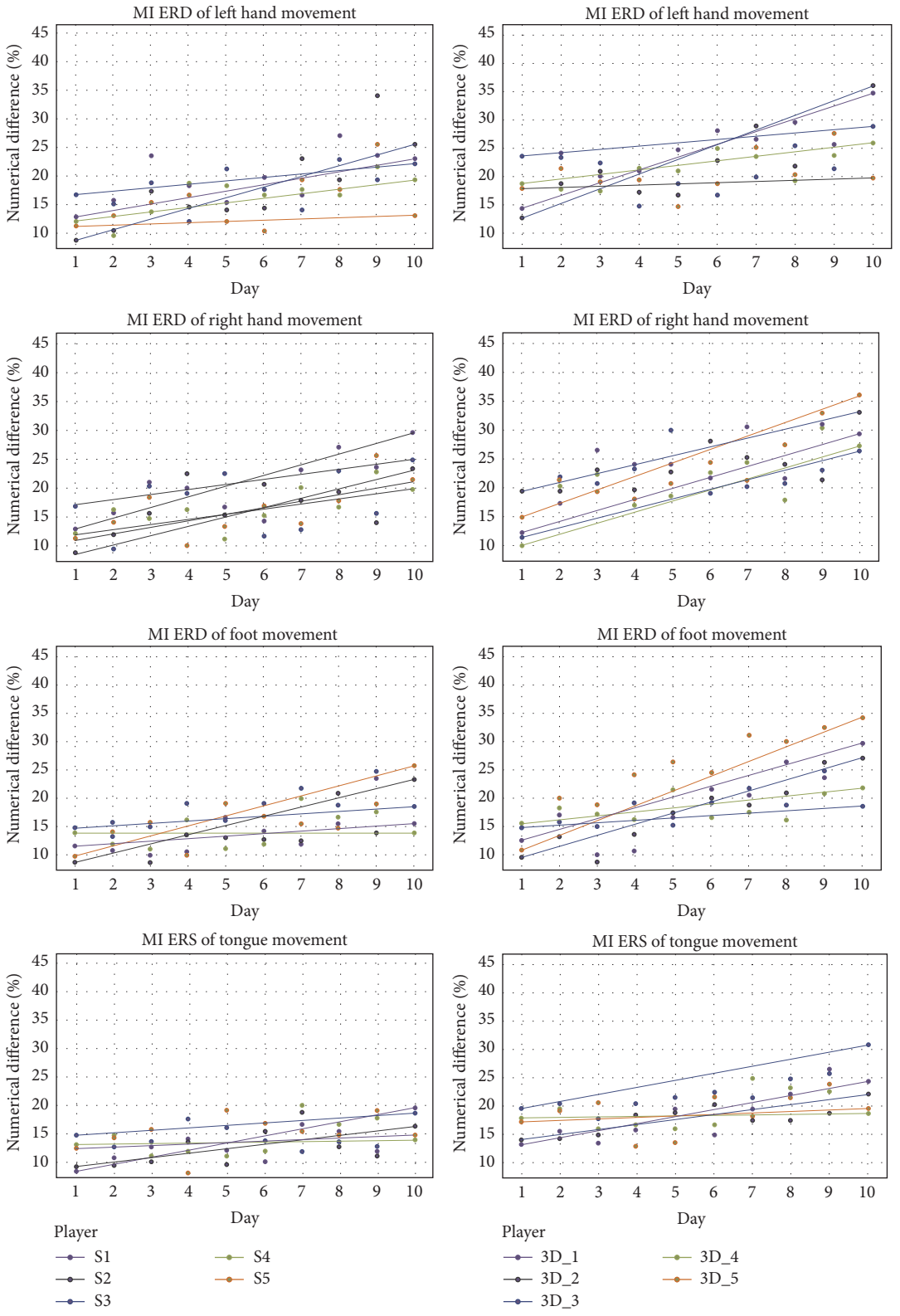

Figure 7: ERD/ERS produced by players in the two games used in the experiment across 10 test days.

Table 5: The details of the 3D Tetris Game-BCI experiment.

	3D_1		3D_2		3D_3		3D_4		3D_5	
	S_I	S_ II	S_I	S_II	S_I	S_II	S_I	S_II	S_I	S_II
Number of right hand MI	52	76	32	83	89	173	87	183	72	176
Number of left hand MI	41	33	25	95	82	116	95	106	68	188
Number of Foots MI	38	44	47	66	71	105	114	127	92	109
Number of Tongue MI	21	35	22	56	79	119	73	98	64	124
Single blink EOG	33	40	30	46	36	70	52	62	42	77
Double blink EOG	47	49	26	34	18	26	18	19	12	21
Number of Block	31	96	48	102	51	132	74	101	42	94
Mean Duration of a run	477 s	1440 s	720 s	1530 s	754 s	1980 s	1260 s	1710 s	630 s	1880 s

these quantitative differences. The main effect for days was significant, $F = 2.427$, $P < 0.005$, but the main effect for groups was not significant, $F = 0.850$, $P = 0.207$. There was a statistically significant group × day interaction, $F = 3.643$, $P = 0.014$. A simple main effects test for days occurred for Group S subjects, $F = 4.213$, $P = 0.0584$; Tukey's HSD test for multiple comparisons revealed significant improvement in ERD values between day 1 and day 4 ($P = 0.0427$) and increasing tendency among day 4 and day 10 ($P = 0.074$). A simple main effect for days was also found for Group 3D players, $F = 7.302$, $P = 0.012$. Tukey's HSD test for multiple comparisons revealed significant improvement in ERD values between day 1 and day 4 ($P = 0.026$) and increasing tendency among day 4 and day 10 ($P = 0.003$).

In order to investigate the impact of individual variability on the effect of ERD/ERS, we applied Welch's t-test on the ERD/ERS quantitative differences of individual players in Groups S and 3D between day 1 and day 10. We found that three players in Group 3D showed statistically significant improvements, $P = 0.02$, $P < 0.05$, and $P < 0.001$. No subjects showed statistical significance in Group S. After 10 training days, the group that performed MI in the 3D Tetris environment showed significant improvement in generating MI-associated ERD/ERS compared with the group in the Screen Game environment. That result suggested that an immersive and rich-control environment for MI would improve the associated mental imagery and enhance MI-based BCI skills.

3.4.2. Game Score. In this research, though 3D Tetris brought the entirely different operating experiences to players compared to 2D Screen Game and a lot of incomparable elements existed between these two BCI paradigms, they all were the method to test the player's spontaneous ERD/ERS production ability.

In the 3D Tetris Game-BCI, the score represented the number of layers of disappearing Block-heaps. So a higher score represented a better ability to control the block objects using mind control. From training day 1 to day 4, players' scores did not show an upward trend, $P = 0.066$. However, from training day 5 to day 10, an obvious uptrend in scores appeared, $P < 0.005$ (Figure 8).

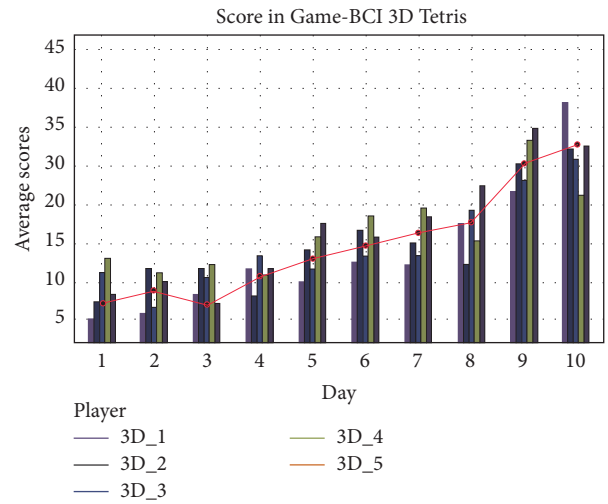

Figure 8: Distribution of players' scores from training day 1 to day 10 in 3D Tetris Game-BCI.

So we separated the 10 training days into two stages: Stage I (S_I) covered from day 1 to day 4 and Stage II (S_II) covered from day 5 to day 10. The details of the 3D Tetris Game-BCI experiment were described in Table 5. The first four rows represented the mean numbers of motor imagery commands used in two stages. The row labeled "Single blink EOG" and "Double blink EOG" meant the mean number of single blink and double blink commands used in two stages. "Number of Block" was the mean number of block groups. "Mean Duration of a run" meant how long players can remain playing. The experimental data showed that when players obtained higher scores (Stage II), they remained playing for longer. In addition, during 10 training days, the Game-BCI output one MI command in 1.43 seconds (var: ±0.028) averagely.

For the 2D Screen Game, the player's mission was to balance numbers relevant to different motor imagery categories. The score was the standard deviation of these four percentage numbers, which meant that a lower score represented better ability to generate motor imagery. However, from training day 1 to day 10, players' scores did not show an obvious downward trend, $P = 0.078$ (Figure 9).

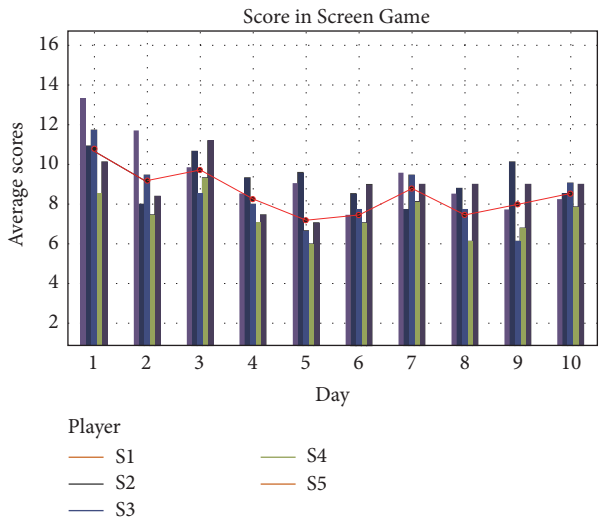

Figure 9: Distribution of players' scores from training day 1 to day 10 in Screen Game.

4. Discussion and Conclusion

In this study, we have shown that the combination of video game and BCI is a new design approach to enhance the stimulation and feedback ability of BCI systems. We implemented a Game-BCI system for 3D Tetris game playing with motor imagery indicated by EEG and blink EOG elements. We proposed and tested two key techniques, multifeature extraction and shared control, for enhancing player's BCI control ability, to demonstrate the feasibility that 3D game environment could enhance player's spontaneous ERD/ERS production ability. Taking the 2D Screen Game as a contrast, we compared the quantitative differences between spatial features extracted from motor imagery EEG collected in two experiments separately. The results of the analysis of ERD/ERS and game scores both suggested that an immersive and rich-control environment would improve user's MI ability and BCI control skills.

4.1. Multifeature Extraction. The method of multifeature extraction, combining independent component analysis and common spatial patterns, is a renovated mode for EEG feature extraction. Independent component analysis (ICA) is a standard tool for data analysis in the area of neural networks and signal processing. The typical application is blind source separation of EEG signals. In raw EEG signals, there are electrooculograms, electromyography, and other artifacts, as well as mutual interferences between signals. The most direct phenomenon is the submergence of small power components exported from other leads, when there is a large power component from a given lead. Extraction via decorrelation of independent components in a multilead time domain with mixed signals could help indicate the energy distribution of each independent component during a certain period or a special cerebral state. The identification of temporal independence is one part of EEG signal processing. Spatial features illustrate EEG expressions of various mental tasks from the perspective of time-varying features of signal energy in the whole brain. In this way, unlike the extraction of time domain features, the spatial domain emphasizes spatial correlations among original signals or among certain types of components. Instead of merely analyzing energy features of a single channel EEG signal, the algorithm considering frequency spectrum variation correlations between different channels facilitates the creation of connections between EEG feature distribution and complex mental tasks. The common spatial pattern method (CSP), based on the theory of matrix simultaneous diagonalization, involves searching for a set of spatial filters, under the effects of which the variance of one type of signal reaches a maximum and the other type of signal reaches a minimum, thereby achieving classification. Because the EEG variance within a specific frequency band is related to its signal energy, the common spatial pattern method was able to achieve optimal classification of EEG signals based on waveband energy features.

In this study, we applied a time model-based residual mutual information minimization independent source signal extraction method based on artifact elimination and characteristic component extraction of EEG signal of limb motor imagery. This method reduces the correlations components under conditions of preserving temporal structures of EEG signals and so provides clear observation of signal characteristics of each component.

To validate the efficiency of multifeature extraction, two computation processes were derived. The spatial filter cspW_Data was trained with feature components. After multifeature extraction, the spatial filter trained with independent components was called cspW_IC. The results of spatial filtering demonstrated that, compared to cspW_Data, cspW_IC could produce more prominent quantitative differences between spatial features extracted from different motor imagery signals.

4.2. 3D Tetris BCI Game. In this research, as a means to assess the utility of the MI control methodology we developed, we integrated BCI design into a 3D Tetris game. The goal was to improve the function in motor imagery training of the BCI system. This attempt follows the idea of gamification for rehabilitation highly respected frontiers. Studies under this new concept, which wants to gamify the process of rehabilitation, have gained wider attention in the rehabilitation field. For example, the Wellapets video game helps teach children how to manage asthma [45]. The social game, Keas, is the leading Health Management platform for employers [46]. The Kognito Co. developed an educational role-playing game to help parents to discuss the underage drinking problem with their children [47]. Run an Empire, a very representative augmented reality game, lets users through "running" way to create their own territory [48]. The goal of systems mentioned above is to help make rehabilitation environments more engaging and more applicable.

Rehabilitation is complex. It involves an ever-changing interaction of the rehabilitation patient with different clinical environments and healthcare providers. It has gone beyond simply creating a fun and exciting application in which to complete rehabilitation exercises and interventions. A

delicate balance of the task and the patient's abilities must be achieved. For BCI systems, the created system should be usable across experimental paradigms and at different phases in the rehabilitation training process. Sollfrank et al. [49] showed that a realistic visualization in 3D of upper and lower limb movements can amplify motor related potentials better than in 2D visualization during subsequent motor imagery. Cho and Lee [50] implemented a real-time game environment system using game player's emotional state information from the BCI sensor to raise the degree of immersion in an FPS game. Kondo and colleagues [51] investigated the effect of static and dynamic visual representations of target movements during BCI neurofeedback training, which revealed that dynamic images showed significant improvement in generating MI-associated ERD compared with static images. Belkacem et al. [52] presented real-time control of a video game with eye movements for an asynchronous and noninvasive communication system using two temporal EEG sensors. EEG-controlled gaming applications allow BCI to provide not only entertainment but also strong motivation for practicing, thereby achieving better control with rehabilitation systems.

In our research, the game part contained more of a gambling element compared to the Game-BCI system above. The 3D visual environment did not completely immerse players but felt more like an operating space. Players paid most attention in the ERD/ERS pattern generation. In order to make players feel that they were completing a complicated control mission with four motor imagery and two EOG commands, an interpretation method of physiological signal was formed based on the concept of shared control. Through evaluating the significance of ERD/ERS generation, we found that 3D Tetris Game-BCI provided an effective approach for players to enhance MI-based BCI skills. During 10 training days, the rapid growth of scoring rate appeared in the last five days. We interpret that outcome to mean that players were willing to use the 3D Tetris Game-BCI system after they mastered the needed skills. So we claim that the pattern of Game-BCI will be a tremendous advance in BCI research field.

Appendix

The algorithm called one-versus-rest (OVR) CSP is an extension of a well-known method called common spatial patterns to multiclass case, to extract signal components specific to one condition from electroencephalography (EEG) data sets of multiple conditions.

In this research, the details of the one-versus-rest CSP algorithm are as follows.

E_R, E_L, E_F, and E_T represented the matrix of independent components (temporal features) related to right hand motor imagery, left hand motor imagery, foot motor imagery, and tongue motor imagery with dimensions $N \times T$. N was the number of independent components, and T is the number of sampling points. The normalized spatial covariance of the independent source signals could be represented as C_R, C_L, C_F, and C_T. The composite spatial covariance could be factorized as

$$C_C = C_R + C_L + C_F + C_T = U_C \lambda_C U_C^T. \tag{A.1}$$

Here, U_C was the matrix of eigenvectors and λ_C was the diagonal matrix of eigenvalues. $P = \sqrt{\lambda_C^{-1}} U_C^T$ denoted the whitening transformation matrix. To see how to extract common spatial patterns specific to right hand motor imagery, let $C_R' = C_L + C_F + C_T$. Then C_R' and C_R are individually transformed as

$$\begin{aligned} S_R &= P R_R P^T, \\ S_R' &= P R_R' P^T. \end{aligned} \tag{A.2}$$

Here, S_R and S_R' share the same eigenvector and the sum of corresponding eigenvalues for two matrices is always one. It can be understood that if S_R can be factored as

$$S_R = U \Lambda_R U^T \tag{A.3}$$

then

$$S_R' = U \Lambda_R' U^T, \tag{A.4}$$

$$\Lambda_R + \Lambda_R' = I. \tag{A.5}$$

Combine (A.2), (A.3), and (A.4) and then obtain

$$\begin{aligned} \Lambda_R &= \left(P^T U\right)^T R_R \left(P^T U\right) = SF_R R_R SF_R^T \\ \Lambda_R' &= \left(P^T U\right)^T R_R' \left(P^T U\right) = SF_R R_R' SF_R^T, \end{aligned} \tag{A.6}$$

where $SF_R = U^T P$. Note that, from (A.5), it is obvious that larger eigenvectors corresponding to larger eigenvalues yield a high variance under condition "right hand motor imagery" and a low variance under other conditions (other kinds of motor imagery). With the projection matrix $W_R = U^T P$ we can get $Z_R = W_R E_R$. Repeating the procedure, we can obtain Z_L, Z_F, and Z_T.

However, the variances of only a small number m of the spatial filtered signals were used as input features for classification. The m first rows of Z_R formed the feature vector Z_I given by the equation

$$Z_I = \log\left(\frac{\operatorname{var}\left(Z_I'\right)}{\sum_{i=1}^{m} \operatorname{var}\left(Z_I'\right)}\right). \tag{A.7}$$

Conflicts of Interest

The authors declare that there are no conflicts of interest regarding the publication of this paper.

Acknowledgments

This work was supported by the State Key Laboratory for Manufacturing Systems Engineering in Xi'an Jiaotong University and the School of Computer Science in Xi'an Polytechnic University.

References

[1] K. Huotari and J. Hamari, "Defining gamification—a service marketing perspective," in *Proceedings of the 16th International Academic MindTrek Conference: "Envisioning Future Media Environments" (MindTrek '12)*, pp. 17–22, Tampere, Finland, October 2012.

[2] S. Deterding, D. Dixon, R. Khaled, and L. Nacke, "From game design elements to gamefulness: defining "gamification"," in *Proceedings of the 15th International Academic MindTrek Conference: Envisioning Future Media Environments (MindTrek '11)*, pp. 9–15, Tampere, Finland, September 2011.

[3] J. Hamari, "Transforming homo economicus into homo ludens: a field experiment on gamification in a utilitarian peer-to-peer trading service," *Electronic Commerce Research and Applications*, vol. 12, no. 4, pp. 236–245, 2013.

[4] J. Hamari, "Do badges increase user activity? A field experiment on the effects of gamification," *Computers in Human Behavior*, vol. 71, pp. 469–478, 2017.

[5] G. Zichermann, *Gamification by Design: Implementing Game Mechanics in Web and Mobile Apps*, O'Reilly Media, Sebastopol, Calif, USA, 1st edition, 2011.

[6] J. Hamari and J. Koivisto, "'Working out for likes': an empirical study on social influence in exercise gamification," *Computers in Human Behavior*, vol. 50, pp. 333–347, 2015.

[7] The Speed Camera Lottery. The Fun Theory.

[8] https://en.wikipedia.org/wiki/Gamification.

[9] "FANGO delivers on Social TV," Impulse Gamer, 2012.

[10] K. Adam, "HOW TO: Gamify Your Marketing," Mashable, 2011.

[11] D. Takahashi, "Website builder DevHub gets users hooked by 'gamifying' its service," VentureBeat, 2010.

[12] O. Toubia, "Idea generation, creativity, and incentives," *Marketing Science*, vol. 25, no. 5, pp. 411–425, 2006.

[13] C. Lister, J. H. West, B. Cannon, T. Sax, and D. Brodegard, "Just a fad? Gamification in health and fitness apps," *JMIR Serious Games*, vol. 2, no. 2, article e9, 2014.

[14] J. Markoff, "In a video game, tackling the complexities of protein folding," *The New York Times*, 2010.

[15] The Gamification of Education. Knewton.

[16] S. De Sousa Borges, V. H. S. Durelli, H. M. Reis, and S. Isotani, "A systematic mapping on gamification applied to education," in *Proceedings of the 29th Annual ACM Symposium on Applied Computing (SAC '14)*, pp. 216–222, March 2014.

[17] https://en.wikipedia.org/wiki/Brain%E2%80%93computer_interface.

[18] T. Hanakawa, "Organizing motor imageries," *Neuroscience Research*, vol. 104, pp. 56–63, 2016.

[19] A. Schlögl, F. Lee, H. Bischof, and G. Pfurtscheller, "Characterization of four-class motor imagery EEG data for the BCI-competition 2005," *Journal of Neural Engineering*, vol. 2, no. 4, pp. L14–L22, 2005.

[20] J. Li, H. Ji, L. Cao, R. Gu, B. Xia, and Y. Huang, "Wheelchair control based on multimodal brain-computer interfaces," in *Neural Information Processing*, vol. 8226, pp. 434–444, Springer, New York, NY, USA, 2013.

[21] J. Winters, "Just short of telepathy: can you interact with the outside world if you can't even blink an eye?" *Psychology Today*, vol. 36, no. 3, p. 44, 2003.

[22] L. A. Farwell and E. Donchin, "Talking off the top of your head: toward a mental prosthesis utilizing event-related brain potentials," *Electroencephalography and Clinical Neurophysiology*, vol. 70, no. 6, pp. 510–523, 1988.

[23] E. Yin, Z. Zhou, J. Jiang, Y. Yu, and D. Hu, "A dynamically optimized SSVEP brain-computer interface (BCI) speller," *IEEE Transactions on Biomedical Engineering*, vol. 62, no. 6, pp. 1447–1456, 2015.

[24] H. Yuan, T. Liu, R. Szarkowski, C. Rios, J. Ashe, and B. He, "Negative covariation between task-related responses in alpha/beta-band activity and BOLD in human sensorimotor cortex: an EEG and fMRI study of motor imagery and movements," *NeuroImage*, vol. 49, no. 3, pp. 2596–2606, 2010.

[25] B. Allison, B. Graimann, and A. Gräser, "Why use a BCI if you are healthy," in *Proceedings of the Brain-Computer Interfaces and Games Workshop at ACE (Advances in Computer Entertainment) (BRAINPLAY '07)*, Salzburg, Austria, June 2007.

[26] J. B. F. Van Erp, F. Lotte, and M. Tangermann, "Brain-computer interfaces: beyond medical applications," *Computer*, vol. 45, no. 4, Article ID 6165246, pp. 26–34, 2012.

[27] https://en.wikipedia.org/wiki/Motor_imagery.

[28] D. Marshall, D. Coyle, S. Wilson, and M. Callaghan, "Games, gameplay, and BCI: the state of the art," *IEEE Transactions on Computational Intelligence and AI in Games*, vol. 5, no. 2, pp. 82–99, 2013.

[29] E. C. Lalor, S. P. Kelly, C. Finucane et al., "Steady-state VEP-based brain-computer interface control in an immersive 3D gaming environment," *EURASIP Journal on Advances in Signal Processing*, vol. 2005, no. 19, Article ID 706906, pp. 3156–3164, 2005.

[30] E. C. Lalor, S. P. Kelly, C. Finucane et al., "Steady-state VEP-based brain-computer interface control in an immersive 3D gaming environment," *EURASIP Journal on Applied Signal Processing*, vol. 2005, no. 19, pp. 3156–3164, 2005.

[31] M. W. Tangermann, M. Krauledat, K. Grzeska et al., "Playing pinball with non-invasive BCI," in *Proceedings of the 22nd Annual Conference on Neural Information Processing Systems (NIPS '08)*, vol. 21, pp. 1641–1648, December 2008.

[32] B. Reuderink, A. Nijholt, and M. Poel, "Affective Pacman: a frustrating game for brain-computer interface experiments," in *Intelligent Technologies for Interactive Entertainment*, vol. 9 of *Lecture Notes of the Institute for Computer Sciences, Social Informatics and Telecommunications Engineering*, pp. 221–227, Springer, Berlin, Germany, 2009.

[33] G. Pires, M. Torres, N. Casaleiro, U. Nunes, and M. Castelo-Branco, "Playing Tetris with non-invasive BCI," in *Proceedings of the IEEE 1st International Conference on Serious Games and Applications for Health, (SeGAH '11)*, pp. 1–6, Braga, Portugal, November 2011.

[34] B. Van de Laar, H. Gürkök, D. Plass-Oude Bos, M. Poel, and A. Nijholt, "Experiencing BCI control in a popular computer game," *IEEE Transactions on Computational Intelligence and AI in Games*, vol. 5, no. 2, pp. 176–184, 2013.

[35] B. Z. Allison, J. Jin, Y. Zhang, and X. Wang, "A four-choice hybrid P300/SSVEP BCI for improved accuracy," *Brain-Computer Interfaces*, vol. 1, no. 1, pp. 17–26, 2014.

[36] M. Wang, I. Daly, B. Z. Allison et al., "A new hybrid BCI paradigm based on P300 and SSVEP," *Journal of Neuroscience Methods*, vol. 244, pp. 16–25, 2015.

[37] E. Yin, T. Zeyl, R. Saab, D. Hu, Z. Zhou, and T. Chau, "An auditory-tactile visual saccade-independent P300 brain-computer interface," *International Journal of Neural Systems*, vol. 26, no. 1, Article ID 1650001, 2016.

[38] E. Yin, T. Zeyl, R. Saab, T. Chau, D. Hu, and Z. Zhou, "A hybrid brain—computer interface based on the fusion of P300

and SSVEP scores," *IEEE Transactions on Neural Systems and Rehabilitation Engineering*, vol. 23, no. 4, pp. 693–701, 2015.

[39] https://en.wikipedia.org/wiki/3D_Tetris.

[40] http://www.bci2000.org/wiki/index.php/-User_Tutorial:Analyzing_the_Initial_Mu_Rhythm_Session.

[41] G. Pfurtscheller, C. Brunner, A. Schlögl, and F. H. Lopes da Silva, "Mu rhythm (de)synchronization and EEG single-trial classification of different motor imagery tasks," *NeuroImage*, vol. 31, no. 1, pp. 153–159, 2006.

[42] T. Li, J. Hong, J. Zhang, and F. Guo, "Brain-machine interface control of a manipulator using small-world neural network and shared control strategy," *Journal of Neuroscience Methods*, vol. 224, pp. 26–38, 2014.

[43] http://cn.mathworks.com/help/nnet/ref/hardlim.html?requestedDomain=www.mathworks.com.

[44] S. Siuly, Y. Li, and P. P. Wen, "Clustering technique-based least square support vector machine for EEG signal classification," *Computer Methods and Programs in Biomedicine*, vol. 104, no. 3, pp. 358–372, 2011.

[45] http://www.wellapets.com.

[46] http://keas.com.

[47] http://www.kognito.com/products/.

[48] http://www.runanempire.com/.

[49] T. Sollfrank, D. Hart, R. Goodsell, J. Foster, and T. Tan, "3D visualization of movements can amplify motor cortex activation during subsequent motor imagery," *Frontiers in Human Neuroscience*, vol. 9, article 463, 2015.

[50] O.-H. Cho and W.-H. Lee, "BCI sensor based environment changing system for immersion of 3D game," *International Journal of Distributed Sensor Networks*, vol. 2014, Article ID 620391, 8 pages, 2014.

[51] T. Kondo, M. Saeki, Y. Hayashi, K. Nakayashiki, and Y. Takata, "Effect of instructive visual stimuli on neurofeedback training for motor imagery-based brain-computer interface," *Human Movement Science*, vol. 43, pp. 239–249, 2015.

[52] A. N. Belkacem, S. Saetia, K. Zintus-Art et al., "Real-time control of a video game using eye movements and two temporal EEG sensors," *Computational Intelligence and Neuroscience*, vol. 2015, Article ID 653639, 10 pages, 2015.

Hindawi
Computational Intelligence and Neuroscience
Volume 2017, Article ID 1323985, 9 pages
https://doi.org/10.1155/2017/1323985

Research Article

Comparison of the BCI Performance between the Semitransparent Face Pattern and the Traditional Face Pattern

Jiao Cheng, Jing Jin, and Xingyu Wang

Key Laboratory of Advanced Control and Optimization for Chemical Processes, Ministry of Education, East China University of Science and Technology, Shanghai, China

Correspondence should be addressed to Jing Jin; jinjingat@gmail.com

Received 18 October 2016; Revised 26 January 2017; Accepted 16 March 2017; Published 9 April 2017

Academic Editor: Mikhail A. Lebedev

Brain-computer interface (BCI) systems allow users to communicate with the external world by recognizing the brain activity without the assistance of the peripheral motor nervous system. P300-based BCI is one of the most common used BCI systems that can obtain high classification accuracy and information transfer rate (ITR). Face stimuli can result in large event-related potentials and improve the performance of P300-based BCI. However, previous studies on face stimuli focused mainly on the effect of various face types (i.e., face expression, face familiarity, and multifaces) on the BCI performance. Studies on the influence of face transparency differences are scarce. Therefore, we investigated the effect of semitransparent face pattern (STF-P) (the subject could see the target character when the stimuli were flashed) and traditional face pattern (F-P) (the subject could not see the target character when the stimuli were flashed) on the BCI performance from the transparency perspective. Results showed that STF-P obtained significantly higher classification accuracy and ITR than those of F-P ($p < 0.05$).

1. Introduction

Brain-computer interface (BCI) is a technology that allow users to communicate with others or control external devices via brain activity alone [1–3]. BCI directly measures brain activities usually based on electroencephalography (EEG) recorded noninvasively through electrodes placed on the surface of the head [4]. The intention of users can be recognized by analyzing the EEG signals of various mental tasks [5, 6] which can help these users directly control external devices through brain activities.

P300-based BCI is one of the most common used BCI systems presented by Farwell and Donchin [7], and this system uses the flash letter pattern. Over the past two decades, the "flash only" paradigm in which the target reverses color or is briefly masked by a solid box [8] is usually used as stimulus to elicit P300 potentials. However, recent studies are focused mostly on a new stimulus that the target is overlapped with a famous face. Such stimuli actually yield better performance compared with the conventional flash only pattern through numerous experiments [8–12]. This result is due to that the face stimuli can elicit other event-related potential (ERP) components not restricted to the P300 components (such as vertex positive potential (VPP), N170, N200, and N400), and these potentials also contribute to the classification accuracy. Zhang et al. [11, 12] reported that VPP and N170 can help improve classification accuracy with stimuli that change to faces. Jin et al. [8, 9, 13] also reported that N400 significantly contributes to improving the classification accuracy in ERP-based BCI system. Currently, a variety of face patterns have been proposed by numerous researchers. Jin et al. [8, 10] presented various types of face paradigms (neutral face, smiling face, shaking neutral face, and shaking smiling face paradigms) and compared multifaces using various familiar faces with single faces. The results indicated that the performance of the ERP-based BCI is enhanced by these face stimuli. Kaufmann et al. [9] introduced face stimuli transparently superimposed on characters in comparison with the flash pattern. Their result showed that such stimuli can generate higher ERP amplitudes and obtain higher classification accuracy than those of the flash letter pattern. However, previous studies

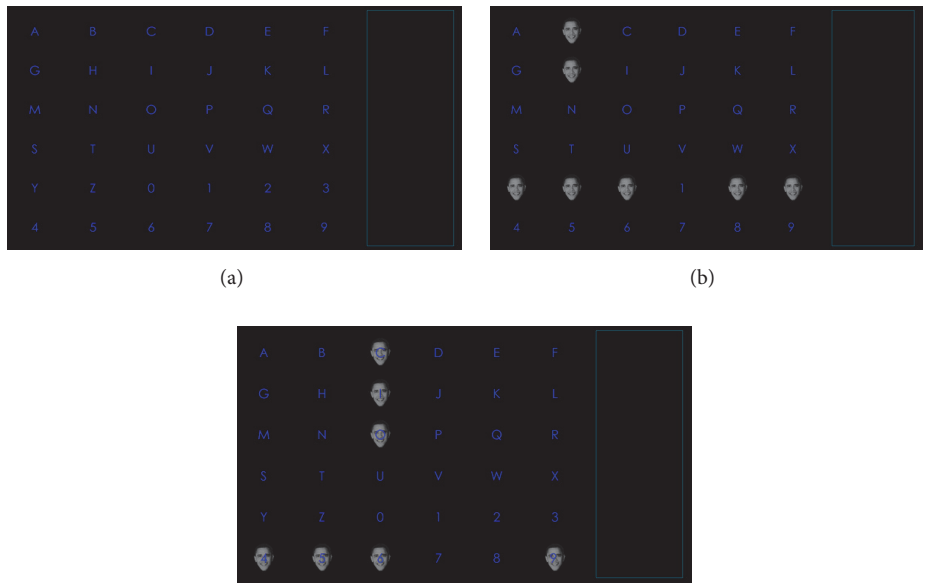

(a) (b)

(c)

Figure 1: The display presented to subjects. (a) 6 × 6 matrix displayed in the monitor; (b) face pattern (F-P); (c) semitransparent face pattern (STF-P).

on face stimuli focused mainly on the effect of various face types (i.e., face expression, face familiarity, and multifaces) on the BCI performance [8, 10, 14]. Studies on the influence of face transparency differences are scarce. Therefore, we investigated the effect of semitransparent face pattern (STF-P) (the subject could see the target character when the stimuli were flashed) and traditional face pattern (F-P) (the subject could not see the target character when the stimuli were flashed) on the BCI performance. Semitransparent faces can increase the psychological salience of the stimulus and allow for uninterrupted attention. Thus, we hypothesized that the persistent visible target character could help subjects focus on the target, increase N200 and N400 amplitudes, and improve the performance of ERP-based BCI using semitransparent face stimuli.

2. Methods

2.1. Subjects. Ten healthy subjects (2 females and 8 males, aged 22–26 years with the mean age of 23.5) participated in this study. The native language of the subjects is Mandarin Chinese. In addition, these subjects are all right-handed and have no known neurological disorders. They signed written consent form prior to the experiment, and the local ethics committee approved the consent form and experimental procedure before any subjects participated. Furthermore, all subjects had no previous BCI experiences.

2.2. Stimuli and Procedure. The subjects sat in a chair in front of the monitor, which displayed a 6 × 6 matrix with characters and numbers (Figure 1(a)) [10]. They were required to silently count the number of times the target flashed and avoid unnecessary movements. In this study, two paradigms were presented to the subjects. The parameters of the two paradigms (i.e., character size, intercharacter distance, background color, and stimulus brightness) were kept constant, except stimulus transparency. Accordingly, the counterbalance of the paradigm presentation could be obtained. In the first paradigm, the face stimulus concealed the target character, and the subject could not see the target character during the time the stimulus was on (Figure 1(b)). We called this paradigm as the traditional face pattern (F-P). In the second paradigm, the face stimulus was made semitransparent, and the subject could see the target character during the time the stimuli were on (Figure 1(c)). We called this paradigm as semitransparent F-P (STF-P). The subjects were tasked to count the number of times the target flashed. The flash configuration was based on binomial coefficients [15, 16]. The binomial coefficients were based on $C(n,k) = n!/(k!(n-k)!)$, $0 \le k \le n$, where n represents the number of flashes per trial and k represents the number of flashes per trial for each element in the matrix. We chose the combination of $C(12,2)$ to denote the 12-flash pattern. Table 1 shows the configuration of the 12-flash pattern combination with 36 flash pattern pairs. The positions in Table 1 corresponded to the positions of the 36 characters in a 6 × 6 matrix.

Each subject was required to complete two paradigms (F-P and STF-P) on the same day. Each paradigm contained one offline block and one online block. The order of the paradigms F-P and STF-P was counterbalanced throughout the experiment (five of ten subjects did the F-P first). During the offline period, each paradigm consisted of three offline runs called one offline block, and each offline run contained 5 target characters that would be spelled by the subjects without any rest. The subjects had 3 min rest between each offline run. In addition, each target character was identified through 16 trials, and each trial was composed of 12 flashes. No feedback

Table 1: Configuration of the 12-flash pattern combination.

1,4	1,5	1,6	1,7	1,8	1,9
2,10	2,5	2,6	2,7	2,8	2,9
3,10	*3,11*	3,6	3,7	3,8	3,9
4,10	*4,11*	4,12	4,7	4,8	4,9
5,10	*5,11*	5,12	1,10	5,8	5,9
6,10	*6,11*	6,12	3,12	*2,11*	6,9

Notes. We named these 12-flash groups as "$\text{flash}_1, \text{flash}_2, \ldots, \text{flash}_{12}$." The numbers in the table represent the target character of the 12 flashes. The same number in the configuration would simultaneously present stimuli. For example, letter "A" was flashed in flash_1 and flash_4. The italicized numbers represent the positions that simultaneously presented face stimuli during flash_{11}.

would be presented to the subjects in the offline experiment. However, during the online period, each paradigm only had one online run called one online block. The number of trials for recognizing each target character was selected automatically by an adaptive strategy [17, 18], and each trial was also composed of 12 flashes. The subjects were required to spell 36 target characters without any rest during the online period, and the system would promptly present the online result whenever the classifier recognized the target character. The stimulus on time was 100 ms and the stimulus onset asynchrony was 250 ms throughout the offline and online experiments. Moreover, an italicized number was used to prompt the subjects of the next target character before each run started, and they had 4 s for target selection. In addition, after finishing the offline experiment, subjects had 4 min rest to prepare for the following online experiment. Copy spelling task was used in the offline and online experiments.

2.3. Calibration. We acquired the EEG signals recorded with g.USBamp and g.EEGcap (Guger Technologies, Graz, Austria) with a sensitivity of 100 μV, band-pass filtered between 0.5 and 30 Hz, and sampled at 256 Hz. A total of 16 corresponding electrode positions were selected in the experiments according to the International 10-20 System (Figure 2) [8]. These positions were Fz, FC1, FC2, C3, Cz, C4, P3, Pz, P4, O1, Oz, O2, P7, P8, F3, and F4. FPz was used as the ground electrode, while right mastoid (A) was used as the reference electrode. These selected electrodes were used to keep track of the EEG signals.

2.4. Feature Extraction Procedure. Feature extraction is an effective method for reducing dimensionality and amount of required computations [18]. In this study, the third-order Butterworth band-pass filter was used to filter the EEG signals; the high pass was 0.5 Hz and low pass was 30 Hz. In addition, we downsampled the EEG signals from 256 Hz to 36.6 Hz by selecting every seventh sample from the filtered EEG. Consequently, we obtained the feature vector with the size of 16 × 29 (16 represents the number of the channels and 29 denotes the time points). In addition, winsorizing was used to remove the electrooculogram interference signals. The 10th and 90th percentiles were computed for each sample. Amplitude values lying below the 10th percentile or above the 90th percentile were then replaced with the 10th percentile or the 90th percentile, respectively [19].

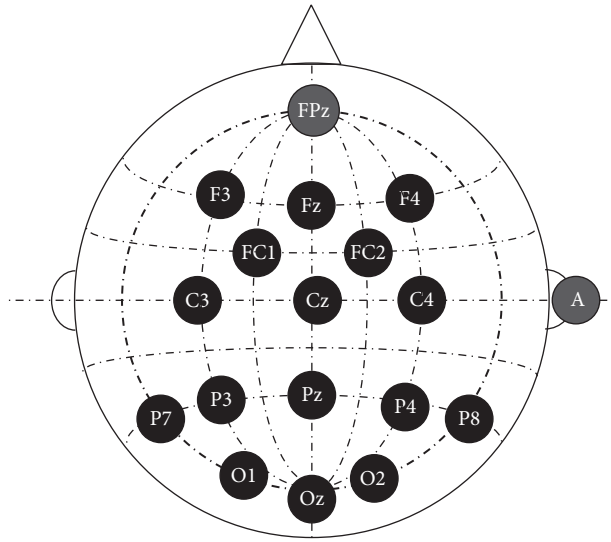

Figure 2: Configuration of the selected electrode positions (FPz was used as the ground electrode; right mastoid (A) was used as the reference electrode).

2.5. Classification Scheme. Bayesian linear discriminant analysis (BLDA) was used to build the classifier model for the online experiment. BLDA can effectively solve the problems of high-dimensional data sets or noise fitting owing to its regularization method. Hoffmann et al. [20] applied such a method to the classification of P300 BCIs and achieved good results.

2.6. Adaptive System Settings. The system was used to judge whether the results of two consecutive outputs were consistent. Accordingly, the final results of system output could be determined. If the results of two consecutive outputs were consistent, then the system exported the result as a feedback. Otherwise, the system would not provide any response until 16 trials were completed. When 16 trials ended, the classifier would automatically select the last output [21].

2.7. Statistical Analysis. We chose paired-samples t-tests (one-sample Kolmogorov-Smirnov test) for normal distribution to investigate the differences in mean amplitudes averaged from each ERP peak point ±20 ms between the F-P and STF-P paradigms. We also used such a method to explore the differences in online classification accuracy and bit rate between the two paradigms. The nonparametric Wilcoxon signed-rank test was used to compare the responses from the report of the subjects, as these data obey an uncertain distribution. The alpha level was $\alpha = 0.05$.

2.8. Subjective Report. After finishing the tasks of two paradigms, we conducted a questionnaire survey of three questions. The three questions were answered by the subjects

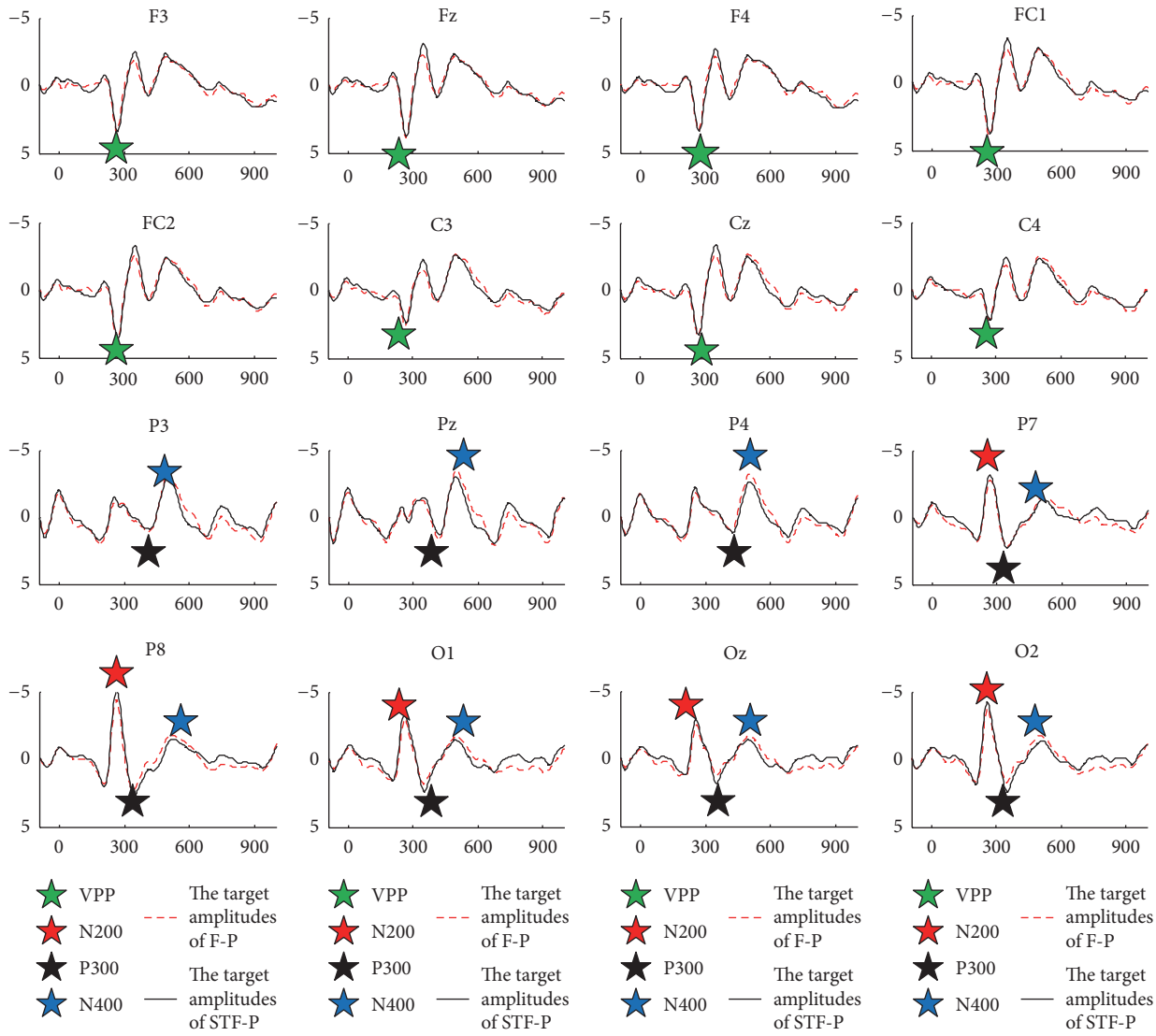

Figure 3: Grand averaged ERPs of target flashes across subjects 1–10 over 16 electrode sites.

on a 1–3 scale. A high score indicated a high degree of tiredness, difficulty, and annoyance (1: minimum; 2: medium; 3: maximum). The questions were as follows:

(1) Did this paradigm make you tired?

(2) Was this paradigm difficult?

(3) Did this paradigm make you annoyed?

3. Results

Figure 3 shows the grand averaged ERPs of target flashes after being baseline corrected by 100 ms prestimulus interval across subjects 1–10 over 16 electrode sites [21]. The two paradigms had similar VPP components over frontal and central areas. However, a few differences were found in N200 and P300 over parietal and occipital sites. STF-P had relatively higher peak values across N200 and P300 than those of F-P over parietal and occipital sites. We explored the differences of VPP, N200, P300, and N400 between STF-P and F-P; for this purpose, we selected Cz for VPP, P8 for N200, Pz for P300, and Cz for N400; these electrode positions typically contain the largest corresponding ERP components [7, 12, 22, 23] and are thus the best examples. Figure 4 shows the mean amplitudes of VPP at Cz, N200 at P8, P300 at Pz, and N400 at Cz for each subject and the N400 amplitude of the first and the third runs at Cz from the two paradigms [8]. The mean amplitude was averaged from each ERP peak point ±20 ms. The N200 amplitude at P8 from STF-P was significantly larger than that of F-P ($t = 2.49$, $p < 0.05$, df = 9, Figure 4(b)). Furthermore, no significant difference was found between the two paradigms across VPP and P300 ($t = 0.35$, $p > 0.05$, df = 9 for VPP, and $t = 1.45$, $p > 0.05$, df = 9 for P300, Figures 4(a) and 4(c)). Meanwhile, the value of P300 was smaller than that of the P300 reported in other studies [19, 24]. Although the N400 at Cz from STF-P showed no significant difference compared with that from F-P ($t = -0.65$, $p > 0.05$, df = 9; Figure 4(d)), the stability of N400

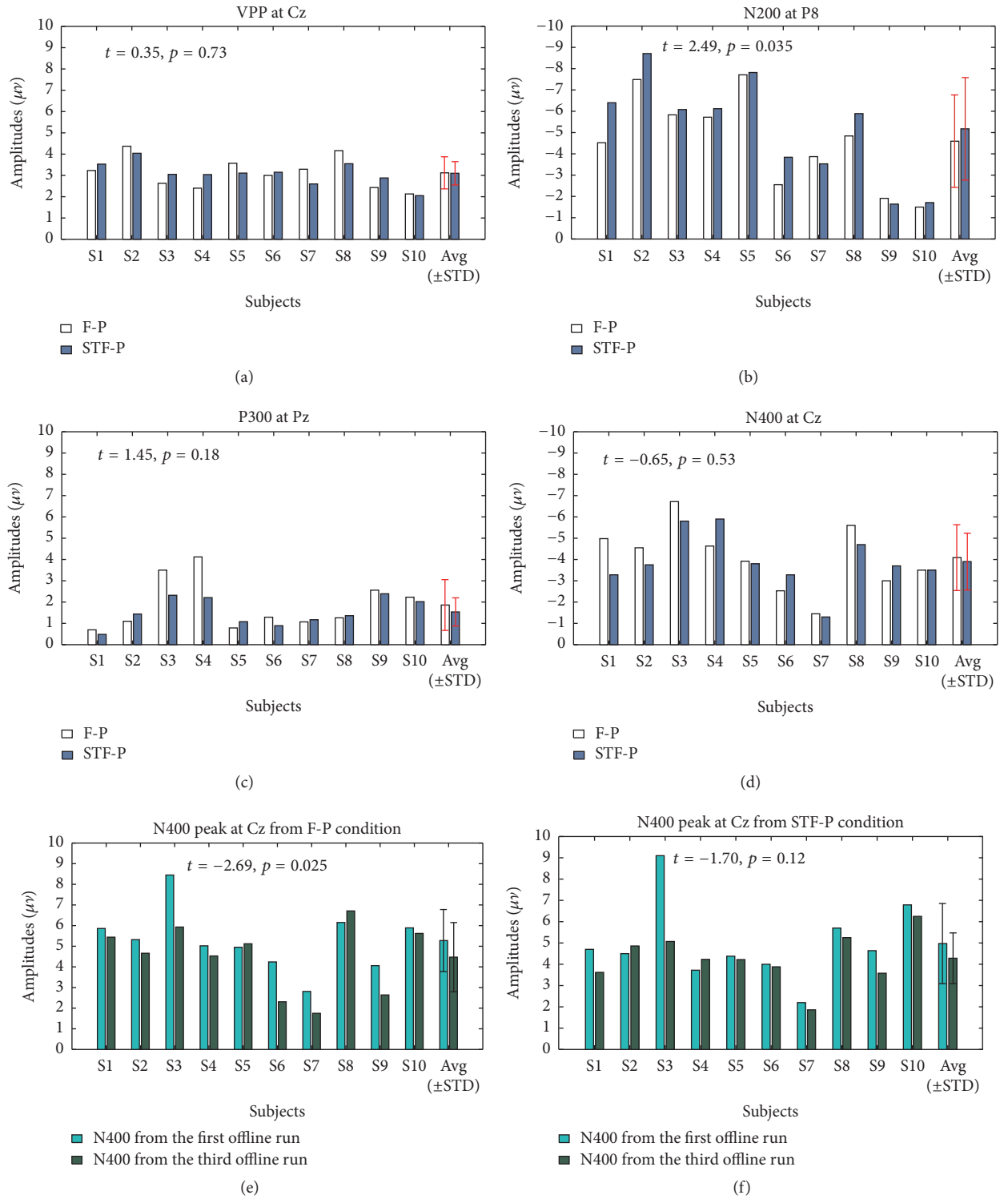

FIGURE 4: Six panels presenting the mean amplitudes averaged from each ERP peak point ±20 ms for each subject, and the differences in the amplitudes of N400 between the first and third offline runs from the two paradigms. These panels indicate the averaged amplitude of VPP at Cz (a); the averaged amplitude of N200 at P8 (b); the averaged amplitude of P300 at Pz (c); the averaged amplitude of N400 at Cz (d); the difference of N400 at Cz from the first and third offline run of the F-P (e); the difference of N400 at Cz from the first and third offline run of the STF-P (f). In addition, "Avg" is the average, "STD" is the standard deviation, and the error bars in the figure represent a standard deviation of each data set.

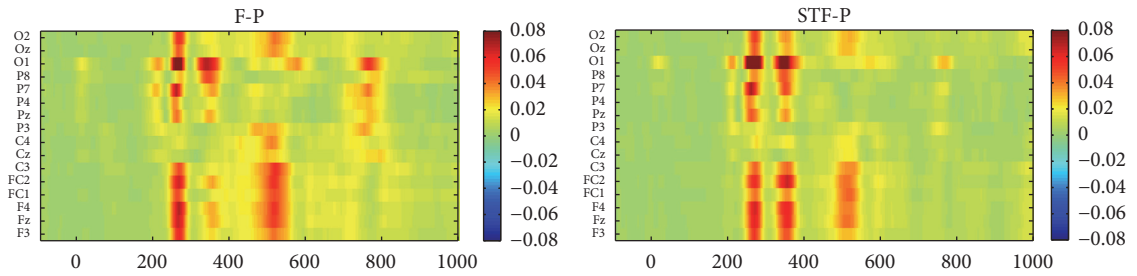

Figure 5: Absolute R-squared values of ERPs from these two patterns at 0–1000 ms averaged from subjects 1–10.

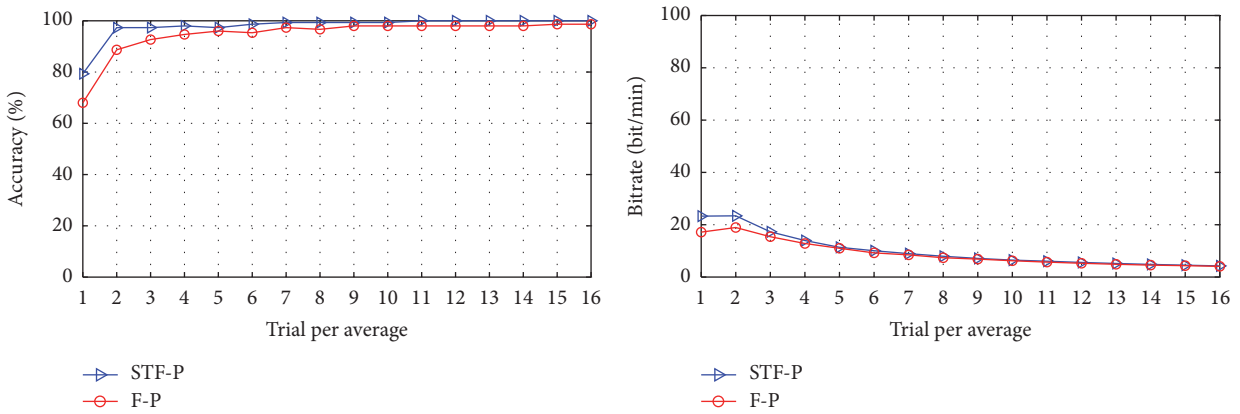

Figure 6: Classification accuracy and raw bit rate based on the offline data.

from STF-P ($t = -1.70$, $p > 0.05$, df = 9; Figure 4(f)) was better than that from F-P ($t = -2.69$, $p < 0.05$, df = 9; Figure 4(e)). Figure 5 shows the absolute R-squared values of ERPs from the two paradigms at 0–1000 ms averaged from subjects 1–10 on 16 electrodes. R-squared values of ERPs reflected the time energy of the signals. The definition is as follows:

$$r^2 = \left(\frac{\sqrt{N_1 N_2}}{N_1 + N_2} \cdot \frac{\text{mean}(X_1) - \text{mean}(X_2)}{\text{std}(X_1 \cup X_2)} \right)^2, \quad (1)$$

where X_1 and X_2 are the features of classes "1" and "2," respectively and N_1 and N_2 are the number of samples.

Figure 6 shows the classification accuracy and raw bit rate based on the offline data [8]. The values were obtained from 15-fold cross-validation. The classification accuracy and bit rate of STF-P were better than those of F-P when 1–16 numbers of trials were used for averaging.

Figure 7 shows the contributions of N200 (between 150 and 300 ms), P300 (between 300 and 450 ms), and N400 (between 450 and 700 ms) on the BCI performance [8]. The two graphs indicated that N200 and P300 components were crucial in the classification accuracy. In addition, the N400 component also contributed to the classification accuracy.

Table 2 shows the online classification accuracy, bit rate, and mean number of trials for each subject. The classification accuracy and bit rate of STF-P were significantly higher than those of F-P ($t = 2.89$, $p < 0.05$, df = 9 for classification accuracy, $t = 4.03$, $p < 0.05$, df = 9 for bit rate). Moreover, the number of trials for averaging of STF-P was significantly less than that of F-P ($t = -2.33$, $p < 0.05$, df = 9).

Table 3 presents the responses of the subjects to the three questions for each paradigm. We further investigated the differences between the two paradigms. For this purpose, we chose the Wilcoxon signed-rank test method owing to the fact that the data satisfy an uncertain distribution. No significant differences were found between the two paradigms in terms of the degree of tiredness ($p > 0.05$), degree of difficulty ($p > 0.05$), and degree of annoyance ($p > 0.05$).

4. Discussion

This study aimed to survey whether any difference would be found between STF-P in which the subject could see the target character during the time the stimuli were on and F-P in which the target character was concealed during the time the stimuli were on. The results showed that the STF-P could elicit larger N200 component and improve the classification accuracy and bit rate of the BCI system compared with the F-P.

The Eriksen flanker task [25] is a commonly used experimental design to obtain N200 and is a kind of a mismatch paradigm [21]. In the present study, the STF-P elicited larger N200 component than the F-P. On the one hand, semitransparent face stimuli may lead to a high mismatch, thereby resulting in a large N200. On the other hand, the psychological salience of the stimuli can be exploited to elicit high ERP components not confined to the P300 components [9].

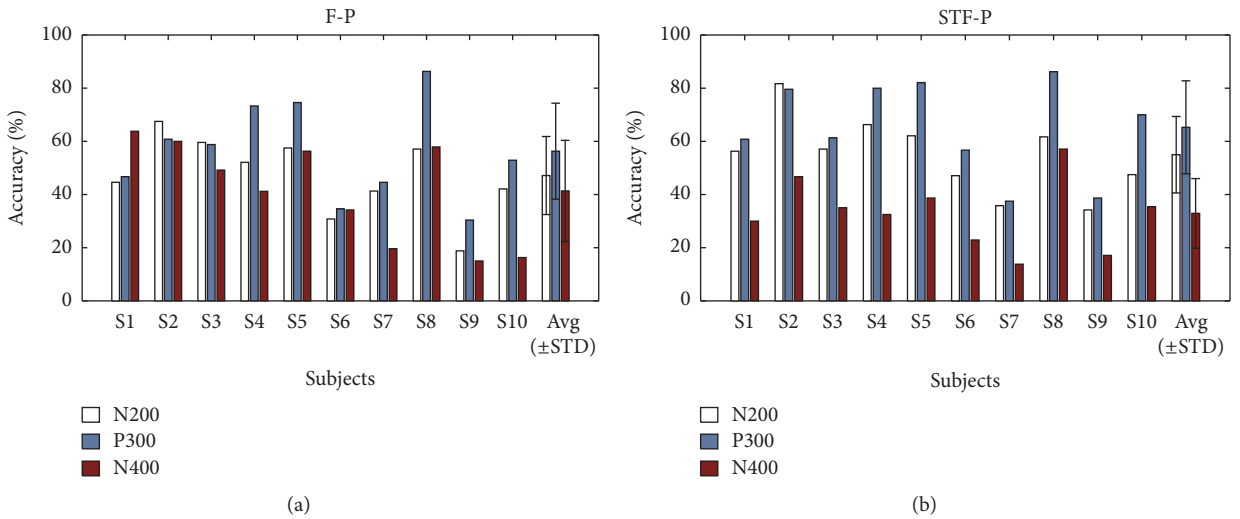

Figure 7: The contributions of N200, P300, and N400 time windows on the classification accuracy.

Table 2: Online classification accuracy, bit rate, and average number of trials for each subject.

		S1	S2	S3	S4	S5	S6	S7	S8	S9	S10	AVG ± STD
ACC (%)	F-P	94.4	94.4	91.7	94.4	80.5	100	94.4	77.8	91.7	100	91.9 ± 7.3
	STF-P	97.2	94.4	97.2	100	88.9	97.2	97.2	83.3	94.4	100	95.0 ± 5.2
RBR (bit/min)	F-P	32.9	42.7	36.3	44.5	32.3	44.3	43.9	29.4	28.6	44.8	38.0 ± 6.7
	STF-P	41.0	44.5	43.0	50.3	39.3	43.0	42.5	36.1	36.6	49.6	42.6 ± 4.8
AVT	F-P	2.78	2.14	2.39	2.06	2.14	2.33	2.08	2.22	3.03	2.31	2.35 ± 0.32
	STF-P	2.36	2.06	2.25	2.06	2.08	2.25	2.28	2.03	2.50	2.08	2.20 ± 0.16

ACC = classification accuracy, RBR = raw bit rate (bit/min), AVT = average number of trials used to classify each character, STF-P = semitransparent face pattern, F-P = face pattern, AVG = average, and STD = standard deviation.

Table 3: Subjects' responses to three questions for each pattern.

		S1	S2	S3	S4	S5	S6	S7	S8	S9	S10	AVG ± STD
Tired	F-P	2	2	2	1	2	2	1	2	1	1	1.6 ± 0.52
	STF-P	1	2	1	2	1	1	1	1	1	1	1.2 ± 0.42
Difficult	F-P	2	1	1	2	1	1	2	2	1	2	1.5 ± 0.53
	STF-P	1	2	1	1	1	2	1	2	1	1	1.3 ± 0.48
Annoyed	F-P	1	2	1	2	1	1	1	2	1	1	1.3 ± 0.48
	STF-P	1	1	1	2	1	1	1	2	1	1	1.2 ± 0.42

F-P = face pattern; STF-P = semitransparent face pattern. AVG is average and STD is standard deviation.

The difference of P300 amplitude between two paradigms in this paper was not clear and no significant difference was found. This phenomenon may be attributed to the low luminosity contrast when the background is black (the gray value of face was set 110, while the background was 255). However, low luminosity contrast leads to low visual fatigue. Li et al. [26] studied the effects of various luminosity contrasts on the BCI performance and found that low luminosity contrast produces small amplitude for P300 on average. A high luminosity contrast can result in bright, noticeable infrequent stimuli; as a result, subjects can easily concentrate their attention and efficiently identify the target characters. Therefore, low brightness may lead to increased effort or attention deployment in subjects. This finding may have an important implication for clinical application.

The effects of repetition can decrease the amplitude of N400, especially for long-term offline data recording [8]. In STF-P, given that the target differed, the stimulus also differed when the subject shifted their focus from one target to another. Since the significant difference of N400 between

the first and third offline run was found in the F-P while not in the STF-P (see Figures 4(e) and 4(f)), it indicated that STF-P contained less repetition effects compared to the F-P.

Classification accuracy and ITR are the important indexes of BCI performance. In previous studies, face paradigms themselves have had good performances in accuracy (mean accuracy was higher than 90%) [8]. Therefore, even 1% increment in accuracy would be a good improvement. In this study, the averaged classification accuracy and bit rate of the STF-P were 95.0%, 42.6 bit/min, while those of the F-P were 91.9%, 38.0 bit/min, and were 3.1%, 4.6 bit/min, higher than those of the F-P. Figure 4(b) showed that the N200 at P8 of the STF-P was significantly higher than that of the F-P. Figure 7 showed that N200 could contribute to classification accuracy. Kaufmann et al. [27] reported that the potential of N200 can enhance the classification accuracy. Jin et al. [8] proved that other components can contribute to the classification accuracy under the condition of small P300 amplitudes. Table 2 showed that the classification accuracy and information transfer rate of the STF-P were significantly higher than that of the F-P ($p < 0.05$). As in all, the STF-P could obtain superior performance compared to the F-P.

This research studied two paradigms only (semitransparency and nontransparency) and focused less on the different transparent degrees based on the state of being transparent. However, this research provided a new idea on the studies of face stimuli and demonstrated that other distinct components could contribute strongly to the BCI performance.

5. Conclusion

In this study, we measured the performance of STF-P and F-P on BCI. The result indicated that STF-P was superior to F-P. In future studies, we will further verify the performance of the STF-P pattern on patients.

Conflicts of Interest

The authors declare that they have no conflicts of interest.

Acknowledgments

This work was supported in part by the Grant National Natural Science Foundation of China, under Grants nos. 61573142, 61203127, 91420302, and 61305028. This work was also supported by the Fundamental Research Funds for the Central Universities (WG1414005, WH1314023, and WH1516018).

References

[1] E. W. Sellers, D. J. Krusienski, D. J. McFarland, T. M. Vaughan, and J. R. Wolpaw, "A P300 event-related potential brain-computer interface (BCI): the effects of matrix size and inter stimulus interval on performance," *Biological Psychology*, vol. 73, no. 3, pp. 242–252, 2006.

[2] F. Nijboer, E. W. Sellers, J. Mellinger et al., "A P300-based brain-computer interface for people with amyotrophic lateral sclerosis," *Clinical Neurophysiology*, vol. 119, no. 8, pp. 1909–1916, 2008.

[3] X.-Y. Wang, F. Cai, J. Jin, Y. Zhang, and B. Wang, "Robot control system based on auditory brain-computer interface," *Control Theory and Applications*, vol. 32, no. 9, pp. 1183–1190, 2015.

[4] M. F. Mason, M. I. Norton, J. D. Van Horn, D. M. Wegner, S. T. Grafton, and C. N. Macrae, "Wandering minds: the default network and stimulus-independent thought," *Science*, vol. 315, no. 5810, pp. 393–395, 2007.

[5] A. Kübler, B. Kotchoubey, J. Kaiser, J. R. Wolpaw, and N. Birbaumer, "Brain-computer communication: unlocking the locked in," *Psychological Bulletin*, vol. 127, no. 3, pp. 358–375, 2001.

[6] J. R. Wolpaw, N. Birbaumer, D. J. McFarland, G. Pfurtscheller, and T. M. Vaughan, "Brain-computer interfaces for communication and control," *Clinical Neurophysiology*, vol. 113, no. 6, pp. 767–791, 2002.

[7] L. A. Farwell and E. Donchin, "Talking off the top of your head: toward a mental prosthesis utilizing event-related brain potentials," *Electroencephalography and Clinical Neurophysiology*, vol. 70, no. 6, pp. 510–523, 1988.

[8] J. Jin, B. Z. Allison, Y. Zhang, X. Wang, and A. Cichocki, "An erp-based bci using an oddball paradigm with different faces and reduced errors in critical functions," *International Journal of Neural Systems*, vol. 24, no. 8, Article ID 1450027, 2014.

[9] T. Kaufmann, S. M. Schulz, C. Grünzinger, and A. Kübler, "Flashing characters with famous faces improves ERP-based brain-computer interface performance," *Journal of Neural Engineering*, vol. 8, no. 5, pp. 173–178, 2011.

[10] J. Jin, B. Z. Allison, T. Kaufmann et al., "The changing face of P300 BCIs: a comparison of stimulus changes in a P300 BCI involving faces, emotion, and movement," *PLoS ONE*, vol. 7, no. 11, Article ID e49688, 2012.

[11] Y. Zhang, Q. Zhao, J. Jin, X. Y. Wang, and A. Cichocki, "A novel BCI based on ERP components sensitive to configural processing of human faces," *Journal of Neural Engineering*, vol. 9, no. 2, pp. 26018–26030, 2012.

[12] D. A. Jeffreys and E. S. A. Tukmachi, "The vertex-positive scalp potential evoked by faces and by objects," *Experimental Brain Research*, vol. 91, no. 2, pp. 340–350, 1992.

[13] T. Kaufmann, S. M. Schulz, A. Köblitz, G. Renner, C. Wessig, and A. Kübler, "Face stimuli effectively prevent brain-computer interface inefficiency in patients with neurodegenerative disease," *Clinical Neurophysiology*, vol. 124, no. 5, pp. 893–900, 2013.

[14] S.-K. Yeom, S. Fazli, K.-R. Müller, and S.-W. Lee, "An efficient ERP-based brain-computer interface using random set presentation and face familiarity," *PLoS ONE*, vol. 9, no. 11, Article ID e111157, 2014.

[15] J. Jin, P. Horki, C. Brunner, X. Wang, C. Neuper, and G. Pfurtscheller, "A new P300 stimulus presentation pattern for EEG-based spelling systems," *Biomedizinische Technik*, vol. 55, no. 4, pp. 203–210, 2010.

[16] J. Jin, B. Z. Allison, E. W. Sellers et al., "Optimized stimulus presentation patterns for an event-related potential EEG-based brain-computer interface," *Medical and Biological Engineering and Computing*, vol. 49, no. 2, pp. 181–191, 2011.

[17] A. Lenhardt, M. Kaper, and H. J. Ritter, "An adaptive P300-based online brain-computer interface," *IEEE Transactions on Neural Systems and Rehabilitation Engineering*, vol. 16, no. 2, pp. 121–130, 2008.

[18] J. Jin, B. Z. Allison, E. W. Sellers et al., "An adaptive P300-based control system," *Journal of Neural Engineering*, vol. 8, no. 3, Article ID 036006, pp. 292–301, 2011.

[19] J. Jin, I. Daly, Y. Zhang, X. Y. Wang, and A. Cichocki, "An optimized ERP brain-computer interface based on facial expression changes," *Journal of Neural Engineering*, vol. 11, no. 3, pp. 1082–1088, 2014.

[20] U. Hoffmann, J.-M. Vesin, T. Ebrahimi, and K. Diserens, "An efficient P300-based brain-computer interface for disabled subjects," *Journal of Neuroscience Methods*, vol. 167, no. 1, pp. 115–125, 2008.

[21] J. Jin, E. W. Sellers, S. Zhou, Y. Zhang, X. Wang, and A. Cichocki, "A P300 brain-computer interface based on a modification of the mismatch negativity paradigm," *International Journal of Neural Systems*, vol. 25, no. 3, pp. 595–599, 2015.

[22] J. R. Folstein and C. Van Petten, "Influence of cognitive control and mismatch on the N2 component of the ERP: a review," *Psychophysiology*, vol. 45, no. 1, pp. 152–170, 2008.

[23] C. C. Duncan, R. J. Barry, J. F. Connolly et al., "Event-related potentials in clinical research: guidelines for eliciting, recording, and quantifying mismatch negativity, P300, and N400," *Clinical Neurophysiology*, vol. 120, no. 11, pp. 1883–1908, 2009.

[24] L. Chen, J. Jin, Y. Zhang, X. Y. Wang, and A. Cichocki, "A survey of the dummy face and human face stimuli used in BCI paradigm," *Journal of Neuroscience Methods*, vol. 239, pp. 18–27, 2015.

[25] B. A. Eriksen and C. W. Eriksen, "Effects of noise letters upon the identification of a target letter in a nonsearch task," *Perception and Psychophysics*, vol. 16, no. 1, pp. 143–149, 1974.

[26] Y. Li, S. Bahn, C. S. Nam, and J. Lee, "Effects of luminosity contrast and stimulus duration on user performance and preference in a P300-based brain-computer interface," *International Journal of Human-Computer Interaction*, vol. 30, no. 2, pp. 151–163, 2014.

[27] T. Kaufmann, E. M. Hammer, and A. Kübler, "ERPs contributing to classification in the P300 BCI," in *Proceedings of the 5th International Brain-Computer Interface Conference*, pp. 136–139, 2013.

Hindawi
Computational Intelligence and Neuroscience
Volume 2017, Article ID 1742862, 25 pages
https://doi.org/10.1155/2017/1742862

Review Article

Progress in EEG-Based Brain Robot Interaction Systems

Xiaoqian Mao,[1] Mengfan Li,[1] Wei Li,[1,2,3] Linwei Niu,[4] Bin Xian,[1] Ming Zeng,[1] and Genshe Chen[5]

[1] *School of Electrical Engineering and Automation, Tianjin University, Tianjin 300072, China*
[2] *Department of Computer & Electrical Engineering and Computer Science, California State University, Bakersfield, CA 93311, USA*
[3] *State Key Laboratory of Robotics, Shenyang Institute of Automation, Shenyang, Liaoning 110016, China*
[4] *Department of Math and Computer Science, West Virginia State University, Institute, WV 25112, USA*
[5] *Intelligent Fusion Technology, Inc., Germantown, MD 20876, USA*

Correspondence should be addressed to Wei Li; wli@csub.edu

Received 28 December 2016; Accepted 21 March 2017; Published 5 April 2017

Academic Editor: Hasan Ayaz

The most popular noninvasive Brain Robot Interaction (BRI) technology uses the electroencephalogram- (EEG-) based Brain Computer Interface (BCI), to serve as an additional communication channel, for robot control via brainwaves. This technology is promising for elderly or disabled patient assistance with daily life. The key issue of a BRI system is to identify human mental activities, by decoding brainwaves, acquired with an EEG device. Compared with other BCI applications, such as word speller, the development of these applications may be more challenging since control of robot systems via brainwaves must consider surrounding environment feedback in real-time, robot mechanical kinematics, and dynamics, as well as robot control architecture and behavior. This article reviews the major techniques needed for developing BRI systems. In this review article, we first briefly introduce the background and development of mind-controlled robot technologies. Second, we discuss the EEG-based brain signal models with respect to generating principles, evoking mechanisms, and experimental paradigms. Subsequently, we review in detail commonly used methods for decoding brain signals, namely, preprocessing, feature extraction, and feature classification, and summarize several typical application examples. Next, we describe a few BRI applications, including wheelchairs, manipulators, drones, and humanoid robots with respect to synchronous and asynchronous BCI-based techniques. Finally, we address some existing problems and challenges with future BRI techniques.

1. Introduction

There are several approaches to brain activity measurements, such as magnetoencephalogram (MEG), near infrared spectroscopy (NIRS), electrocorticogram (ECoG), functional magnetic resonance imaging (fMRI), and electroencephalogram (EEG) [1]. Brain machine interface (BMI) [2, 3] or Brain Computer Interface (BCI) [4–6] provides a new nonmuscular channel for sending messages and commands to the external world. A BCI creates an additional communication channel for users who are not able communicate via normal pathways and computers. In BCI systems, the signal acquisition devices are generally divided into two categories: invasive and noninvasive. In an invasive BCI system, arrays of microelectrodes are permanently implanted in the cerebral cortex [7]. The brain signals are recorded from ensembles of single brain cells (also known as single units) or the activity of multiple neurons (also known as multiunits) [8]. Schmidt investigated the possibility of making long-term connections to the central nervous system with microelectrodes to control external devices [9]. In the year 2000, Nicolelis had successfully realized an invasive BMI on a night monkey, which reconstructed its arm movements to obtain food by operating a joystick. This open-loop BMI-based system was upgraded to test a closed-loop motor control on a macaque monkey. The monkey was able to control movements of a robot arm to grasp an object by a moving cursor on a video screen via visual feedback [10]. In terms of human beings, Hochberg et al. demonstrated the ability of two people with long-standing tetraplegia to use a neural interface system to

control a robotic arm to perform three-dimensional reach and grasp movements [11]. Participants controlled the arm and hand over a broad space without explicit training, using signals decoded from a small, local population of motor cortex neurons, recorded from a 96-channel microelectrode array. Schwartz et al. comprehensively reviewed invasive BMI technologies for mind-controlled robot systems [12].

An EEG device, as a representative of noninvasive technology, found a wide application in both clinical and research fields [13–16] due to its low cost and portability. Invasive BCI systems are mainly used to restore special sensations, such as visual sense, and motor functions for paralyzed patients. The quality of neural signals is relatively high because the microelectrodes are directly implanted into the cerebral grey matter. However, invasive BCI systems have the disadvantage of easily causing immune reaction and callus, which most likely lead to the regression and disappearance of neural signals.

In order to solve these problems, many researchers have focused on noninvasive BCI systems because of their ease of use, portability, low cost, and low damage to human bodies. Different from the invasive BCI systems, which record the single-unit activity from within cortex, the noninvasive BCI systems use EEGs to record brain electrical activities from the scalp [17]. Therefore, noninvasive BCI systems have found a wider application. Early in the 1990s, Niels Birbaurmer had translated the EEG signals of paralyzed patients into control commands to control the cursor of a computer. In the following years, the EEG-based BCI has been largely researched to analyze the characteristics of brain signals from the scalp and apply it to control intelligent devices to assist paralyzed patients with their daily lives. The typically used signal acquisition devices include a series of products (g.USBamp [18–20], g.BSamp [21, 22], and g.BCIsys [23]) made by g.tec in Austria, Cerebus [24–28] made by BlackRock Microsystems in USA, a series of products with 64, 128, or 256 channels (SynAmps 2 [29–33]) made by Compumedics Neuroscan in Australia, wireless Emotiv EPOC [34–36] made by Emotiv Systems in USA, BrainNet-36 [37], ANT-Neuro [38], FlexComp Infiniti encoder [39], and so forth. And the most commonly used BCI operating system is BCI2000 [40] because it is highly flexible and interchangeable and especially can incorporate alone or in combination with any brain signals, signal processing methods, output devices, and operating protocols.

Based on brain activity patterns, the EEG-based BCI systems are categorized into four different types: event-related desynchronization/synchronization (ERD/ERS) [41], steady-state visual evoked potential (SSVEP) [42], event-related potential (ERP) [43], and slow cortical potential (SCP) [44]. Among them, the SSVEP, ERPs, ERD/ERS, and their hybrids [45–48] attract the interests of researchers.

In the application of BCI-based cognitive models to control external mechanical devices, such as a robot arm [49], a wheelchair [50], or a humanoid robot [34], Brain Robot Interaction (BRI) [24, 51, 52] has become more and more popular. A BRI system is a closed-loop control system that uses brain signals in combination with surrounding information feedback. The collected brain activities must be decoded to generate commands for robots to execute an action or a task that an operator wants to fulfill. The robot must provide feedback of the surroundings to the operator, to assist in making proper decisions. Therefore, an ideal setup for a BRI system usually consists of evoking sources (for SSVEP or ERP) to generate specific brain signals, signal acquisition devices, data analyzing systems, and control objects, among which the signal generating and data analyzing are the most challenging and worthy researching tasks. More and more researchers focus their attention on discovering new evoking mechanisms and testing novel decoding algorithms.

In this paper, we present a comprehensive review and a critical analysis of the three main EEG models with respect to brain signal generation, methods of feature extraction, and feature classification. Then, we list some applications of synchronous and asynchronous BRI systems, especially for humanoid robots. Last, we focus on discussing the challenges and future perspectives of brain signal modeling and the difficulties of BRI.

2. EEG-Based Brain Signal Models

2.1. SSVEP

2.1.1. Evoking Mechanism. In EEG-based brain signal models, SSVEP is generated by visual stimuli. From retinal photoreceptors, visual percepts propagate first to the visual areas and next to the rest of the brain [53]. Following the presentation of visual stimuli, sensory evoked potentials (SEPs) and termed visually evoked potentials (VEPs) can be recorded in the visual areas. VEPs elicited by brief stimuli are usually transient responses of the visual system. Transient evoked potentials are responses of the system under study to sudden changes (jumps or steps) in the input [54]. About 50 years ago, Regan started experimenting with long stimulus trains, consisting of sinusoidally modulated monochromatic light [55]. These stimuli produced a stable VEP of small amplitude, which could be extracted by averaging over multiple trials. These EEG waves were termed as "steady-state" visually evoked potentials (SSVEP) of the human visual system. SSVEPs can also be found in animals, such as in primates [56] or in cats [57].

SSVEP is a steady-state physical response to outside periodic stimuli and generated at the primary visual cortex without triggering senior visual information process [62]. Since SSVEP is generated at the occipital EEG electrodes (including Oz, O1, and O2 [63]), the corresponding areas have the strongest power. Although the electrodes used in SSVEP vary from person to person, the most reasonable electrodes used in SSVEP mainly include Oz, O1, O2, Pz, P3, P4, and some surrounding electrodes located at the occipital. Researchers had concluded that SSVEP evoking frequencies had a wide range from 1 to at least 90 Hz, and the steady-state potentials exhibited clear resonance phenomena around 10, 20, 40, and 80 Hz [64]. The most commonly used frequencies range from 4 to 60 Hz. In terms of SSVEP evoking, the repetitive visual stimulus (RVS) [58] mainly include simple square flicker, checkerboard, gratings, and light-emitting diode (LED) [65].

2.1.2. Experimental Paradigm. SSVEP-based BCIs allow users to select a target by means of an eye-gaze. The user visually fixes attention on a target and the BCI identifies the target through SSVEP features analysis [172]. Considering a BCI as a communications channel, SSVEP-based BCIs can be classified into three categories depending on the specific stimulus sequence modulation in use [173]: time modulated VEP (t-VEP) BCIs, frequency modulated VEP (f-VEP) BCIs, and pseudorandom code modulated VEP (c-VEP) BCIs. VEPs that react to different stimulus sequences should be orthogonal or near orthogonal to each other in some domain, to ensure reliable identification of the target. In a t-VEP BCI, the flash sequences of different targets are orthogonal in time. That is, the flash sequences for different targets are either strictly nonoverlapping or stochastic. In an f-VEP BCI, each target is flashed at a unique frequency, generating a periodic sequence of evoked responses with the same fundamental frequency as its harmonics. In a c-VEP BCI, pseudorandom sequences are used. The duration of ON and OFF states of each target's flash is determined by a pseudorandom sequence. Signal modulations can optimize the information transfer rate. Indeed, code modulation provides the highest communication speed.

To elicit an SSVEP, a RVS has to be presented to the user. The RVS can be rendered on a computer screen by alternating graphical patterns or with external light sources able to emit modulated light. Alternating graphical patterns mainly include single graphic and pattern reversal stimuli. Single graphic stimuli could be a rectangle, square, arrow, or robot picture and rendered on a computer screen and appear from and disappear into the background at a specified rate, as shown in Figure 1(a). Pattern reversal stimuli could be a checkerboard or grating that is rendered by oscillatory alternation of graphical patterns, as shown in Figure 1(b). They consist of at least two patterns that are alternated at a specified number of alternations per second. The external light can flash with any frequency and the graphical patterns with only certain frequencies because of the computer screen refresh rate limitations.

2.2. ERP

2.2.1. Evoking Mechanism. ERP is generated when a specific stimulus acts on the sensory system of the brain or some mental factor occurs. Subsequently, ERP is evoked in response to the emerging or disappearing of the stimuli. Classical ERPs include several positive and negative waves, such as P1, N1, P2, N2, and P3 (namely, P300) according to the emerging sequences and polarities. The N1 is associated with attention [174] and P2 with stimulus encoding [175]. N2 has been associated with "response selection" or "response activation" [176] and P300 with "context updating" [177] or "context closure" [178]. As the "exogenous component," the P1, N1, and P2 components are easily influenced by physical stimuli characters, while as the "endogenous component," N2 and P3 are not influenced by physical stimuli characters.

In 1965, Sutton et al. discovered an electrical potential that exhibited a positive fluctuation within approximately 300 ms after the presentation of an unexpected event (visual, auditory, etc.) [179]. Smith et al. named this potential "P300" potential based on its polarity and relatively fixed latency [180]. A P300 potential is induced prominently in channels Pz, Fz, and Cz in the midline centroparietal regions, and its latency varies from 300 ms to 800 ms when a set of visual stimuli are presented unexpectedly in a random sequence [181]. Therefore, the most commonly used electrodes in ERP are mainly located in the midline centroparietal regions, such as Fz, Cz, Pz, Oz, and their surrounding ones. The P300 component has a relatively high amplitude of 5–20 μV and can be found in EEG after a single stimulus without superposition, so it has wide applications in BRI.

2.2.2. Experimental Paradigm. A P300 system often uses stimuli with different characters, contents, and decoding methods to run the corresponding cognitive process of the subject, according to the different contents and purposes of the research. The visually evoked P300 system often adapts the visual oddball paradigm, in which two different visual stimuli are presented to the subject randomly and the standard stimulus appears generally and the bias stimulus incidentally. The bias stimulus is called target stimulus when the subject reacts to it. The P300 component will be observed in 300 ms after the target stimulus appears [182]. Except the evoking paradigm of presenting a single visual stimulus in turn, researchers have put forward more and more P300 evoking paradigms to present more stimuli efficiently in the P300-based character speller system.

Farwell and Donchin first put forward a P300 speller system [59]: a 6-by-6 matrix containing the letters of the alphabet and a few 1-word commands (see Figure 2) were displayed on a computer-controlled CRT screen. The "stimulus events" that occurred in the test consist of intensifications of either a row or a column of the matrix. The detection was achieved by repeatedly flashing rows and columns of the matrix. When the element containing the chosen character was flashed, a P300 was elicited, and it was this P300 that was detected by the computer. Treder and Blankertz put forward a Hex-o-Spell paradigm and Figure 3 shows a screenshot of the visual speller [60]. Figure 3(a) was the group level. The group containing the target symbol "B" (group "ABCDE") was intensified. Figure 3(b) was the transition phase. The symbols of the selected group were expanded onto the other discs. Figure 3(c) was the symbol level. The nontarget disc with the symbol "A" was intensified. The empty disc at the bottom was intended as a backdoor for returning to the group level in case the wrong group was selected. Acqualagna and Blankertz developed rapid serial visual presentation (RSVP) as a paradigm for mental typewriting for patients unable to overtly fixate the target symbol [61]. Figure 4 showed the process of the paradigm. First, the sentence was presented on the display. After the fixation cross, the RSVP of the symbols starts. The target letter was highlighted on the top of screen. Participants had to concentrate on the target letter and were asked to silently count its number of occurrences. The data recorded in this phase were used to train the classifier. In the online phase, the classifier selected the symbol with the best score and displayed it.

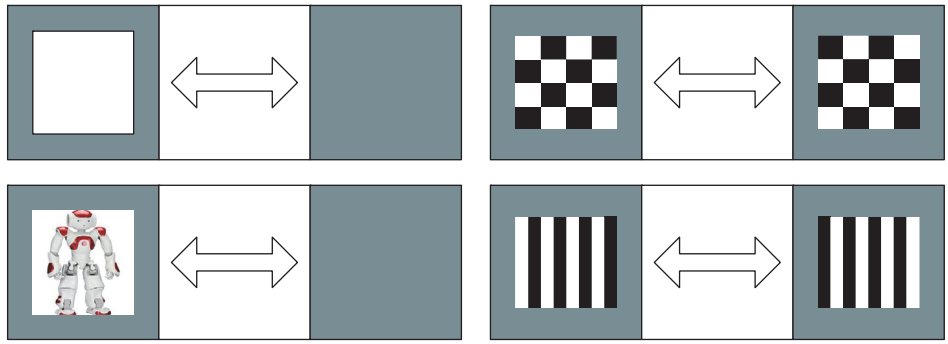

(a) Single graphic stimuli (b) Pattern reversal stimuli

Figure 1: (a) Single graphic stimuli: the graphical object alternately appears and disappears in the background. (b) Pattern reversal stimuli: at least two patterns are alternated at a specified frequency [58].

A	G	M	S	Y	*
B	H	N	T	Z	*
C	I	O	U	*	TALK
D	J	P	V	FLN	SPAC
E	K	Q	W	*	BKSP
F	L	R	X	SPL	QUIT

Figure 2: The rows and columns of the matrix were flashed alternately [59].

Researchers have recently paid attention to some other ERPs to improve the performance of the ERP-based BCI. Jin et al. use faces as visual stimuli to induce N400 potential to make the ERP more obvious [183, 184]. Jin et al. apply mismatch paradigm to evoke mismatch negativity to improve the accuracy and information transfer rate [185].

2.3. MI

2.3.1. Generation Mechanism. Motor imagery may be seen as mental rehearsal of a motor act without any overt motor output. It is broadly accepted that mental imagination of movements involves similar brain regions/functions which are involved in programming and preparing such movements [188]. Pfurtscheller and Neuper showed independent imagination of movements versus planning of voluntary movements of either the right or the left hand; the most prominent EEG changes were localized over the corresponding primary sensorimotor cortex [189]. During the imagination of a right hand or left hand movement, for example, a similar ERD can be found over the contralateral hand area and an ERS over the ipsilateral hand area. Traditionally, transient increases and decreases in spectral power recorded in the human EEG have been termed event-related synchronization (ERS) and desynchronization (ERD), respectively [190]. Both phenomena are time-locked but not phase-locked to the event and they are highly frequency band specific. It has long been known that movements elicit frequency specific changes in the EEG [191–193] and changes in spectral power in the μ (8–14 Hz) and β (15–30 Hz) frequency bands can be observed during both voluntary [194] and passive movements [195].

During overt execution of the movement, the initially contralateral ERD develops a bilateral distribution [196], whereas during mental simulation this ERD remains mostly limited to the contralateral hemisphere. This means that the suppression of μ and central β rhythms is more pronounced at the contralateral hemisphere when subjects imagine one-sided hand movements than when they actually perform such movements. These ERD phenomena are used as the classification basis in MI. The most representative MI-ERD phenomena are generated by imaging the movement of left hand, right hand, and feet and are distributed on primary motor cortex (M1). The corresponding areas locate at the EEG electrodes of C3, C4, and Cz which are also the most used electrodes in MI.

2.3.2. Experimental Paradigm. In MI, producing the EEG signal is an important factor in a successful BCI. Therefore, the issues concerned with human training are worth considering. Different from SSVEP or ERP, the MI needs a longer training period in order to generate the ERD/ERS phenomena. It may take months of training before the user achieves the desirable level of performance. In order for the user to acquire self-control of an EEG response, some kind of feedback is essential, at least in the beginning, and the feedback can speed up the learning process and improve performance.

The MI training process usually consists of offline and online training. A period of offline training is essential for adjusting user's EEG signals and training the recognition algorithm. Time for a single training trial is often 9 seconds (see Figure 5). During the trial, an arrow with random direction (left or right) is displayed on the computer screen and the user imagines movement of the left or right hand according to the direction of the arrow. During the first two seconds of one trial, nothing is displayed on computer screen. At $t = 2$ s, a fixation cross appears with a short beep. From $t = 3$ s to 9 s, the user is asked to carry out the MI task while the fixation cross with left or right direction displayed on the screen. Then several trials of training data will be used to generate a template of recognition algorithm. The train generated template is stored to recognize online training. For online

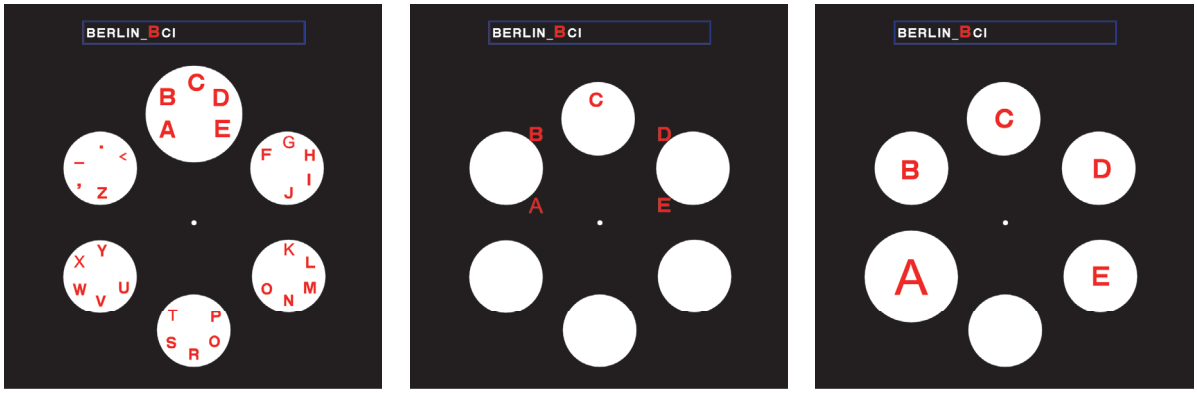

(a) (b) (c)

Figure 3: Screenshot of Hex-o-Spell paradigm [60].

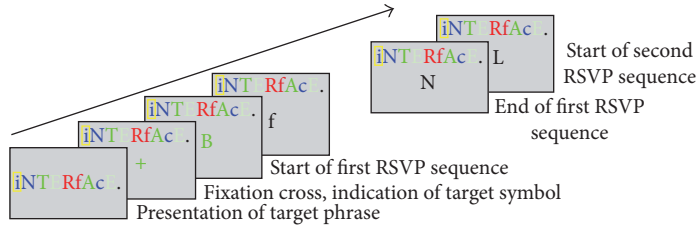

Figure 4: RSVP paradigm [61].

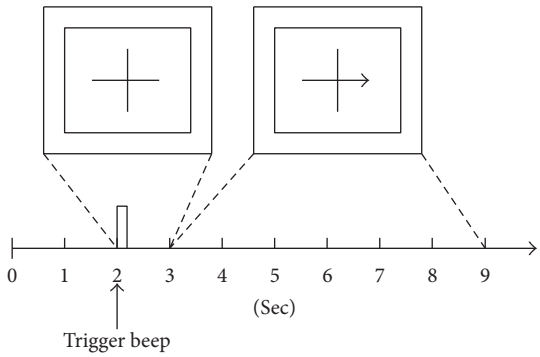

Figure 5: Timing scheme for one training trial [39].

training, Neuper et al. used a feedback bar to inform the user of the imaging results [197]. The feedback stimulus began to extend horizontally towards the right or left side according to the classification result. Yu et al. used a hybrid BCI with SSVEP and MI to extend the feedback bar in the targeted direction [198]. Alimardani et al. asked the subjects to watch first-person images of robots through a head mounted display [18]. A lighting ball in front of robot's hands gave motor imagery cue and subjects held images of a grasp for their own corresponding hand. Classifier detected two classes of results (right or left) and sent a motion command to robot's hand.

3. Brain Signal Decoding Methods

An essential factor in the successful operation of BCI systems is the methods used to process the brain signals [58]. This paper summarizes different signal processing schemes that have been used in BCI systems. It specifically focuses on the following signal processing components of a BCI: the preprocessing, feature extraction, and feature classification. As for various brain signal evoking mechanisms, this paper chooses the most commonly used paradigms (SSVEP, P300, MI) as the objects to summarize the brain signal processing methods.

3.1. Preprocessing Methods. Preprocessing methods in BCI mainly include frequency domain filtering and spatial filtering. Band-pass filters and notch filters are the most commonly used methods in frequency domain filtering, which can extract the characteristic signals located in the stimulus frequency and remove noise and artifacts. These filters are designed according to frequency characteristics of related signals. Often, the frequency range of a band-pass filter is designed according to the stimulation frequencies or their harmonics, while a notch filter is used to remove power line interference. Spatial filters can expand the signal-to-noise ratio of the brain signal response, by processing brain signal data of multiple channels. Signals from multiple channels are less affected by noise than signals from a unipolar or bipolar system. The spatial filtering technique can be also used to extract features. Generally, the spatial filtering methods include minimum energy combination (MEC), canonical correlation analysis (CCA), common average reference (CAR), principal component analysis (PCA), independent component analysis (ICA), and autocorrelation (AC). MEC is used to cancel nuisance signals as much as possible. CCA computes the relation between two multivariable data sets

Table 1: Preprocessing methods in different EEG paradigms.

EEG paradigms	Authors	Preprocessing methods
SSVEP	Bevilacqua et al. [66]	2–60 Hz for band-pass filter, notch filter at 50 Hz
	Müller-Putz and Pfurtscheller [21]	0.5–30 Hz for band-pass filter, notch filter at 50 Hz
	Ortner et al. [67]	0.5–100 Hz for band-pass filter, notch filter at 50 Hz
	Wu et al. [65]	0.3–40 Hz for band-pass filter
	Muller et al. [37]	3–60 Hz for band-pass filter, CAR
	Júnior et al. [68]	CCA
	Wang et al. [69]	CCA
	Zhang et al. [70]	Multiset CCA
	Nan et al. [71]	MEC, CCA
	Pouryazdian and Erfanian [72]	PCA
P300	Rakotomamonjy and Guigue [73]	8-order, 0.1–10 Hz band-pass Chebyshev Type I filter
	El Dabbagh and Fakhr [74]	8 order, 0.1–20 Hz band-pass Chebyshev Type I filter
	Mak et al. [75]	0.5–30 Hz band-pass
	Panicker et al. [38]	3 order, 0.5–12 Hz Butterworth filter
	Lugo et al. [76]	0.1–30 Hz band-pass filter
	Lotte et al. [77]	25 Hz low-pass filter
	Li et al. [25]	1–10 Hz band-pass filter
	Spüler et al. [78]	0.5–16 Hz band-pass filter, CAR
	Casagrande et al. [79]	CAR
	Syan and Harnarinesingh [80]	10-order low-pass Hamming-window filter with 6 dB cutoff at 30 Hz, CAR, PCA
MI	Park et al. [81]	5-order, 8–30 Hz Butterworth filter
	Coyle et al. [22]	R^2CA with a standard 8–26 Hz band
	Wang et al. [82]	FB (Filter Bank) with 4–8, 8–12, . . . , 36–40 Hz
	Devlaminck et al. [83]	A set of spatial filters
	Ang et al. [84]	FB
	Li et al. [85]	8–30 Hz band-pass filter
	Yao et al. [29]	8–26 Hz band-pass filter
	Song et al. [39]	4-order Butterworth IIR filter, Laplacian filter
	Wu and Ge [86]	CAR, FIR (Finite Impulse Response) filter
	Zhou et al. [87]	8–35 Hz band-pass filter, ICA
	Sharma and Baron [88]	PCA, tensor ICA
	Bashar et al. [89]	Autocorrelation

after linear combinations of original data. For the CAR method, the average value of all electrodes is subtracted from the channel of interest to make the EEG recording nearly reference-free. PCA is used to decompose signals into components of responses of brain activities. It aims to reduce the dimension of original data. ICA is often used to separate movement related independent components from EEG data. AC enhances the weak EEG signal, reduces noise, and makes it suitable for analysis. Table 1 lists some preprocessing methods of different EEG paradigms.

3.2. Feature Extraction Methods. The feature extraction is a key issue in signal processing and plays an important role to the whole BCI system. A variety of methods have been used in different EEG paradigms. Several commonly used feature extraction methods are described as follows.

3.2.1. Fourier-Based Transform (FT). The FT contains Fast Fourier Transform (FFT) and Discrete Fourier Transform (DFT). FT methods are mainly used for power spectrum density analysis (PSDA). FFT is a fast computation algorithm for DFT, which could influence the practical applications. In real applications, the available stimulation frequencies may be limited because the frequency resolutions are limited to a given data segment length. The advantages include simplicity and small computation time.

In SSVEP-based BCI, Wang et al. used 256-point FFT to transform EEG signals into the frequency domain representing 5 frequencies of 9 Hz, 11 Hz, 13 Hz, 15 Hz, and 17 Hz [30]. A 128-point FFT averaged the three spectral components around the target frequency when the subjects did not focus on any stimuli. The average value was used to recognize an idle state of a subject. Mouli et al. used maximum amplitudes of the FFT to distinguish different target stimuli of 7, 8, 9, and 10 Hz [90]. Müller-Putz and Pfurtscheller computed the frequency components by estimating the power density spectrum of the EEG signal with split-radix FFT and averaged the three spectral components around the target frequency

[21]. Hwang et al. estimated the EEG data using the FFT with a frequency resolution of 0.1 Hz and constructed the feature vectors by the arithmetic sum of the stimulation frequencies and the second harmonic frequencies [91]. As for DFT, Oikonomou et al. used the FFT algorithm as the estimation of DFT coefficients [92]. Diez et al. also used the FFT as an estimation of the power spectral density based on the DFT [93]. All these studies which used FFT as the estimation of DFT show the computational advantages of FFT. FFT has a wide use in SSVEP systems from low and medium to a high range of frequencies. DFT is often estimated by FFT because of its small computational time.

The P300 components are not sensitive to frequency, so there is no study of it using FFT as feature extraction methods. However, the MI paradigm generates the μ and β rhythms responses when motor imagery is active. A few studies have tried to recognize the MI tasks using FFT. For example, Hiroyasu et al. used β rhythms (13–16 Hz or 13–30 Hz) and μ rhythms (8–12 Hz) as the feature values of recognition [111]. The FFT overlap processing was performed to calculate the power spectrum transitions. Jin et al. utilized FFT to analyze the frequency range of μ and β so as to analyze the energy of EEG and get its features [112].

3.2.2. Wavelet Transform (WT). EEG signals are nonstationary whose frequency components vary as a function of time [199]. The analysis of such signals can be facilitated by Wavelet Transform which provide flexible time-frequency resolution. WT is based on FT and is an adjustable-window Fourier analysis [200]. The advantage of WT over FT is that it is easy to choose different mother wavelet functions to analyze different types of signals. WT is potentially one of the most powerful signal processing techniques because of its ability to adjust to signal components and its multiresolution which is broadly used to analyze EEG signals.

In SSVEP-based BCI, Zhang et al. introduced Continuous Wavelet Transform (CWT) into SSVEP feature extraction and classification [94]. The choice of mother wavelet is the key issue in CWT. They investigated different types of wavelets and compared the performances in SSVEP classification. Experimental results showed that Complex Morlet wavelet outperformed others and especially had advantages in short EEG data segment. Kumari and Somani used the coefficients of CWT as the feature vectors to find the location of high-frequency components in SSVEP [95].

In P300-based BCI, Demiralp et al. used the WT to identify the most significant response property reflecting the P300 wave [102]. The application of a 5 octave quadratic B-spline-WT on single sweeps yielded discrete coefficients in each octave with an appropriate time resolution for each frequency range. The main feature indicating a P300 response was the positivity of the 4th delta (0.5–4 Hz) coefficient after stimulus onset. Vareka and Mautner applied Daubechies7 wavelet to an averaged target epoch in DWT [103]. The P300 component is obtained by the signal reconstructed from the approximation coefficients of level 6. Guo et al. used Daubechies4 (db4) as the mother wavelet of DWT because of the similarity between db4 and P300 [104]. The decomposition level was set from 4 to 6. They tested the method in traditional P300 speller system. Also, Pan et al. used a WT-based method to recognize P300 components in P300 speller systems [105]. They applied the Mallat algorithm to calculate the coefficients of WT and decomposed the signals into satisfied resolution, which resulted in multiresolution of WT. Vequeira et al. also used WT on P300 speller system as the feature extraction method to help patients with oral communications problems [106].

In MI-based BCI, the CWT gives a highly redundant representation of EEG signals in the time-scale domain [199], so it can be applied for the precise localization of ERD/ERS components in the time-scale domain. Hsu and Sun applied CWT together with Student's two-sample t-statistics for 2D time-scale feature extraction [113]. The 2D time-scale yielded a highly redundant representation of EEG signals in the time-frequency domain, from which the precise location of event-related brain desynchronization and synchronization (ERD and ERS) components could be obtained. Then, the CWTs of EEG data performing left and right MI in both C3 and C4 channels were analyzed, respectively. Xu and Song used DWT to execute multiresolution decomposition for a signal [114]. They chose the decomposition level of 4 and the wavelet of Daubechies order 10. The extracted wavelet coefficients showed the distribution of the motor imagery signal in time and frequency and the component D3 (8–16 Hz) was within the μ rhythm and D2 (16–32 Hz) was within the β rhythm. Bashar et al. proposed Dual Tree Complex Wavelet Transform (DTCWT) domain to identify left and right hand motor imagery movements [89]. DTCWT is a recent enhancement to the DWT which has additional properties including nearly shift invariant and directionally selective of two and higher dimensions [201]. It is more efficient in time-frequency localization of EEG signals. They applied DTCWT to decompose EEG signals into three levels and reconstruct these components using the inverse DTCWT approximately corresponding to the physiological EEG subbands delta, theta, alpha, and beta, respectively. Then, EEG signals in lower frequency bands and μ rhythms (7.5–12.5 Hz) were extracted.

According to the references we have consulted, the Wavelet Transform (WT) is suitable for various kinds of EEG paradigms analysis because of its optimal resolution in both the time and frequency domain. Therefore, WT has a wide application in SSVEP, P300, and MI paradigms for feature extraction.

3.2.3. Hilbert-Huang Transform (HHT). HHT, consisting of empirical mode decomposition (EMD) and Hilbert spectral analysis (HAS) [202], is a recently developed adaptive data analysis method, which has been used extensively in EEG research. The key part of HHT is EMD with which any complicated data set can be decomposed into a finite and often small number of intrinsic mode functions (IMFs). An IMF is an oscillator function with time-varying frequencies that can represent the local characteristics of nonstationary signals [203]. Different from FFT, which is based on cosine functions, HHT is self-adaptive and can acquire better performance in some signal segments, so it can be used in analyzing both stationary and nonstationary signals. However, HHT computation time is higher than that of FT.

In SSVEP-based BCI, Huang et al. used HHT for the recognition of high-frequency SSVEP signals [96]. The original signals were transformed into 11-order IMF, which satisfied the requirements of the HT, by the method of EMD. Then, HT method was used on each order of IMF above to calculate its instantaneous frequency. All those results were used to create an integrated time-frequency figure. The component of its corresponding frequency could be seen from its frequency diagram by analyzing the corresponding levels with FFT. Ruan et al. applied HHT to decompose the independent components by ICA to obtain IMF needed and analyzed IMF by frequency domain analysis or power spectrum estimation [97]. They could identify the subjects at the target stimulus frequency according to the spectrum peak in the spectrum diagram and frequency diagram. Zhang et al. put forward an Improved HHT (IHHT) to extract time-frequency feature of High-Frequency Combination Coding-Based SSVEP (HFCC-SSVEP) [98]. The extraction method consists of synchronous averaging, band-pass filtering, EMD, selection of IMF, instantaneous frequency, and Hilbert spectrum. Besides, the HT has also been employed to compute SSVEP phases [99, 100]. According to the investigation above, HHT provides an effective solution for high-frequency SSVEP.

In P300-based BCI, there is no reference using HHT to extract the P300 components. While in MI-based BCI, HHT is an effective way to extract μ and β rhythms. Wang et al. used HHT to analyze three motor imagery tasks [115]. The raw signal was decomposed using EMD and several IMFs were gained. Then, the Hilbert spectrum was calculated based on the IMF1 and IMF2. In each motor imagery task, local instantaneous energies, within specific frequency band of electrode C3 and C4, were selected as the features. Jerbic et al. investigated the perspective of HHT for extracting time-frequency information used for MI classification [116]. The IMFs obtained by EMD were mapped into time-frequency-energy matrix, constraining frequency scale to 1 Hz wide frequency bins (range 6–40 Hz). Liu et al. devised a feature, Degree of Imagery (DOI) based on HHT, which can effectively detect the ERD during motor imagery, thereby improving the classification performance [117]. In this paper, they thought that not all of the IMFs were useful for the detection of ERD, so they calculated partial IMFs to accomplish the EMD process in practice in order to improve the computational speed of HHT. Furthermore, they demonstrated that DOI could improve the detection and classification of ERD effect.

The HHT is useful for EEG paradigms that are sensitive to frequency. From the references referred to above, HHT provides an effective solution for high-frequency SSVEP. Also, the μ and β rhythms in motor imagery can be extracted by HHT.

3.2.4. Independent Component Analysis (ICA). ICA is a recently developed method with the goal of finding a linear representation of non-Gaussian data so that components are statistically independent or as independent as possible. Such a representation seems to capture the essential structure of the data in many applications, including feature extraction and signal separation [204]. ICA can be performed in two different ways, namely, spatial ICA that extracts unique independent spatial maps and temporal ICA that extracts independent time courses. The electrodes "record" the mixed EEG signal at different locations around the scalp. Therefore, it is reasonable to apply ICA on EEG signals to identify those independent sources and map them to needed components.

In SSVEP-based BCI, ICA is often used to extract EEG signals from raw signals. Wang et al. employed ICA to decompose EEGs over the visual cortex into SSVEP signal and background noise [101]. Thirteen ICs were calculated as sources through ICA and the four with most significant power at stimulation frequency were supposed to be signal activities of SSVEP while the remaining were considered as noise activities.

In P300-based BCI, Li et al. chose FastICA to perform ICA in a P300 speller system because of its fast speed and high reliability [107]. They computed 16 ICs and selected 3 ICs with the largest difference in their coefficients as the P300 related ones. The activation status of these 3 ICs in different channels was used as the feature for P300 identification. Turnip et al. put forward a nonlinear independent components analysis (NICA) extraction method for P300 [108]. With the NICA method, a level of accuracy was attained after about 240 iterations, which were less than 1800 iterations in the same level without using the proposed feature extraction. The results showed that NICA accelerated the network's training process and the tracking error convergence was faster. Li et al. applied ICA to select the channels whose brain signals contained large N200 and P300 potentials and small artifacts as the optimal channels to extract the features [26]. They separated the source signals that produced ERP, muscle artifacts, or ocular artifacts.

In MI-based BCI, Naeem et al. studied three different ICA algorithms (Infomax, FastICA, and SOBI) and compared them to Common Spatial Patterns (CSP), Laplacian derivations, and standard bipolar derivations [118]. Among the ICA algorithms, the best performance was achieved by Infomax when using 22 components as well as for the selected 6 components by visual inspection. Guo et al. explored a dynamic ICA based on the sliding window Infomax algorithm to analyze motor imagery EEG [119]. The method could get a dynamic mixing matrix with the new data input, which was unlike the static mixing matrix in traditional ICA algorithms. The feature patterns were based on the total energy of dynamic mixing matrix coefficients in a certain time window.

In most cases, ICA is used to separate the noise/interference from the raw EEG signals in preprocessing. While in feature extraction, ICA usually combines other feature extraction algorithms to classify the different targets in various EEG paradigms.

3.2.5. Common Spatial Pattern (CSP). The CSP method is a powerful signal processing technique that was shown to superiorly extract discriminative information, compared to other spatial filters such as bipolar, Laplacian, or CAR [205]. The principle of CSP is yielding a set of spatial filters that are designed to minimize the variance of one class while maximizing it for the other class. Ortner et al. advised that the CSP method needs more electrodes than others [206]. CPS can suppress noise by using the data from many electrodes and

hence needs a minimum number of electrodes to perform well. However, because CSP is based on the Fisher discriminative criterion, it can only reflect the separative ability of the mean power of two classes. In practice, this mean power separation may be insufficient to reflect the discrimination of samples around the decision boundary. From the statistics viewpoint, arithmetic mean is sensitive to outliers. Artifacts such as eye and muscle activities may dominate over the EEG signal, and thus they may give excessive power in some channels. Because of CSP simply pooling the covariance matrixes of trials together, if an artifact happens to be unevenly distributed in different experiment conditions, CSP will capture it with high eigenvalue. This will distort the following CSP spatial filter [207].

In P300-based BCI, Pires et al. proposed an application of standard CSP combined with an approach of feature combination based on probabilistic models of spatial filtered data embedded in a Bayesian classifier [109]. The result showed that CSP could be effectively used on P300. Amini et al. used morphological, intelligent segmentation, CSP, and combined features (segmentation+CSP) in the feature extraction block [110]. Within the P300 oddball principle context, they considered two spatiotemporal matrixes which represented the P300 potential evoked by the target event and the ongoing EEG for nontarget events, respectively. Then the set of features was obtained via the CSP technique. A statistical analysis was applied for evaluating the fitness of each feature in discriminating between target and nontarget signals.

Indeed, the CSP is an effective method especially for MI classification. Many improved CSP-based methods have been put forward recently to enhance the classification accuracy. Samek et al. proposed a method called stationary CSP (sCSP) which regularizes the CSP solution towards stationary subspaces; that is, the CSP is extended to be invariant to nonstationarities in the data [120]. CSP reduced variations of the extracted features by assuming that the variations were not task-related like eye movements or electrode artifacts. The results showed that the sCSP was competitive compared with the state-of-the-art CSP method. He et al. proposed an EMD-based CSP method to realize the data-related and adaptive frequency band selection [121]. The IMFs decomposed from the EMD and the amplitude modulated signal by instantaneous amplitude (IA) calculated from HT were fully explored and employed. Use of the EMD filter property avoided manually dividing the frequency band, which was usually adopted in the traditional CSP method. Moreover, it could be expected that a small number of informative frequency band related IMFs would lead to higher algorithm efficiency. To address the problem of selecting the subject-specific frequency band for the CSP algorithm, the Filter Band CSP (FBCSP) algorithm was proposed for MI-BCI. The FBCSP algorithm classifies single-trial EEG based on selected features computed from subject-specific temporal-spatial filters. Keng et al. used FBCSP on BCI competition IV Datasets 2a and 2b to classify 4 classes (left hand, right hand, feet, and tongue) and 2 classes (left hand and right hand) of MI tasks, respectively [122]. Also, Chin et al. used FBCSP to classify 4 classes of MI tasks [123]. To improve the CSP algorithm's robustness against outliers, Yong et al. first investigated how multivariate outliers affected the performance of the CSP algorithm and then proposed a modified version of the algorithm whereby the classical covariance estimates are replaced by the robust covariance estimates obtained using Minimum Covariance Determinant (MCD) estimator [208]. Median Absolute Deviation (MAD) is also used to robustly estimate the variance of the projected EEG signals. The results showed that the proposed algorithm is able to reduce the influence of the outliers. Then, Kai et al. tested the RFBCSP algorithm on BCI competition IV Datasets 2b and the results revealed a promising direction of RFBCSP for robust classifications of EEG measurements in MI-BCI [124].

In the context of Brain Computer Interfaces, the Common Spatial Patterns method is widely used for classification of motor imagery events. However, it is not very often used for classification of event-related potentials such as P300. Meanwhile, there is no reference describing the applications of CSP on SSVEP-based BCI.

All the feature extraction methods we have referred to are most commonly used in BCI, including SSVEP, P300, and MI. Due to article length limitations, we cannot list all the feature extraction methods one by one. Table 2 summarizes the methods mentioned above in different EEG paradigms.

3.3. Feature Classification Methods. Nonstationarities are ubiquitous in EEG signals. They are especially apparent in the use of EEG-based BCI. Therefore the stability of a classifier is a significant factor in the discrimination of targets in various paradigms. Overall, it was agreed that simplicity is generally best and therefore, the use of linear methods is recommended wherever possible. Furthermore, linear classifiers are generally more robust than nonlinear ones. This is because linear classifiers have fewer free parameters to tune and are thus less prone to overfitting. It was also agreed that nonlinear methods in some applications can provide better results, particularly with complex and/or other very large data sets [209].

In the following, the paper introduces the most commonly used classification methods and their applications in BCI systems, which mainly include Linear Discriminant Analysis (LDA), Support Vector Machines (SVM), neural networks, nonlinear Bayesian classifiers, nearest neighbor classifiers, and combinations of classifiers [210]. Table 3 summarizes partial applications of classification methods on SSVEP, P300, MI, and so forth.

3.3.1. LDA (FLDA). The aim of LDA (also known as Fisher's LDA) is to use hyperplanes to separate the data representing the different classes [211]. For a two-class problem, the class of a feature vector depends on which side of the hyperplane the vector is (see Figure 6). LDA finds the optimal projection which maximizes the distance between the two-class means and minimizes the interclass variances. The separating hyperplane is perpendicular to the projection direction [186]. The strategy generally used for multiclass BCI is the "One Versus the Rest" (OVR) strategy which consists in separating each class from all the others.

This technique is simple and has a very low computational requirement, which makes it suitable for online BCI system.

Table 2: Feature extraction methods in different EEG paradigms.

EEG paradigms	Authors	Feature extraction methods
SSVEP	Wang et al. [30]	Average and FFT, 5 targets (9, 11, 13, 15, 17 Hz)
	Mouli et al. [90]	FFT, 4 targets (7, 8, 9, 10 Hz)
	Müller-Putz and Pfurtscheller [21]	FFT, 4 targets (6, 7, 8, 13 Hz)
	Hwang et al. [91]	FFT, spelling system (5–7.9 Hz with a span of 0.1 Hz)
	Oikonomou et al. [92]	FFT as an estimation of DFT, 5 target (6.66, 7.5, 8.57, 10, 12 Hz)
	Diez et al. [93]	FFT as an estimation of DFT, 4 targets (37, 38, 39, 40 Hz)
	Zhang et al. [94]	CWT, 4 targets (15, 12, 10, 8.57 Hz)
	Kumari and Somani [95]	CWT, 3 targets (8, 14, 28 Hz)
	Huang et al. [96]	HHT (34, 35, 37, 38, 45, 48 Hz)
	Ruan et al. [97]	HHT (11, 12 Hz)
	Zhang et al. [98]	IHHT (25, 33.33, 40 Hz)
	Molina et al. [99]	HT (all integer frequencies from 30 to 40 Hz, 4 phases)
	Zhu et al. [100]	HT (all integer frequencies from 32 to 40 Hz, 4 phases)
	Wang et al. [101]	ICA (13 Hz)
P300	Demiralp et al. [102]	WT (5 octave quadratic B-spline-WT), auditory oddball paradigm (800, 1200 Hz tones)
	Vareka and Mautner [103]	DWT (Daubechies7), oddball paradigm (traditional OQ experiment)
	Guo et al. [104]	DWT (Daubechies4), P300 speller (6 by 6 matrix)
	Pan et al. [105]	WT (Mallat), P300 Speller (6 by 6 matrix)
	Vequeira et al. [106]	WT (bior), P300 Speller (6 by 6 matrix)
	Li et al. [107]	FastICA, P300 Speller
	Turnip et al. [108]	NICA, EPFL BCI group data
	Li et al. [26]	ICA, oddball paradigm (6 targets)
	Pires et al. [109]	CSP, P300 arrow paradigm
	Amini et al. [110]	morphological, intelligent segmentation, CSP and combined features (segmentation+CSP), P300 Speller
MI	Hiroyasu et al. [111]	FFT, left or right hand (13–16 Hz or 13–30 Hz, 8–12 Hz)
	Jin et al. [112]	FFT, left or right hand (8–30 Hz)
	Hsu and Sun [113]	CWT, left or right hand
	Xu and Song [114]	DWT (Daubechies10), left or right hand
	Bashar et al. [89]	DTCWT, left or right hand
	Wang et al. [115]	HHT, left or right hand, foot
	Jerbic et al. [116]	HHT, left or right hand
	Liu et al. [117]	HHT, left or right hand
	Naeem et al. [118]	ICA, left or right hand, foot, tongue
	Guo and Wu [119]	Dynamic ICA, BCI competition 2003 data set III
	Samek et al. [120]	sCSP, Dataset IVa, BCI Competition III
	He et al. [121]	EMD-based CSP, BCI Competition IV dataset I
	Ang et al. [122] Chin et al. [123]	FBCSP, BCI Competition IV 2a (4 classes) and 2b (2 classes)
	Kai et al. [124]	RFBCSP, BCI Competition IV 2b (2 classes)

Table 3: Feature classification methods in different EEG paradigms.

EEG paradigms	Authors	Classification methods
SSVEP	Chu et al. [125]	LDA, 3 classes (20, 15, 12 Hz)
	Bi et al. [126]	LDA, 2 classes (12, 13 Hz)
	Oikonomou et al. [92]	LDA, 5 classes (6.66, 7.5, 8.57, 10, 12 Hz)
	Maggi et al. [127]	RLDA, 5 classes (6, 7, 8, 10 Hz, idle)
	Singa and Haseena [128]	SVM, 4 classes (7, 9, 11, 13 Hz)
	Bi et al. [129]	SVM, 3 classes (12, 13 Hz, idle)
	Sakurada et al. [130]	SVM, 4 classes (6, 7, 8, nonfixation)
	Jian and Tang [35]	OVO RBF SVM, 5 classes (8, 10, 12, 14, 15 Hz)
	Cecotti and Gräser [131]	TDNN, 5 classes (13, 14, 15, 16, 17 Hz)
	Cecotti [132]	CNN, 5 classes (6.66, 7.5, 8.57, 10, 12 Hz)
	Hartmann and Kluge [133]	HMM, 3 classes (10, 12, 15 Hz)
	Ko et al. [134]	kNN, 2 classes (15, 20 Hz)
	Oikonomou et al. [92]	kNN, 5 classes (6.66, 7.5, 8.57, 10, 12 Hz)
P300	Gareis et al. [135]	LDA, P300 Speller
	Onishi and Natsume [136]	Ensemble Stepwise LDA, P300 Speller
	Elwardy et al. [137]	Disjunctive Normal Unsupervised LDA, P300 Speller
	Li et al. [31]	SVM, P300 speller
	Raju et al. [138]	Least Square SVM (LS-SVM), Competition III, Dataset II (P300 Speller)
	Li et al. [139]	Self-Training Semisupervised SVM, P300 Speller
	Yang et al. [140]	LVQNN, 7 classes (oddball paradigm)
	Turnip et al. [141]	MNN, raw data in Hoffmann et al.
	Cecotti and Gräser [142]	CNN, P300 Speller
	Helmy et al. [143]	HMM, raw data in Hoffmann et al.
	Speier et al. [144]	HMM, P300 Speller
	Syan and Harnarinesingh [80]	kNN, P300 Speller, BCI Competition II
	Chikara and Ko [145]	kNN, 2 classes
MI	Chen et al. [32]	LDA, 2 classes (left or right hand)
	Steyrl et al. [146]	Shrinkage RLDA, 2 classes (right hand and feet)
	Vidaurre et al. [147]	KALDA, 2 classes (left or right hand)
	Rathipriya et al. [148]	SVM, 2 classes, Dataset IVa (right hand, foot) and IVb (left hand, foot), BCI Competition III
	Oskoei et al. [149]	supervised and unsupervised SVM, 3 classes, Dataset V, BCI Competition III (left or right hand, word association)
	Siuly and Li [150]	LS-SVM, 2 classes, Dataset IVa and IVb, BCI Competition III
	Hamedi et al. [151]	BP, 3 classes (left or right hand, tongue)
	Wei et al. [152]	LVQNN, 2 classes (left or right hand)
	Hazrati and Erfanian [153]	APNN, 2 classes (left or right hand), BCI competition 2003, data set III
	Haselsteiner and Pfurtscheller [154]	TDNN, 2 classes (left or right hand)
	Siuly et al. [155]	Naïve Bayes, 2 classes, Dataset IVa and IVb, BCI Competition III
	Obermaier et al. [156]	HMM, 2 classes (left or right hand)
	Suk and Lee [157]	HMM, Dataset IIa, BCI Competition IV (2008), 4 classes (left or right hand, feet, tongue)
	Bashar et al. [89]	kNN, 2 classes (left or right hand), BCI Competition 2003 data set (motor imagery III)
	Bashar and Bhuiyan [158]	BCI Competition II data set (GRAZ motor imagery III)
	Diana Eva and Tarniceriu [159]	kNN, 2 classes (left or right hand), BCI Competition 2002

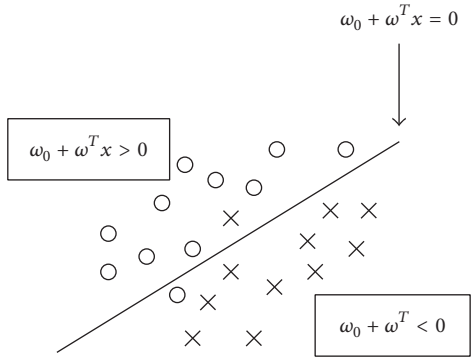

Figure 6: A hyperplane which separates two classes: the "circles" and the "crosses" [186].

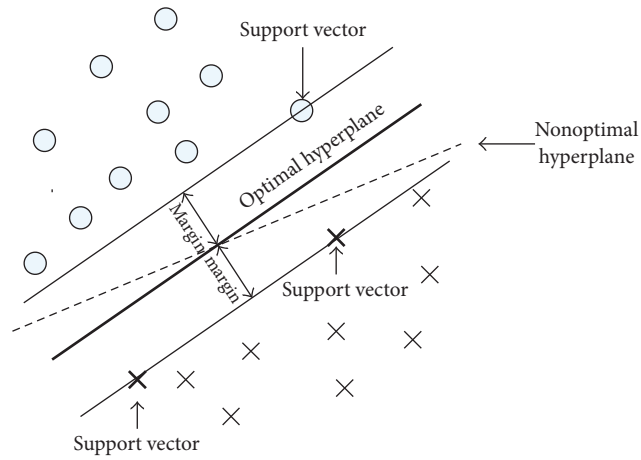

Figure 7: SVM find the optimal hyperplane for generalization [187].

Additionally, FLDA is simple to use and generally provides good results. It has been successfully used in a variety of BCI systems. Since the main drawback is its linearity, it may provide poor results on complex nonlinear EEG data. This can be resolved by using a kernel function [212].

To classify the time-varying EEG signals better, an adaptive LDA classifier is needed. Kalman adaptive LDA (KALDA) is an adaptive version of LDA based on Kalman filtering, in which the Kalman gain changes the update coefficient and varies the adaptation speed according to the property of the data [147]. KALDA is a supervised classifier. Maggi et al. put forward a regularized linear discriminant analysis (RLDA) which is based on the modified samples covariance matrix method [127]. The RLDA included a boosting algorithm based on a cyclic minimization of the classification error in the training set and an algorithm for outlier rejection. The multiclass identification problem was solved by means of a combination of binary classifiers using a one-versus-all approach.

3.3.2. Support Vector Machines (SVM). SVMs are becoming popular in a wide variety of biological applications [213]. A SVM is a computer algorithm that learns by example to assign labels to objects. It is also discriminates classes by constructing a linear optimal hyperplane, which is induced from the maximum margin principle between two classes [214]. The selected hyperplane is the one that maximizes the margins, that is, the distance from the nearest training points (see Figure 7). Also, the OVR strategy is used for multiclass BCI.

One of the major advantages of the SVM approach is its flexibility. Using the basic concepts of maximizing margins, duality, and kernels, the paradigm can be adapted to many types of inference problems [187]. Additionally, the usage of SVM is simple. The decision rule of SVM is a simple linear function in the kernel space which makes SVM stable and has a low variance. A low variance may be a key for low classification error in BCI because BCI features are very unstable over time. Furthermore, the robustness of SVM enables SVM to obtain ideal results even with very high dimensional feature vectors and a small training set. However, SVM classifiers have a longer computational time than others.

In order to maintain the classification accuracy and overall performance of the system, online classification and adaptive schemes which modify BCI classification parameters in real-time are particularly important. Jian and Tang applied One Again One Radial Basis Function Support Vector Machine (OAO RBF SVM) to classification in order to improve the short time window classification accuracy [35]. Moreover, they presented a signal quality evaluation method which cancelled the decision of the RBF SVM when signal quality was low and prone to be misclassified. Making no decision could reduce the cost of making a wrong decision. Oskoei et al. applied supervised and unsupervised adaptive schemes to online SVM that classified BCI data [149]. Online SVM processed fresh samples as they came and updated existing support vectors without referring to pervious samples. It was shown that the performance of online SVM was similar to that of the standard SVM, and both supervised and unsupervised schemes improved the classification hit rate. To reduce the time-consuming training sessions, there are also semisupervised SVM learning algorithms. Li et al. designed a Self-Training Semisupervised SVM algorithm for classification in small training data cases [139]. This algorithm converges fast and has low computational burden. They illustrated that the algorithm can be used to significantly reduce training efforts and improve adaptability of a BCI system.

3.3.3. Neural Networks. Neural networks are highly efficient in classification of data and are similar to the working of the human neurons. The method is especially useful when a perfectly algorithmic solution cannot be formulated, but adequate data must be available. Considering these features, a neural network is the best possible solution to classify the BCI. Among all the neural networks used in BCI, the Multilayer Perception (MLP) is the most widely used methods.

MLP is a feedforward artificial NN, in which the Backpropagation (BP) network is the most famous and active model in all the feedforward neural networks. Its kernel is the BP algorithm. BP neural network consists of input layers, hidden layers, and output layers. The number of hidden layers is determined by practical situations. The relationship

between the input pattern and the corresponding output pattern can be obtained by learning arithmetic and can be any nonlinear function.

Besides, there are many other neural networks used in the field of BCI, such as Convolutional Neural Network (CNN), CCA-NN, Learning Vector Quantization (LVQ) Neural Network, Multilayer Neural Network (MNN), Adaptive Probabilistic Neural Network (APNN), Time Delay Neural Network (TDNN), and Time-Dependent Neural Networks (TDNN). Table 3 lists partial practices in different EEG paradigms.

3.3.4. Bayesian Classifiers. The classification principle of the Bayesian classifier is to calculate the posterior probability using Bayesian formulas according to the prior probability of an object, namely, the probability of some class to which the object belongs. The class with the highest posterior probability is the one to which the object belongs. Bayesian classifiers mainly include naïve Bayes classifier, Hidden Markov Model (HMM), and Bayesian Graphical Network (BGN). All these classifiers produce nonlinear decision boundaries. They are generative, which enables them to perform more efficient rejection of uncertain samples than discriminative classifiers. However, Bayesian classifiers are not as widespread as linear classifiers or Neural Networks in BCI applications. The naïve Bayes classifier and HMM have been employed for BCI, but BGN is not commonly used because of its long computational time.

The naïve Bayes classifier greatly simplifies learning by assuming that features are independent given class. Although independence is generally a poor assumption, in practice naïve Bayes often competes well with more sophisticated classifiers [215]. The naïve Bayes classifier is mainly used in motor imagery.

HMMs are very efficient for the classification of time series. They are popular in the field of speech recognition and signal processing, and recently they have been applied to mental task classification of temporal sequences of BCI features and even to the classification of raw EEG. HMMs can also naturally accommodate variable-length models, permit reading of these models, and make sense of them. There are some applications using it in SSVEP, P300, and MI.

3.3.5. Nearest Neighbor Classifiers. These classifiers are very simple. A feature vector is assigned to a class with respect to its nearest neighbor(s). The neighbor can be a feature vector or a class prototype. If the number of samples is large, it makes sense to use it, instead of the single nearest neighbor. The majority vote of the nearest k neighbors is called k Nearest Neighbor (kNN). kNN is the most widely used classifier among nearest neighbor classifiers.

kNN classifier is rarely applied in SSVEP and P300. However, it has a good performance in MI and has a higher accuracy rate than many other classifiers, such as LDA, Naïve Bayes, and SVM.

Recently, the combination of several classifiers has been employed to solve the feature classifications in BCI. The combination of similar classifiers may outperform the use of the individual classifiers on its own. There are many strategies of classifier combination in BCI applications, such as Boosting [216], Voting [217], and Stacking [218]. Here, we will not explain them in detail. The detailed explanations can be found in the referenced paper [210].

4. Typical BRI Systems

4.1. Wheelchair Control. As a simple intelligent device, a wheelchair is primarily considered as a BCI-based control object because of its small degree of freedom (DOF). Galán et al. designed an asynchronous and noninvasive EEG-based BCI for continuous mental control of a wheelchair. The subject was able to mentally drive both a real and a simulated wheelchair from a starting point to a goal along a prespecified path by executing three different mental tasks (left hand imagination movement to turn left, rest to go forward, and word association to turn right) [219]. Iturrate et al. used a noninvasive brain-actuated wheelchair that relied on a P300 neurophysiological protocol to realize an autonomous navigation system which drove the wheelchair to the desired location while avoiding collisions with obstacles in the environment detected by the laser scanner [220]. Rebsamen et al. used a slow P300-based BCI to select a destination among a list of predefined locations and a faster MI-based BCI to stop the wheelchair, which provides mobility to BCI users in a safe way [221]. Philips et al. developed an adaptive shared control system of a brain-actuated simulated wheelchair aiming at providing an extra assistance when a subject was in difficult situations. Despite three possible discrete mental steering commands of forward, left, and right, three levels of assistance, including collision avoidance, obstacle avoidance, and orientation recovery, would be triggered whenever the user had difficulties in driving the wheelchair towards the goal [222]. Vanacker et al. introduced a shared control system that helped the subject in driving an intelligent wheelchair with a noninvasive brain interface. The subject's steering intentions were estimated from EEG signals and passed through to the shared control system before being sent to the wheelchair motors [223]. Li et al. proposed a hybrid BCI system combining P300 and SSVEP to improve the performance of asynchronous control and applied the paradigm to produce a "go/stop" command in real-time wheelchair control [224]. In this way, the wheelchair probably plays the role of a human's legs, which guides the disabled or elderly to the place where they want to go.

4.2. Manipulator Control. Manipulators mainly refer to a variety of robot arms and mechanical prosthetics. Most of the manipulators have a relatively small DOF, which are able to imitate a human's arm to finish different kinds of tasks. Palankar et al. applied a P300 BCI to control a 7-DOF wheelchair-mounted robotic arm. The BCI interface consists of 15 stimuli corresponding to 14 movements of the robot arm and one stop command, which interpret the user's intention to direct the robot along a step-by-step path to a desired position [225]. Li et al. proposed a BMI system to perform the motion of a serial manipulator in the whole workspace. Small-world neural network (SWNN) was used to classify five brain states based on motor imagery and shared

control. The control strategy used six 2-tuple commands to achieve motion control of the manipulator in 3D Cartesian space [226]. Iáñez et al. used four cognitive processes or "tasks" and a rest state to control a robot arm with 6 DOF [227]. Pohlmeyer et al. let a marmoset monkey control the movements of a robot arm for a reaching task using a reinforcement learning (RL) BMI. The monkey was required to move a robot arm to one of two LED targets to receive a food reward [228]. Wang et al. presented a protocol for a three-mode MI-based BCI, in which left/right hand and foot motor imageries were adopted. The three modes constructed eight commands to control a 5-DOF robotic arm to finish "left," "right," "up," "down," "ahead," "aback," "hold," and "put." Using the system, the subject was able to move the robotic arm to an appropriate position from the initial position to grab an object, put the object down in a designated position, and move the arm back to the initial position [229]. Elstob and Secco developed a low cost EEG-based BCI prosthetic using MI and realized the open or close of the whole hand by detecting the left or right MI [230]. Müller-Putz and Pfurtscheller used four red LED bars mounted on the hand prosthesis to elicit SSVEP and controlled the prosthesis to finish the tasks of turning right/left and opening/closing hand [21]. Here, controlling a manipulator mainly aims at dealing with some grasping and carrying objects, which takes the place of a human's arms in the BRI system.

4.3. Drone Control. Drones are becoming more and more popular in our daily lives. They are widely used in transportation, air shooting, and entertainment. In the application of BRI, Chen et al. established an SSVEP-based BCI system using fuzzy tracking and control algorithm on an air swimmer drone vehicle. The air swimmer drone vehicle was able to elevate, dive, turn left, go forward, and turn right. The system aims at helping subjects with amyotrophic lateral sclerosis (ALS) participate in communication or entertainment [231]. Kos'Myna et al. put forward a bidirectional feedback in MI BCIs, in which the subject was able to control a drone within 5 minutes. They applied the system to the piloting of an AR.Drone 2.0 Quadcopter to do tasks involving taking off, flying in a straight line until a target is reached, and landing the drone [232]. Doud et al. used a MI-based BCI to realize a continuous control of a virtual helicopter through golden rings positioned and oriented randomly throughout a 3D virtual space [233]. In addition, LaFleur et al. realized a quadcopter control in three-dimensional space using a noninvasive MI-based BCI. The subject could pilot the AR Drone Quadcopter safely through suspended-foam rings with the help of the visual feedback of the quadcopter's video on the computer screen [234]. Due to its flexibility and diversity, the drone is a good option for the disabled to communicate with the world.

4.4. Humanoid Robot Control. One of the greatest challenges to the BRI systems is the control a humanoid robot, because it has very complex mechanical kinematics and dynamics characters. Bell et al. established an EEG-based BCI interface that can be used to command a partially autonomous humanoid robot to perform complex tasks such as walking to specific locations and picking up desired objects [235]. Li et al. used a 32-channel EEG device to acquire a subject's brainwaves and controlled a humanoid robot, KT-X PC robot, by identifying mental activities when the subject was thinking "turning right," "turning left," or "walking forward." By doing this, they primarily investigated the relationship between complex humanoid robot behaviors and human mental activities [236, 237]. Zhao et al. developed an OpenViBE-based brainwave control system for Cerebot and used the platform to control a humanoid robot NAO to finish four robot-walking behaviors: turning right, turning left, walking forward, and walking backward [27].

In this section, we focus on the development of BRI system from synchronous to asynchronous systems. The controlled objects mainly aim at humanoid robots. Tables 4 and 5 list some BRI applications of controlling humanoid robots with synchronous and asynchronous BCI, respectively.

Table 4 shows that NAO is the most commonly used humanoid robot in BRI systems. There is a wide application for humanoid robots used in BCI including SSVEP, P300, MI, and even their hybrids. Most of them are synchronous systems. Even though the asynchronous BCI systems have been explored a lot in theory, the practical application techniques in social environment are still immature. This is because the detection of idle state is difficult and complex, and the additional classification of idle state is at the cost of accuracy. Therefore, the accuracy of the classification in an asynchronous BRI system often cannot satisfy an operator's demands.

Additionally, the BRI system is still on the level of lab research, and there are few applications currently available. Still, some BRI systems based on BCI have realized online control of intelligent peripherals and feedback. New application systems are emerging continuously. The BRI system has applications in medical and nonmedical fields. In the medical field, patients with a normal functioning mind but a disabled body can use the BRI system to communicate with others and control some intelligent peripherals, such as an intelligent wheelchair, mechanical prosthesis, virtual typewriter, or humanoid robot. While in the nonmedical field, the BRI system can be applied to state supervising of the operator, games, general amusement, and smart homes.

To realize the practical application in daily lives, the safety of the BRI system will be the most significant factor. Considering the safety of the operator, the concept of "brain switch" is put forward. Namely, the brain switch avoids generating task commands in a nontask state, so the brain switch plays an important role in a practical BRI system. For example, when operating a wheelchair or prosthesis, a trigger error may put the operator in danger. The asynchronous BCI system provides a solution by acting as a brain switch. The asynchronous BCI system detects the idle state of brain activities and prevents the output of the control commands while idle. Most BCIs are based on synchronous protocols where the operator must follow a fixed repetitive scheme to switch from one mental task to the next. In these synchronous BCI systems, the EEG recognized phenomena are time-locked to a cue, with a typical trial lasting 4 to 10 s or longer. In contrast, asynchronous BCI relies on asynchronous protocols

Table 4: Control of a humanoid robot with synchronous BCI.

EEG paradigms	Authors	Robot model	Control commands
SSVEP	Güneysu and Akin [34]	NAO	Left, right, down, up (hand)
	Zhao et al. [160]	NAO	Turn left, right, walk forward, backward for one-step walking, turn left, right, move forward, stop for continuous walking, head left, right, camera selecting top or bottom, object grasping and lifting
	Caglayan and Arslan [36]	Kondo KHR-3HV	Raise left or right arm
	Zhao et al. [28]	NAO	Walk forward and backward, turning left and right
	Gergondet et al. [23]	HRP-2	Walk forward and backward, turning left and right
	Wang et al. [161]	NAO	Human face detection and tracking
P300	Zhao et al. [28]	NAO	Walk forward and backward, shift left and right, turn left and right
	Li et al. [162]	NAO	Walk forward and backward, shift left and right, turn left and right
	Tang et al. [163]	NAO	Turn left and right (with different angle), move forward (with different speed), stand up, sit down, wave hand, turn on/off the system
	Liu et al. [164]	Adult-size robot	Walk forward and backward, turn left and right
MI	Bouyarmane et al. [165]	Humanoid robot HRP2	Go up and down
	Batula et al. [166]	DARwIn-OP	Walk forward and backward, turn left and right
	Cohen et al. [167]	HOAP3	Walk forward, turn left and right
P300+MI	Finke et al. [19]	Honda's Humanoid Robot	Walk forward and backward, sidestep left and right, turn left and right
SSVEP+MI	Duan et al. [20]	NAO	Walk forward, turn left and right, grasp motion

Table 5: Control of a humanoid robot with asynchronous BCI.

EEG paradigms	Authors	Robot model	Control commands
SSVEP	Deng et al. [168]	HanGood HGR-3M	Turn left, right, walk forward, stop
MI	Jiang et al. [169]	NAO	Walk forward, stop, turn left and right
	Jiang et al. [170]	NAO	Stop motion, open/close hand, shoulder up and down, elbow up and down
	Chae et al. [33]	NAO	Head left and right, body left and right, walk forward, stop
SSVEP+P300+MI	Choi and Jo [171]	NAO	Walk forward, body turn, head turn, object recognition

in which the operator makes voluntary, self-paced decisions on when to stop performing a BCI task and when to start the next one. This makes the system very flexible and natural to operate and yields rapid response times [238].

5. Future Perspectives

Over past years, a number of research groups have had success with EEG-based BCI paradigms, including SSVEP, ERP, MI, and their hybrids. Some BRI groups have demonstrated that some BRI systems have the potential for BRI practical applications, such as assisting the elders or disabled persons in daily tasks. However, there are still many technical problems with BCI and BRI that need to be addressed, especially with humanoid robots interaction. In the following, we summarize some difficulties and challenges in future research.

5.1. Novel EEG Evoking Patterns. The existing EEG evoking patterns have developed rapidly with respect to principles, coding, and decoding. The classification accuracy has not reached the maturity to control intelligent devices outside a laboratory setting. For example, the visual evoking patterns SSVEP and ERP need visual stimuli equipment, while the MI pattern has the disadvantages of long training time, limited commands, and relatively low classification accuracy. Therefore, novel EEG evoking patterns are essential to begin a new epoch for BCI development. Novel EEG evoking patterns mainly focus on being free of visual stimuli, applying more

efficient algorithms to generate more decoding commands, and evoking higher classification accuracy.

5.2. Adaptive EEG Decoding Methods. The performance of BCI varies from one person to another and is easily affected by an operator's mental state. To obtain a good performance in the BCI system, the operator must be trained for a while, especially for MI. Therefore, the generality of EEG decoding methods remains unsolved. Considering the similarities and differences among humans, adaptive EEG decoding methods need to be designed so the classification models have a better performance with respect to self-studying and self-correcting. Liu et al. adaptively change repetition number by comparing the classification results with a threshold [239]; Jin et al. detected the same target stimulus twice in limited repetitions, by automatically adjusting the repetition number [240]. In theory, an adaptive classification method plays an important role in online BRI systems.

5.3. Portable EEG Device. In a BCI system, the acquisition of the brain signals is the primary function and is the key in guaranteeing the stability and accuracy of the system. With the development of the sensors and amplifiers, the noise attached to the brain signals can be largely restrained. Even though an EEG device has high-precision and high reliability, such as the Cerebus, it is heavy and not portable. Even though the Emotive EPOC is more portable than Cerebus, it has limited channels, which makes it not suitable for multichannel analysis. In the visual evoking paradigms, such as SSVEP or P300, an evoking device is essential, but a LCD screen or a LED device is not suitable for real-world application. A more portable EEG acquisition device is needed and a wearable visual evoking device, such as a Google glass, may solve the problem.

5.4. Dynamics and Kinematics and Control Architecture of Robots. In terms of interaction between humans and robots, the dynamics and kinematics of robots are supposed to greatly influence the performance of a BRI system, whether for wheelchairs, manipulator, drones, or humanoid robots. On one hand, the dynamics determines the motion characters, such as the speed, acceleration, and stability. In addition, the dynamics of robots can solve the matching problem between the robot's motion and the information transfer rate (ITR) of BCI. The research of dynamics is used to calculate the time cost of each motion of a robot, which can give guidance for choosing the corresponding ITR. Thus, the entire executing efficiency of a BRI system will be improved greatly. On the other hand, the kinematics of robots plays an important role in path planning, path optimizing, and global path modeling.

A humanoid robot has an especially sophisticated control architecture that consists of sensor fusion, modeling, path planning, and motion control. Solving these problems will greatly prompt the development of BRI in three ways. First, a humanoid robot is generally equipped with different kinds of sensors, such as sonars, cameras, bumpers, and GPS. Taking advantage of the robot's intelligence will assist the operator to finish tasks more efficiently and relieves the mental pressure of the operator. Second, a humanoid robot has a complex mechanical kinematics and dynamics problem, but it can friendly interact with users. Therefore, the application of a humanoid robot in BRI system is becoming more and more popular. Modeling a humanoid robot's mechanical kinematics and dynamics can keep the robot upright walking and assist in path planning and motion control. Third, the former BRI systems mostly control the humanoid robot at a low level and do not combine the operator's intention with the intelligence of the robot for higher level decision making. How and when the brain signals are inserted into the BCI are important considerations for BRI development. For example, path planning can be realized by a camera and GPS, which will never or rarely need the involvement of brain signals. Brain signals only play a role in supervising the process and gives guidance in the case of an emergency. Thus, a human does not need to care about the detailed path a humanoid robot develops but just needs to set a destination. When an emergency occurs, a humanoid robot will be prevented from creating a path and the operator must maneuver via brain signals. Last, there will be conflicts between the user and the robot, so it becomes quite significant to find an appropriate solution to these conflicts. Developing a strategy to find the optimal balance between automation and operator control will be the vital issue in solving the problem.

5.5. Evaluation Index System. A system usually needs evaluation indexes to judge its performance. A good evaluation index system should be suitable for different types of systems. For BCI systems, the commonly used evaluation indexes are classification accuracy and ITR. However, both indexes only judge a single experiment of a subject. When conducting the same BCI experiment on the same subject, the indexes must be recalculated. Therefore, the indexes are not adaptive even to the same subject. Average values may solve the problem, but they will cover the differences of the same subject in different spirit status. The evaluation index system of the BCI needs not only classification accuracy and ITR, but also indexes that are able to represent the differences in the same subject. Additionally, the evaluation index system should comprehensively evaluate the entire performance of a BCI system for different subjects.

5.6. Individual Differences. The character and amplitude of the brain signal vary from person to person, which leads to the individual differences in the sensitivity and performance of BRI systems. Usually, a person who is familiar with the experimental procedure or has experimental experience will have a high accuracy rate. It is possible for some persons to have a terrible performance in EEG-based BRI systems even after a long training period. Particularly, the MI training process always takes a long time for people to master the skills. Therefore, how to diminish the individual differences between persons still remains to be solved. Additionally, the existing BRI systems mainly use normal functioning people as volunteers, even though there are some applications for special people such as the elderly and patients with neurological conditions. Many experiments are needed to explore the individual differences between a normal functioning person

and the disabled or the elderly, for the application of the BRI systems as a service.

5.7. Combination of EEG with Other Detecting Means. Despite EEG-based brain signal detecting, there are also many other modern devices capable of detecting a person's brain activity. Some researchers attempted to explore brain activities by combining EEG with functional near infrared spectroscopy (fNIRS) and functional magnetic resonance imaging (fMRI). For instance, Leamy et al. combined fNIRS and EEG to improve motor cortex activity classification during an imagined movement-based task [241]. Putze et al. developed a hybrid BCI which uses EEG and fNIRS to discriminate and detect visual and auditory stimulus processing and found the fusion of the two significantly increased accuracies [242]. Mulert et al. integrated fMRI and EEG to understand brain activities in an auditory oddball paradigm and the results suggest their combination results in an improved understanding of the spatiotemporal dynamics of brain activity [243]. With the emerging of the combination of EEG with other brain signal detecting methods, this technique will be particularly useful in the design of BCI devices and BRI systems.

Conflicts of Interest

The authors declare that there are no conflicts of interest regarding the publication of this paper.

Acknowledgments

This research work was funded by the National Natural Science Foundation of China under Grant no. 61473207.

References

[1] S. Amiri, A. Rabbi, L. Azinfar et al., "A review of P300, SSVEP, and hybrid P300/SSVEP brain-computer interface systems," in *Brain-Computer Interface Systems—Recent Progress and Future Prospects*, InTech, 2013.

[2] M. D. Serruya, N. G. Hatsopoulos, L. Paninski, M. R. Fellows, and J. P. Donoghue, "Brain-machine interface: instant neural control of a movement signal," *Nature*, vol. 416, no. 6877, pp. 141–142, 2002.

[3] B. Wodlinger, J. E. Downey, E. C. Tyler-Kabara, A. B. Schwartz, M. L. Boninger, and J. L. Collinger, "Ten-dimensional anthropomorphic arm control in a human brain-machine interface: difficulties, solutions, and limitations," *Journal of Neural Engineering*, vol. 12, no. 1, Article ID 016011, 2015.

[4] J. R. Wolpaw, N. Birbaumer, W. J. Heetderks et al., "Brain-computer interface technology: a review of the first international meeting," *IEEE Transactions on Rehabilitation Engineering*, vol. 8, no. 2, pp. 164–173, 2000.

[5] A. Burns, H. Adeli, and J. A. Buford, "Brain-computer interface after nervous system injury," *Neuroscientist*, vol. 20, no. 6, pp. 639–651, 2014.

[6] A. Ortiz-Rosario and H. Adeli, "Brain-computer interface technologies: from signal to action," *Reviews in the Neurosciences*, vol. 24, no. 5, pp. 537–552, 2013.

[7] A. B. Schwartz, "Cortical neural prosthetics," *Annual Review of Neuroscience*, vol. 27, pp. 487–507, 2004.

[8] M. A. Lebedev and M. A. L. Nicolelis, "Brain-machine interfaces: past, present and future," *Trends in Neurosciences*, vol. 29, no. 9, pp. 536–546, 2006.

[9] E. M. Schmidt, "Single neuron recording from motor cortex as a possible source of signals for control of external devices," *Annals of Biomedical Engineering*, vol. 8, no. 4, pp. 339–349, 1980.

[10] M. A. L. Nicolelis, "Brain–machine interfaces to restore motor function and probe neural circuits," *Nature Reviews Neuroscience*, vol. 4, no. 5, pp. 417–422, 2003.

[11] L. R. Hochberg, D. Bacher, B. Jarosiewicz et al., "Reach and grasp by people with tetraplegia using a neurally controlled robotic arm," *Nature*, vol. 485, no. 7398, pp. 372–375, 2012.

[12] A. B. Schwartz, X. T. Cui, D. J. Weber, and D. W. Moran, "Brain-controlled interfaces: movement restoration with neural prosthetics," *Neuron*, vol. 52, no. 1, pp. 205–220, 2006.

[13] J. R. Wolpaw, N. Birbaumer, D. J. McFarland, G. Pfurtscheller, and T. M. Vaughan, "Brain-computer interfaces for communication and control," *Clinical Neurophysiology*, vol. 113, no. 6, pp. 767–791, 2002.

[14] J. Ibáñez, J. I. Serrano, M. D. del Castillo, J. A. Gallego, and E. Rocon, "Online detector of movement intention based on EEG—application in tremor patients," *Biomedical Signal Processing and Control*, vol. 8, no. 6, pp. 822–829, 2013.

[15] S. Waldert, H. Preissl, E. Demandt et al., "Hand movement direction decoded from MEG and EEG," *Journal of Neuroscience*, vol. 28, no. 4, pp. 1000–1008, 2008.

[16] S. Coyle, T. Ward, C. Markham, and G. McDarby, "On the suitability of near-infrared (NIR) systems for next-generation brain-computer interfaces," *Physiological Measurement*, vol. 25, no. 4, pp. 815–822, 2004.

[17] T. M. Vaughan, W. J. Heetderks, L. J. Trejo et al., "Brain-computer interface technology: a review of the Second International Meeting," *IEEE Transactions on Neural Systems & Rehabilitation Engineering A Publication of the IEEE Engineering in Medicine & Biology Society*, vol. 11, no. 2, pp. 94–109, 2003.

[18] M. Alimardani, N. Shuichi, and H. Ishiguro, "The effect of feedback presentation on motor imagery performance during BCI-teleoperation of a humanlike robot," in *Proceedings of the 5th IEEE RAS and EMBS International Conference on Biomedical Robotics and Biomechatronics (BioRob '14)*, pp. 403–408, IEEE, São Carlos, Brazil, August 2014.

[19] A. Finke, A. Knoblauch, H. Koesling, and H. Ritter, "A hybrid brain interface for a humanoid robot assistant," in *Proceedings of the 33rd Annual International Conference of the IEEE Engineering in Medicine and Biology Society (EMBS '11)*, pp. 7421–7424, September 2011.

[20] F. Duan, D. Lin, W. Li, and Z. Zhang, "Design of a multimodal EEG-based hybrid BCI system with visual servo module," *IEEE Transactions on Autonomous Mental Development*, vol. 7, no. 4, pp. 332–341, 2015.

[21] G. R. Müller-Putz and G. Pfurtscheller, "Control of an electrical prosthesis with an SSVEP-based BCI," *IEEE Transactions on Biomedical Engineering*, vol. 55, no. 1, pp. 361–364, 2008.

[22] D. Coyle, J. Garcia, A. R. Satti, and T. M. McGinnity, "EEG-based continuous control of a game using a 3 channel motor imagery BCI: BCI game," in *Proceedings of the IEEE Symposium on Computational Intelligence, Cognitive Algorithms, Mind, and Brain (CCMB '11)*, pp. 1–7, IEEE, Singapore, April 2011.

[23] P. Gergondet, S. Druon, A. Kheddar, C. Hintermüller, C. Guger, and M. Slater, "Using brain-computer interface to steer a humanoid robot," in *Proceedings of the IEEE International*

Conference on Robotics and Biomimetics (ROBIO '11), pp. 192–197, December 2011.

[24] J. Zhao, W. Li, X. Mao, and M. Li, "SSVEP-based experimental procedure for brain-robot interaction with humanoid robots," *Journal of Visualized Experiments*, vol. 2015, no. 105, 2015.

[25] M. Li, W. Li, and H. Zhou, "Increasing N200 potentials via visual stimulus depicting humanoid robot behavior," *International Journal of Neural Systems*, vol. 26, no. 1, Article ID 1550039, 2016.

[26] W. Li, M. Li, and W. Li, "Independent component analysis-based channel selection to achieve high performance of N200 and P300 classification," in *Proceedings of the IEEE 14th International Conference on Cognitive Informatics & Cognitive Computing*, pp. 384–389, IEEE, Beijing, China, July 2015.

[27] J. Zhao, Q. Meng, W. Li et al., "An OpenViBE-based brainwave control system for Cerebot," in *Proceedings of the IEEE International Conference on Robotics and Biomimetics*, pp. 1169–1174, Shenzhen, China, December 2013.

[28] J. Zhao, W. Li, and M. Li, "Comparative study of SSVEP- and P300-based models for the telepresence control of humanoid robots," *PLoS ONE*, vol. 10, no. 11, Article ID e0142168, 2015.

[29] L. Yao, J. Meng, X. Sheng, D. Zhang, and X. Zhu, "A novel calibration and task guidance framework for motor imagery BCI via a tendon vibration induced sensation with kinesthesia illusion," *Journal of Neural Engineering*, vol. 12, no. 1, Article ID 016005, 2015.

[30] H. Wang, T. Li, and Z. Huang, "Remote control of an electrical car with SSVEP-Based BCI," in *Proceedings of the IEEE International Conference on Information Theory and Information Security (ICITIS '10)*, pp. 837–840, December 2010.

[31] Q. Li, J. Li, S. Liu et al., "Improving the performance of P300-speller with familiar face paradigm using support Vector machine ensemble," in *Proceedings of the International Conference on Network and Information Systems for Computers*, pp. 606–610, January 2015.

[32] C.-Y. Chen, C.-W. Wu, C.-T. Lin, and S.-A. Chen, "A novel classification method for motor imagery based on Brain-Computer Interface," in *Proceedings of the International Joint Conference on Neural Networks (IJCNN '14)*, pp. 4099–4102, July 2014.

[33] Y. Chae, J. Jeong, and S. Jo, "Toward brain-actuated humanoid robots: asynchronous direct control using an EEG-Based BCI," *IEEE Transactions on Robotics*, vol. 28, no. 5, pp. 1131–1144, 2012.

[34] A. Güneysu and H. L. Akin, "An SSVEP based BCI to control a humanoid robot by using portable EEG device," in *Proceedings of the International Conference of the IEEE Engineering in Medicine & Biology Society*, pp. 6905–6908, 2013.

[35] H.-L. Jian and K.-T. Tang, "Improving classification accuracy of SSVEP based BCI using RBF SVM with signal quality evaluation," in *Proceedings of the International Symposium on Intelligent Signal Processing and Communication Systems (ISPACS '14)*, pp. 302–306, December 2014.

[36] O. Caglayan and R. B. Arslan, "Humanoid robot control with SSVEP on embedded system," in *Proceedings of the 5th International Brain-Computer Interface Meeting: Defining the Future*, pp. 260–261, June 2013.

[37] S. M. T. Muller, T. F. Bastos-Filho, and M. Sarcinelli-Filho, "Using a SSVEP-BCI to command a robotic wheelchair," in *Proceedings of the IEEE International Symposium on Industrial Electronics (ISIE '11)*, pp. 957–962, IEEE, Gdansk, Poland, 2011.

[38] R. C. Panicker, S. Puthusserypady, and Y. Sun, "An asynchronous P300 BCI with SSVEP-based control state detection," *IEEE Transactions on Biomedical Engineering*, vol. 58, no. 6, pp. 1781–1788, 2011.

[39] W. Song, X. Wang, S. Zheng, and Y. Lin, "Mobile robot control by BCI based on motor imagery," in *Proceedings of the 6th International Conference on Intelligent Human-Machine Systems and Cybernetics (IHMSC '14)*, pp. 383–387, August 2014.

[40] G. Schalk, D. J. McFarland, T. Hinterberger, N. Birbaumer, and J. R. Wolpaw, "BCI2000: a general-purpose brain-computer interface (BCI) system," *IEEE Transactions on Biomedical Engineering*, vol. 51, no. 6, pp. 1034–1043, 2004.

[41] G. Pfurtscheller, "Functional brain imaging based on ERD/ERS," *Vision Research*, vol. 41, no. 10-11, pp. 1257–1260, 2001.

[42] E. Sellers, Y. Arbel, and E. Donchin, "BCIs that uses event related potentials," in *Brain-Computer Interfaces: Principles and Practice*, J. Wolpaw and E. W. Wolpaw, Eds., p. 300, Oxford University Press, 2012.

[43] W. Sittiprapaporn, "The design and interpretation of EEGs, FFTs, visual EPs, auditory EPs and auditory P300 ERPs studies with topographic brain mapping," *Journal of Engineering and Applied Sciences*, vol. 7, no. 6, pp. 399–404, 2012.

[44] R. Veit, U. Strehl, T. Hinterberger, M. Erb, W. Grodd, and N. Birbaumer, "Self-regulation of slow cortical potentials: an event-related fMRI study," *NeuroImage*, vol. 11, no. 5, article S32, 2000.

[45] B. Z. Allison, J. Jin, Y. Zhang, and X. Wang, "A four-choice hybrid P300/SSVEP BCI for improved accuracy," *Brain-Computer Interfaces*, vol. 1, no. 1, pp. 17–26, 2014.

[46] M. Wang, I. Daly, B. Z. Allison et al., "A new hybrid BCI paradigm based on P300 and SSVEP," *Journal of Neuroscience Methods*, vol. 244, pp. 16–25, 2015.

[47] L. Bi, K. Jie, X. Fan, and Y. Li, "A SSVEP Brain-computer Interface with the Hybrid Stimuli of SSVEP and P300," in *Proceedings of the ICME International Conference on Complex Medical Engineering (CME '13)*, pp. 211–214, Beijing, China, 2013.

[48] L. W. Ko, S. C. Lin, M. S. Song et al., "Developing a few-channel hybrid BCI system by using motor imagery with SSVEP assist," in *Proceedings of the International Joint Conference on Neural Networks (IJCNN '14)*, IEEE, Beijing, China, 2014.

[49] G. N. Ranky and S. Adamovich, "Analysis of a commercial EEG device for the control of a robot arm," in *Proceedings of the 2010 IEEE 36th Annual Northeast Bioengineering Conference*, pp. 1–2, IEEE, New York, NY, USA, 2010.

[50] D. A. Craig and H. T. Nguyen, "Adaptive EEG thought pattern classifier for advanced wheelchair control," in *Proceedings of the 32nd Annul International Conference of the IEEE Engineering in Medicine & Biology Society IEEE Engineering in Medicine & Biology Society*, pp. 2544–2547, IEEE, Lyon, France, 2007.

[51] S. Bozinovski and A. Bozinovski, "Mental states, EEG manifestations, and mentally emulated digital circuits for brain-robot interaction," *IEEE Transactions on Autonomous Mental Development*, vol. 7, no. 1, pp. 39–51, 2015.

[52] C. S. Crawford, M. Andujar, F. Jackson et al., "User experience evaluation towards cooperative brain-robot interaction," in *Proceedings of the International Conference on Human-Computer Interaction (HCI '15)*, pp. 184–193, Los Angeles, Calif, USA, 2015.

[53] F.-B. Vialatte, M. Maurice, J. Dauwels, and A. Cichocki, "Steady-state visually evoked potentials: focus on essential paradigms and future perspectives," *Progress in Neurobiology*, vol. 90, no. 4, pp. 418–438, 2010.

[54] E. Basar, T. Demiralp, M. Schürmann, C. Basar-Eroglu, and A. Ademoglu, "Oscillatory brain dynamics, wavelet analysis, and cognition," *Brain and Language*, vol. 66, no. 1, pp. 146–183, 1999.

[55] D. Regan, "Some characteristics of average steady-state and transient responses evoked by modulated light," *Electroencephalography and Clinical Neurophysiology*, vol. 20, no. 3, pp. 238–248, 1966.

[56] K. Nakayama and M. Mackeben, "Steady state visual evoked potentials in the alert primate," *Vision Research*, vol. 22, no. 10, pp. 1261–1271, 1982.

[57] G. Rager and W. Singer, "The response of cat visual cortex to flicker stimuli of variable frequency," *European Journal of Neuroscience*, vol. 10, no. 5, pp. 1856–1877, 1998.

[58] D. Zhu, J. Bieger, G. G. Molina, and R. M. Aarts, "A survey of stimulation methods used in SSVEP-based BCIs," *Computational Intelligence and Neuroscience*, vol. 2010, Article ID 702357, 12 pages, 2010.

[59] L. A. Farwell and E. Donchin, "Talking off the top of your head: toward a mental prosthesis utilizing event-related brain potentials," *Electroencephalography and Clinical Neurophysiology*, vol. 70, no. 6, pp. 510–523, 1988.

[60] M. S. Treder and B. Blankertz, "(C)overt attention and visual speller design in an ERP-based brain-computer interface," *Behavioral and Brain Functions*, vol. 6, no. 4, article 28, 13 pages, 2010.

[61] L. Acqualagna and B. Blankertz, "Gaze-independent BCI-spelling using rapid serial visual presentation (RSVP)," *Clinical Neurophysiology*, vol. 124, no. 5, pp. 901–908, 2013.

[62] J. Ding, G. Sperling, and R. Srinivasan, "Attentional modulation of SSVEP power depends on the network tagged by the flicker frequency," *Cerebral Cortex*, vol. 16, no. 7, pp. 1016–1029, 2006.

[63] H. H. Jasper, "The ten twenty electrode system of the international federation," *Electroencephalography & Clinical Neurophysiology*, vol. 10, pp. 371–375, 1958.

[64] C. S. Herrmann, "Human EEG responses to 1-100 Hz flicker: resonance phenomena in visual cortex and their potential correlation to cognitive phenomena," *Experimental Brain Research*, vol. 137, no. 3-4, pp. 346–353, 2001.

[65] Z. Wu, Y. Lai, Y. Xia, D. Wu, and D. Yao, "Stimulator selection in SSVEP-based BCI," *Medical Engineering and Physics*, vol. 30, no. 8, pp. 1079–1088, 2008.

[66] V. Bevilacqua, G. Tattoli, D. Buongiorno et al., "A novel BCI-SSVEP based approach for control of walking in Virtual Environment using a Convolutional Neural Network," in *Proceedings of the International Joint Conference on Neural Networks (IJCNN '14)*, pp. 4121–4128, July 2014.

[67] R. Ortner, B. Z. Allison, G. Korisek, H. Gaggl, and G. Pfurtscheller, "An SSVEP BCI to control a hand orthosis for persons with tetraplegia," *IEEE Transactions on Neural Systems and Rehabilitation Engineering*, vol. 19, no. 1, pp. 1–5, 2011.

[68] J. I. D. S. Júnior, S. N. D. C. Leite, T. B. D. S. Costa et al., "Spectral vs. canonical correlation analysis for feature extraction in BCI-SSVEP systems," in *Proceedings of the Brain Congress*, 2016.

[69] Y. Wang, Y.-T. Wang, and T.-P. Jung, "Visual stimulus design for high-rate SSVEP BCI," *Electronics Letters*, vol. 46, no. 15, pp. 1057–1058, 2010.

[70] Y. Zhang, G. X. Zhou, J. Jin, X. Wang, and A. Cichocki, "Frequency recognition in SSVEP-based BCI using multiset canonical correlation analysis," *International Journal of Neural Systems*, vol. 24, no. 4, Article ID 1450013, pp. 1072–1092, 2014.

[71] W. Nan, M. W. Chi, B. Wang et al., "A comparison of minimum energy combination and canonical correlation analysis for SSVEP detection," in *Proceedings of the 5th International IEEE/EMBS Conference on Neural Engineering (NER '11)*, pp. 469–472, Cancun, Mexico, April 2011.

[72] S. Pouryazdian and A. Erfanian, "Detection of steady-state visual evoked potentials for brain-computer interfaces using PCA and high-order statistics," in *Proceedings of the World Congress on Medical Physics and Biomedical Engineering*, vol. 25, no. 9, pp. 480–483, Munich, Germany, September 2009.

[73] A. Rakotomamonjy and V. Guigue, "BCI competition III: dataset II- ensemble of SVMs for BCI P300 speller," *IEEE Transactions on Biomedical Engineering*, vol. 55, no. 3, pp. 1147–1154, 2008.

[74] H. El Dabbagh and W. Fakhr, "Multiple classification algorithms for the BCI P300 speller diagram using ensemble of SVMs," in *Proceedings of the IEEE GCC Conference and Exhibition*, pp. 393–396, February 2011.

[75] J. N. Mak, D. J. McFarland, T. M. Vaughan et al., "EEG correlates of P300-based brain-computer interface (BCI) performance in people with amyotrophic lateral sclerosis," *Journal of Neural Engineering*, vol. 9, no. 2, Article ID 026014, 2012.

[76] Z. Lugo, J. Rodriguez, A. Lechner et al., "A vibrotactile P300-based brain-computer interface for consciousness detection and communication," *Clinical EEG and Neuroscience*, vol. 45, no. 1, pp. 14–21, 2014.

[77] F. Lotte and C. Guan, "An efficient P300-based brain-computer interface with minimal calibration time," in *Proceedings of the Assistive Machine Learning for People with Disabilities Symposium (NIPS'09)*, Vancouver, Canada, 2009.

[78] M. Spüler, M. Bensch, S. Kleih, W. Rosenstiel, M. Bogdan, and A. Kübler, "Online use of error-related potentials in healthy users and people with severe motor impairment increases performance of a P300-BCI," *Clinical Neurophysiology*, vol. 123, no. 7, pp. 1328–1337, 2012.

[79] A. Casagrande, J. Jarmolowska, M. Turconi et al., "PolyMorph: increasing P300 spelling efficiency by selection matrix polymorphism and sentence-based predictions," *Computer Science*, 2015.

[80] C. S. Syan and R. E. S. Harnarinesingh, "Comparison of preprocessing and classification techniques for single-trial and multi-trial P300-based brain computer interfaces," *American Journal of Applied Sciences*, vol. 7, no. 9, pp. 1219–1225, 2010.

[81] C. Park, D. Looney, N. Ur Rehman, A. Ahrabian, and D. P. Mandic, "Classification of motor imagery BCI using multivariate empirical mode decomposition," *IEEE Transactions on Neural Systems and Rehabilitation Engineering*, vol. 21, no. 1, pp. 10–22, 2013.

[82] C. Wang, K. S. Phua, K. A. Kai et al., "A feasibility study of non-invasive motor-imagery BCI-based robotic rehabilitation for stroke patients," in *Proceedings of the 4th International IEEE/EMBS Conference on Neural Engineering (NER '09)*, pp. 271–274, IEEE, Antalya, Turkey, May 2009.

[83] D. Devlaminck, B. Wyns, M. Grosse-Wentrup, G. Otte, and P. Santens, "Multisubject learning for common spatial patterns in motor-imagery BCI," *Computational Intelligence and Neuroscience*, vol. 2011, Article ID 217987, 2011.

[84] K. K. Ang, C. Guan, K. S. Phua et al., "Transcranial direct current stimulation and EEG-based motor imagery BCI for upper limb stroke rehabilitation," in *Proceedings of the International Conference of the IEEE Engineering in Medicine & Biology Society*, pp. 4128–4131, August 2012.

[85] J. Li and L. Zhang, "Active training paradigm for motor imagery BCI," *Experimental Brain Research*, vol. 219, no. 2, pp. 245–254, 2012.

[86] Y. Wu and Y. Ge, "A novel method for motor imagery EEG adaptive classification based biomimetic pattern recognition," *Neurocomputing*, vol. 116, pp. 280–290, 2013.

[87] B. Zhou, X. Wu, L. Zhang, Z. Lv, and X. Guo, "Robust spatial filters on three-class motor imagery EEG data using independent component analysis," *Journal of Biosciences and Medicines*, vol. 2, no. 2, pp. 43–49, 2014.

[88] N. Sharma and J.-C. Baron, "Does motor imagery share neural networks with executed movement: a multivariate fMRI analysis," *Frontiers in Human Neuroscience*, vol. 7, no. 2, article 564, 2013.

[89] S. K. Bashar, A. R. Hassan, and M. I. H. Bhuiyan, "Identification of motor imagery movements from EEG signals using Dual Tree Complex Wavelet Transform," in *Proceedings of the International Conference on Advances in Computing, Communications and Informatics (ICACCI '15)*, pp. 290–296, Kochi, India, August 2015.

[90] S. Mouli, R. Palaniappan, I. P. Sillitoe, and J. Q. Gan, "Performance analysis of multi-frequency SSVEP-BCI using clear and frosted colour LED stimuli," in *Proceedings of the 13th IEEE International Conference on BioInformatics and BioEngineering (BIBE '13)*, pp. 1–4, IEEE, Chania, Greece, November 2013.

[91] H.-J. Hwang, J.-H. Lim, Y.-J. Jung, H. Choi, S. W. Lee, and C.-H. Im, "Development of an SSVEP-based BCI spelling system adopting a QWERTY-style LED keyboard," *Journal of Neuroscience Methods*, vol. 208, no. 1, pp. 59–65, 2012.

[92] V. P. Oikonomou, G. Liaros, K. Georgiadis et al., "Comparative evaluation of state-of-the-art algorithms for SSVEP-based BCIs," 2016.

[93] P. F. Diez, V. A. Mut, E. M. Avila Perona, and E. Laciar Leber, "Asynchronous BCI control using high-frequency SSVEP," *Journal of NeuroEngineering and Rehabilitation*, vol. 8, no. 1, article 39, 2011.

[94] Z. Zhang, X. Li, and Z. Deng, "A CWT-based SSVEP classification method for brain-computer interface system," in *Proceedings of the International Conference on Intelligent Control and Information Processing (ICICIP '10)*, pp. 43–48, August 2010.

[95] M. Kumari and S. Somani, "Enhancing the Classification Accuracy of SSVEP based BCI using CWT method along with ANN," *International Journal of Advanced Research in Engineering & Management*, vol. 1, pp. 81–89, 2015.

[96] M. Huang, P. Wu, Y. Liu et al., "Application and contrast in brain-computer interface between Hilbert-Huang transform and wavelet transform," in *Proceedings of the International Conference for Young Computer Scientists*, pp. 1706–1710, IEEE Computer Society, 2008.

[97] X. G. Ruan, K. Xue, and M. Li, "Feature extraction of SSVEP-based brain-computer interface with ICA and HHT method," in *Proceedings of the 11th World Congress on Intelligent Control and Automation*, pp. 2418–2423, IEEE, June-July 2014.

[98] F. Zhang, C. Han, L. Li, X. Zhang, J. Xie, and Y. Li, "Research on high-frequency combination coding-based SSVEP-BCIs and its signal processing algorithms," *Shock and Vibration*, vol. 2015, Article ID 194230, 12 pages, 2015.

[99] G. G. Molina, D. Zhu, and S. Abtahi, "Phase detection in a visual-evoked-potential based brain computer interface," in *Proceedings of the 18th European Signal Processing Conference (EUSIPCO '10)*, pp. 949–953, August 2010.

[100] D. Zhu, G. Garcia-Molina, V. Mihajlović, and R. M. Aarts, "Online BCI implementation of high-frequency phase modulated visual stimuli," in *Universal Access in Human-Computer Interaction. Users Diversity: 6th International Conference, UAHCI 2011, Held as Part of HCI International 2011, Orlando, FL, USA, July 9–14, 2011, Proceedings, Part II*, vol. 6766 of *Lecture Notes in Computer Science*, pp. 645–654, Springer, Berlin, Germany, 2011.

[101] Y. Wang, Z. Zhang, X. Gao, and S. Gao, "Lead selection for SSVEP-based brain-computer interface," in *Proceedings of the 26th Annual International Conference of the IEEE Engineering in Medicine and Biology Society (EMBC '04)*, pp. 4507–4510, September 2004.

[102] T. Demiralp, A. Ademoglu, M. Schürmann, C. Basar-Eroglu, and E. Basar, "Detection of P300 waves in single trials by the wavelet transform (WT)," *Brain and Language*, vol. 66, no. 1, pp. 108–128, 1999.

[103] L. Vareka and P. Mautner, "Off-line analysis of the P300 event-related potential using discrete wavelet transform," in *Proceedings of the 36th International Conference on Telecommunications and Signal Processing (TSP '13)*, pp. 569–572, IEEE, July 2013.

[104] S. Guo, S. Lin, and Z. Huang, "Feature extraction of P300s in EEG signal with discrete wavelet transform and fisher criterion," in *Proceedings of the 8th International Conference on BioMedical Engineering and Informatics (BMEI '15)*, pp. 200–204, October 2015.

[105] W. Pan, S. Ji-Zhong, and S. J. He, "Research of P300 feature extraction algorithm based on wavelet transform and fisher distance," *International Journal of Education and Management Engineering*, vol. 1, no. 6, pp. 47–50, 2011.

[106] M. Viqueira, B. G. Zapirain, and A. Mendez, "Wavelet transform for the analysis of EEG signals in patients with oral communications problems," in *Proceedings of the 11th IEEE International Symposium on Signal Processing and Information Technology (ISSPIT '11)*, pp. 140–143, Bilbao, Spain, December 2011.

[107] K. Li, R. Sankar, Y. Arbel et al., "Single trial independent component analysis for P300 BCI system," in *Proceedings of the International Conference of the IEEE Engineering in Medicine & Biology Society*, pp. 4035–4038, IEEE, September 2009.

[108] A. Turnip, M. Siahaan, S. Suprijanto, and A. K. Waafi, "P300 detection using nonlinear independent component analysis," in *Proceedings of the 3rd International Conference on Instrumentation, Control and Automation (ICA '13)*, pp. 104–109, IEEE, August 2013.

[109] G. Pires, U. Nunes, and M. Castelo-Branco, "P300 spatial filtering and coherence-based channel selection," in *Proceedings of the 4th International IEEE/EMBS Conference on Neural Engineering (NER '09)*, pp. 311–314, May 2009.

[110] Z. Amini, V. Abootalebi, and M. T. Sadeghi, "Comparison of performance of different feature extraction methods in detection of P300," *Biocybernetics and Biomedical Engineering*, vol. 33, no. 1, pp. 3–20, 2013.

[111] T. Hiroyasu, Y. Ohkubo, and U. Yamamoto, "Electroencephalographic method using fast Fourier transform overlap processing for recognition of right- or left-handed elbow flexion motor imagery," in *Proceedings of the IEEE Symposium on Computational Intelligence in Brain Computer Interfaces (CIBCI '14)*, pp. 24–29, December 2014.

[112] J. Jin, X.-Y. Wang, and X. Zhang, "Recognition of right and left motor imagery based on energy features," *Journal of East China University of Science and Technology*, vol. 33, no. 4, pp. 536–540, 2007.

[113] W.-Y. Hsu and Y.-N. Sun, "EEG-based motor imagery analysis using weighted wavelet transform features," *Journal of Neuroscience Methods*, vol. 176, no. 2, pp. 310–318, 2009.

[114] B. Xu and A. Song, "Pattern recognition of motor imagery EEG using wavelet transform," *Journal of Biomedical Science and Engineering*, vol. 1, no. 1, pp. 64–67, 2008.

[115] L. Wang, G. Xu, J. Wang et al., "Application of Hilbert-Huang transform for the study of motor imagery tasks," in *Proceedings of the International Conference of the IEEE Engineering in Medicine & Biology Society*, pp. 3848–3851, 2008.

[116] A. B. Jerbic, P. Horki, S. Sovilj, V. Isgum, and M. Cifrek, "Hilbert-Huang time-frequency analysis of motor imagery EEG data for brain-computer interfaces," in *Proceedings of the 6th European Conference of the International Federation for Medical and Biological Engineering (MBEC '14)*, pp. 62–65, September 2014.

[117] Y.-H. Liu, C.-A. Cheng, and H.-P. Huang, "Novel feature of the EEG based motor imagery BCI system: degree of imagery," in *Proceedings of the International Conference on System Science and Engineering (ICSSE '11)*, pp. 515–520, IEEE, June 2011.

[118] M. Naeem, C. Brunner, R. Leeb, B. Graimann, and G. Pfurtscheller, "Seperability of four-class motor imagery data using independent components analysis," *Journal of Neural Engineering*, vol. 3, no. 3, pp. 208–216, 2006.

[119] X. Guo and X. Wu, "Motor imagery EEG classification based on dynamic ICA mixing matrix," in *Proceedings of the 4th International Conference on Bioinformatics and Biomedical Engineering*, pp. 1–4, IEEE, Chengdu, China, June 2010.

[120] W. Samek, C. Vidaurre, K.-R. Müller, and M. Kawanabe, "Stationary common spatial patterns for brain-computer interfacing," *Journal of Neural Engineering*, vol. 9, no. 2, Article ID 026013, 2012.

[121] W. He, P. Wei, L. Wang, and Y. Zou, "A novel EMD-based Common Spatial Pattern for motor imagery brain-computer interface," in *Proceedings of the IEEE-EMBS International Conference on Biomedical and Health Informatics (BHI '12)*, pp. 216–219, January 2012.

[122] K. K. Ang, Z. Y. Chin, C. Wang, C. Guan, and H. Zhang, "Filter bank common spatial pattern algorithm on BCI competition IV datasets 2a and 2b," *Frontiers in Neuroscience*, vol. 6, article 39, 2012.

[123] Z. Y. Chin, K. Ang, C. Wang et al., "Multi-class filter bank common spatial pattern for four-class motor imagery BCI," in *Proceedings of the IEEE Engineering in Medicine & Biology Society Conference*, pp. 571–574, September 2009.

[124] K. A. Kai, Y. C. Zheng, H. Zhang et al., "Robust filter bank common spatial pattern (RFBCSP) in motor-imagery-based brain-computer interface," in *Proceedings of the Annual International Conference of the IEEE on Engineering in Medicine and Biology Society (EMBC '09)*, vol. 2009, pp. 578–581, 2009.

[125] Y. Chu, X. Zhao, J. Han, Y. Zhao, and J. Yao, "SSVEP based brain-computer interface controlled functional electrical stimulation system for upper extremity rehabilitation," in *Proceedings of the IEEE International Conference on Robotics and Biomimetics (ROBIO '14)*, pp. 2244–2249, IEEE, Bali, Indonesia, December 2014.

[126] L. Bi, Y. Li, K. Jie, and X.-A. Fan, "A new SSVEP brain-computer interface based on a head up display," in *Proceedings of the 7th ICME International Conference on Complex Medical Engineering (CME '13)*, pp. 201–204, May 2013.

[127] L. Maggi, S. Parini, L. Piccini, G. Panfili, and G. Andreoni, "A four command BCI system based on the SSVEP protocol," in *Proceedings of the 28th Annual International Conference of the IEEE Engineering in Medicine and Biology Society (EMBS '06)*, pp. 1264–1267, September 2006.

[128] R. Singla and B. A. Haseena, "BCI based wheelchair control using steady state visual evoked potentials and support Vector machines," *International Journal of Soft Computing & Engineering*, vol. 3, no. 3, 2013.

[129] L. Bi, X.-A. Fan, K. Jie, T. Teng, H. Ding, and Y. Liu, "Using a head-up display-based steady-state visually evoked potential brain-computer interface to control a simulated vehicle," *IEEE Transactions on Intelligent Transportation Systems*, vol. 15, no. 3, pp. 959–966, 2014.

[130] T. Sakurada, T. Kawase, K. Takano, T. Komatsu, and K. Kansaku, "A BMI-based occupational therapy assist suit: asynchronous control by SSVEP," *Frontiers in Neuroscience*, vol. 7, article 172, 2013.

[131] H. Cecotti and A. Gräser, "Time Delay Neural Network with Fourier transform for multiple channel detection of Steady-State Visual Evoked Potentials for Brain-Computer Interfaces," in *Proceedings of the 16th European Signal Processing Conference (EUSIPCO '08)*, pp. 1–5, August 2008.

[132] H. Cecotti, "A time-frequency convolutional neural network for the offline classification of steady-state visual evoked potential responses," *Pattern Recognition Letters*, vol. 32, no. 8, pp. 1145–1153, 2011.

[133] M. Hartmann and T. Kluge, "Hidden Markov Models for SSVEP-based brain computer interfaces with decision-feedback training," *Frontiers in Neuroinformatics*, 2009.

[134] L.-W. Ko, S.-C. Lin, W.-G. Liang, O. Komarov, and M.-S. Song, "Development of SSVEP-based BCI using common frequency pattern to enhance system performance," in *Proceedings of the IEEE Symposium on Computational Intelligence in Brain Computer Interfaces (CIBCI '14)*, pp. 30–35, December 2014.

[135] I. Gareis, Y. Atum, G. Gentiletti et al., "On the use of LDA performance as a metric of feature extraction methods for a P300 BCI classification task," *Journal of Physics*, vol. 332, no. 1, Article ID 012021, 2011.

[136] A. Onishi and K. Natsume, "Overlapped partitioning for ensemble classifiers of P300-based brain-computer interfaces," *PLoS ONE*, vol. 9, no. 4, Article ID e93045, 2014.

[137] M. Elwardy, T. Tasdizen, and M. Cetin, "Disjunctive normal unsupervised LDA for P300-based brain-computer interfaces," in *Proceedings of the 24th Signal Processing and Communication Application Conference (SIU '16)*, pp. 2261–2264, Zonguldak, Turkey, May 2016.

[138] V. N. Raju, I.-H. Ra, and R. Sankar, "A P300-based BCI classification algorithm using least square support vector machine," *International Journal of Software Engineering and Its Applications*, vol. 9, no. 5, pp. 247–254, 2015.

[139] Y. Li, H. Li, C. Guan, and Z. Chin, "A self-training semi-supervised support vector machine algorithm and its applications in brain computer interface," in *Proceedings of the IEEE International Conference on Acoustics, Speech and Signal Processing (ICASSP '07)*, pp. I385–I388, April 2007.

[140] X. Yang, J. Dai, H. Zhang et al., "P300 wave based person identification using LVQ neural network," *Journal of Convergence Information Technology*, vol. 6, no. 3, pp. 296–302, 2011.

[141] A. Turnip, S. S. Hutagalung, J. Pardede et al., "P300 detection using a multilayer neural network classifier based on adaptive feature extraction," *International Journal of Brain & Cognitive Sciences*, vol. 2, no. 5, pp. 63–75, 2013.

[142] H. Cecotti and A. Gräser, "Convolutional neural networks for P300 detection with application to brain-computer interfaces," *IEEE Transactions on Pattern Analysis and Machine Intelligence*, vol. 33, no. 3, pp. 433–445, 2011.

[143] S. Helmy, T. Al-Ani, Y. Hamam, and E. El-madbouly, "P300 based brain-computer interface using Hidden Markov Models," in *Proceedings of the International Conference on Intelligent*

Sensors, Sensor Networks and Information Processing, pp. 127–132, IEEE, Sydney, Australia, 2009.

[144] W. Speier, C. Arnold, J. Lu, A. Deshpande, and N. Pouratian, "Integrating language information with a hidden markov model to improve communication rate in the P300 speller," *IEEE Transactions on Neural Systems and Rehabilitation Engineering*, vol. 22, no. 3, pp. 678–684, 2014.

[145] R. K. Chikara and L.-W. Ko, "Classification of EEG-P300 signals using phase locking value and pattern recognition classifiers," in *Proceedings of the Conference on Technologies and Applications of Artificial Intelligence (TAAI '15)*, pp. 367–372, IEEE, Tainan, Taiwan, November 2015.

[146] D. Steyrl, R. Scherer, O. Förstner et al., "Motor imagery brain-computer interfaces: random forests vs regularized LDA -non-linear beats linear," in *Proceedings of the 6th International Brain-Computer Interface Conference*, Graz, Austria, September 2014.

[147] C. Vidaurre, A. Schlögl, R. Cabeza, R. Scherer, and G. Pfurtscheller, "Study of on-line adaptive discriminant analysis for EEG-based brain computer interfaces," *IEEE Transactions on Biomedical Engineering*, vol. 54, no. 3, article no. 28, pp. 550–556, 2007.

[148] N. Rathipriya, S. Deepajothi, and T. Rajendran, "Classification of motor imagery ecog signals using support vector machine for brain computer interface," in *Proceedings of the 5th International Conference on Advanced Computing (ICoAC '13)*, pp. 63–66, December 2013.

[149] M. A. Oskoei, J. Q. Gan, and H. Hu, "Adaptive schemes applied to online SVM for BCI data classification," in *Proceedings of the Annual International Conference of the IEEE on Engineering in Medicine and Biology Society (EMBC '09)*, pp. 2600–2603, Minneapolis, Minn, USA, 2009.

[150] S. Siuly and Y. Li, "Improving the separability of motor imagery EEG signals using a cross correlation-based least square support vector machine for brain-computer interface," *IEEE Transactions on Neural Systems and Rehabilitation Engineering*, vol. 20, no. 4, pp. 526–538, 2012.

[151] M. Hamedi, S.-H. Salleh, A. M. Noor, and I. Mohammad-Rezazadeh, "Neural network-based three-class motor imagery classification using time-domain features for BCI applications," in *Proceedings of the IEEE Region 10 Symposium (IEEE TENSYMP '14)*, pp. 204–207, April 2014.

[152] Y. Wei, Y. Zhou, J. Ma et al., "Signal feature extraction and classification method based on EMD and LVQ neural network," *Journal of Data Acquisition & Processing*, no. 5, pp. 683–687, 2014.

[153] M. K. Hazrati and A. Erfanian, "An online EEG-based brain-computer interface for controlling hand grasp using an adaptive probabilistic neural network," *Medical Engineering and Physics*, vol. 32, no. 7, pp. 730–739, 2010.

[154] E. Haselsteiner and G. Pfurtscheller, "Using time-dependent neural networks for EEG classification," *IEEE Transactions on Rehabilitation Engineering*, vol. 8, no. 4, pp. 457–463, 2000.

[155] Siuly, H. Wang, and Y. Zhang, "Detection of motor imagery EEG signals employing Naïve Bayes based learning process," *Measurement*, vol. 86, pp. 148–158, 2016.

[156] B. Obermaier, C. Guger, C. Neuper, and G. Pfurtscheller, "Hidden Markov models for online classification of single trial EEG data," *Pattern Recognition Letters*, vol. 22, no. 12, pp. 1299–1309, 2001.

[157] H.-I. Suk and S.-W. Lee, "Two-layer hidden Markov models for multi-class motor imagery classification," in *Proceedings of the Workshop on Brain Decoding: Pattern Recognition Challenges in Neuroimaging (WBD '10)*, pp. 5–8, August 2010.

[158] S. K. Bashar and M. I. H. Bhuiyan, "Classification of motor imagery movements using multivariate empirical mode decomposition and short time Fourier transform based hybrid method," *Engineering Science & Technology*, vol. 19, no. 3, pp. 1457–1464, 2016.

[159] O. Diana Eva and D. Tarniceriu, "Substitution of spatial filters from relaxation to motor imagery for EEG based brain computer interface," in *Proceedings of the 19th International Conference on System Theory, Control and Computing (ICSTCC '15)*, pp. 147–150, October 2015.

[160] J. Zhao, Q. Meng, W. Li, M. Li, and G. Chen, "SSVEP-based hierarchical architecture for control of a humanoid robot with mind," in *Proceedings of the 11th World Congress on Intelligent Control and Automation (WCICA '14)*, pp. 2401–2406, July 2014.

[161] X.-Y. Wang, F. Cai, J. Jin, Y. Zhang, and B. Wang, "Robot control system based on auditory brain-computer interface," *Control Theory & Applications*, vol. 32, no. 9, pp. 1183–1190, 2015.

[162] M. Li, W. Li, J. Zhao et al., "A P300 model for Cerebot—a mind-controlled humanoid robot," in *Robot Intelligence Technology and Applications 2*, pp. 495–502, Springer, 2014.

[163] J. Tang, J. Jiang, Y. Yu, and Z. Zhou, "Humanoid robot operation by a brain-computer interface," in *Proceedings of the 7th International Conference on Information Technology in Medicine and Education (ITME '15)*, pp. 476–479, November 2015.

[164] J.-C. Liu, H.-C. Chou, C.-H. Chen, Y.-T. Lin, and C.-H. Kuo, "Time-shift correlation algorithm for P300 event related potential brain-computer interface implementation," *Computational Intelligence and Neuroscience*, vol. 2016, Article ID 3039454, 22 pages, 2016.

[165] K. Bouyarmane, J. Vaillant, N. Sugimoto et al., "BCI control of whole-body simulated humanoid by combining motor imagery detection and autonomous motion planning," in *Neural Information Processing*, pp. 310–318, Springer, Berlin, Germany, 2013.

[166] A. M. Batula, J. Mark, Y. E. Kim et al., "Developing an optical brain-computer interface for humanoid robot control," in *Proceedings of the 10th International Conference on Foundations of Augmented Cognition: Neuroergonomics and Operational Neuroscience*, July 2016.

[167] O. Cohen, S. Druon, S. Lengagne et al., "fMRI-Based robotic embodiment: controlling a humanoid robot by thought using real-time fMRI," *Presence: Teleoperators and Virtual Environments*, vol. 23, no. 3, pp. 229–241, 2014.

[168] Z. Deng, X. Li, K. Zheng, and W. Yao, "A humanoid robot control system with SSVEP-based asynchronous brain-computer interface," *Jiqiren/Robot*, vol. 33, no. 2, pp. 129–135, 2011.

[169] J. Jiang, A. Wang, Y. Ge, and Z. Zhou, "Brain-actuated humanoid robot control using one class motor imagery task," in *Proceedings of the Chinese Automation Congress (CAC '13)*, pp. 587–590, November 2013.

[170] J. Jiang, Z. Zhou, E. Yin, Y. Yu, Y. Liu, and D. Hu, "A novel Morse code-inspired method for multiclass motor imagery brain-computer interface (BCI) design," *Computers in Biology and Medicine*, vol. 66, pp. 11–19, 2015.

[171] B. Choi and S. Jo, "A low-cost EEG system-based hybrid brain-computer interface for humanoid robot navigation and recognition," *PLoS ONE*, vol. 8, no. 9, Article ID e74583, 2013.

[172] L. F. Nicolas-Alonso and J. Gomez-Gil, "Brain computer interfaces, a review," *Sensors*, vol. 12, no. 2, pp. 1211–1279, 2012.

[173] G. Bin, X. Gao, Y. Wang, B. Hong, and S. Gao, "VEP-based brain-computer interfaces: time, frequency, and code modulations [Research Frontier]," *IEEE Computational Intelligence Magazine*, vol. 4, no. 4, pp. 22–26, 2009.

[174] S. A. Hillyard and T. W. Picton, "Electrophysiology of cognition," in *Handbook of Physiology. The Nervous System, Higher Functions of the Brain*, F. Plum, Ed., 2010.

[175] R. W. McCarley, S. F. Faux, M. E. Shenton, P. G. Nestor, and J. Adams, "Event-related potentials in schizophrenia: their biological and clinical correlates and new model of schizophrenic pathophysiology," *Schizophrenia Research*, vol. 4, no. 2, pp. 209–231, 1991.

[176] E. Snyder and S. A. Hillyard, "Long-latency evoked potentials to irrelevant, deviant stimuli," *Behavioral Biology*, vol. 16, no. 3, pp. 319–331, 1976.

[177] D. Karis, T. Bashore, M. Coles et al., "Cognitive psychophysiology and human information processing," in *Psychophysiology: Systems, Processes, and Applications*, Guilford Press, New York, NY, USA, 1986.

[178] R. Verleger, "Event-related potentials and cognition: a critique of the context updating hypothesis and an alternative interpretation of P3," *Behavioral and Brain Sciences*, vol. 11, no. 3, pp. 343–356, 1988.

[179] S. Sutton, M. Braren, J. Zubin, and E. R. John, "Evoked-potential correlates of stimulus uncertainty," *Science*, vol. 150, no. 3700, pp. 1187–1188, 1965.

[180] D. B. D. Smith, E. Donchin, L. Cohen, and A. Starr, "Auditory averaged evoked potentials in man during selective binaural listening," *Electroencephalography and Clinical Neurophysiology*, vol. 28, no. 2, pp. 146–152, 1970.

[181] J. Jin, B. Z. Allison, T. Kaufmann et al., "The changing face of P300 BCIs: a comparison of stimulus changes in a p300 bci involving faces, emotion, and movement," *PLoS ONE*, vol. 7, no. 11, Article ID e49688, 2012.

[182] M. Ergen, S. Marbach, A. Brand, C. Başar-Eroğlu, and T. Demiralp, "P3 and delta band responses in visual oddball paradigm in schizophrenia," *Neuroscience Letters*, vol. 440, no. 3, pp. 304–308, 2008.

[183] J. Jin, I. Daly, Y. Zhang, X. Wang, and A. Cichocki, "An optimized ERP brain-computer interface based on facial expression changes," *Journal of Neural Engineering*, vol. 11, no. 3, Article ID 036004, 2014.

[184] J. Jin, B. Z. Allison, Y. Zhang, X. Wang, and A. Cichocki, "An ERP-based BCI using an oddball paradigm with different faces and reduced errors in critical functions," *International Journal of Neural Systems*, vol. 24, no. 8, Article ID 1450027, 2014.

[185] J. Jin, E. W. Sellers, S. Zhou, Y. Zhang, X. Wang, and A. Cichocki, "A P300 brain-computer interface based on a modification of the mismatch negativity paradigm," *International Journal of Neural Systems*, vol. 25, no. 3, Article ID 1550011, 2015.

[186] K. Fukunaga, "Statistical pattern recognition," *Mathematics in Science and Engineering*, vol. 66, no. 12-1, pp. 35–79, 1970.

[187] K. P. Bennett and C. Campbell, "Support vector machines: hype or hallelujah?" *ACM SIGKDD Explorations Newsletter*, vol. 2, no. 2, pp. 1–13, 2000.

[188] M. Jeannerod, "Mental imagery in the motor context," *Neuropsychologia*, vol. 33, no. 11, pp. 1419–1432, 1995.

[189] G. Pfurtscheller and C. Neuper, "Motor imagery activates primary sensorimotor area in humans," *Neuroscience Letters*, vol. 239, no. 2-3, pp. 65–68, 1997.

[190] L. Leocani, C. Toro, P. Manganotti, P. Zhuang, and M. Hallett, "Event-related coherence and event-related desynchronization/synchronization in the 10 Hz and 20 Hz EEG during self-paced movements," *Electroencephalography and Clinical Neurophysiology*, vol. 104, no. 3, pp. 199–206, 1997.

[191] G. E. Chatrian, M. C. Petersen, and J. A. Lazarte, "The blocking of the rolandic wicket rhythm and some central changes related to movement," *Electroencephalography and Clinical Neurophysiology*, vol. 11, no. 3, pp. 497–510, 1959.

[192] H. Gastaut, "Electrocorticographic study of the reactivity of rolandic rhythm," *Revue Neurologique*, vol. 87, no. 2, pp. 176–182, 1952.

[193] H. Jasper, "Electrocorticograms in man: effect of voluntary movement upon the electrical activity of the precentral gyrus," *European Archives of Psychiatry & Clinical Neuroscience*, vol. 183, no. 1, pp. 163–174, 1948.

[194] G. Pfurtscheller and A. Aranibar, "Event-related cortical desynchronization detected by power measurements of scalp EEG," *Electroencephalography and Clinical Neurophysiology*, vol. 42, no. 6, pp. 817–826, 1977.

[195] F. Cassim, C. Monaca, W. Szurhaj et al., "Does post-movement beta synchronization reflect an idling motor cortex?" *NeuroReport*, vol. 12, no. 17, pp. 3859–3863, 2001.

[196] C. Toro, G. Deuschl, R. Thatcher, S. Sato, C. Kufta, and M. Hallett, "Event-related desynchronization and movement-related cortical potentials on the ECoG and EEG," *Electroencephalography and Clinical Neurophysiology*, vol. 93, no. 5, pp. 380–389, 1994.

[197] C. Neuper, A. Schlögl, and G. Pfurtscheller, "Enhancement of left-right sensorimotor EEG differences during feedback-regulated motor imagery," *Journal of Clinical Neurophysiology*, vol. 16, no. 4, pp. 373–382, 1999.

[198] T. Yu, J. Xiao, F. Wang et al., "Enhanced motor imagery training using a hybrid BCI with feedback," *IEEE Transactions on Biomedical Engineering*, vol. 62, no. 7, pp. 1706–1717, 2015.

[199] V. J. Samar, A. Bopardikar, R. Rao, and K. Swartz, "Wavelet analysis of neuroelectric waveforms: a conceptual tutorial," *Brain and Language*, vol. 66, no. 1, pp. 7–60, 1999.

[200] N. E. Huang, H. H. Liu, N. E. Huang et al., "The empirical mode decomposition and the Hilbert spectrum for nonlinear and non-stationary time series analysis," *Proceedings of the Royal Society of London A: Mathematical, Physical & Engineering Sciences*, vol. 454, no. 1971, pp. 903–995, 1998.

[201] I. W. Selesnick, R. G. Baraniuk, and N. G. Kingsbury, "The dual-tree complex wavelet transform," *IEEE Signal Processing Magazine*, vol. 22, no. 6, pp. 123–151, 2005.

[202] N. E. Huang, S. R. Long, and Z. Shen, "The mechanism for frequency downshift in nonlinear wave evolution," *Advances in Applied Mechanics*, vol. 32, no. 8, pp. 59–117, 1996.

[203] P.-L. Lee, H.-C. Chang, T.-Y. Hsieh, H.-T. Deng, and C.-W. Sun, "A brain-wave-actuated small robot car using ensemble empirical mode decomposition-based approach," *IEEE Transactions on Systems, Man, and Cybernetics. Part A: Systems and Humans*, vol. 42, no. 5, pp. 1053–1064, 2012.

[204] A. Hyvärinen and E. Oja, "Independent component analysis: algorithms and applications," *Neural Networks*, vol. 13, no. 4-5, pp. 411–430, 2000.

[205] C. Guger, H. Ramoser, and G. Pfurtscheller, "Real-time EEG analysis with subject-specific spatial patterns for a brain-computer interface (BCI)," *IEEE Transactions on Rehabilitation Engineering*, vol. 8, no. 4, pp. 447–456, 2000.

[206] R. Ortner, J. Scharinger, A. Lechner, and C. Guger, "How many people can control a motor imagery based BCI using common spatial patterns?" in *Proceedings of the 7th International IEEE/EMBS Conference on Neural Engineering (NER '15)*, pp. 202–205, April 2015.

[207] X. Lei, P. Yang, P. Xu et al., "Common spatial pattern ensemble classifier and its application in brain-computer interface," *Journal of Electronic Science & Technology of China*, vol. 7, no. 1, pp. 17–21, 2009.

[208] X. Yong, R. K. Ward, and E. G. Birch, "Robust common spatial patterns for EEG signal preprocessing," in *Proceedings of the 30th Annual International Conference of the IEEE Engineering in Medicine & Biology Society*, pp. 2087–2090, Vancouver, Canada, August 2008.

[209] K.-R. Müller, C. W. Anderson, and G. E. Birch, "Linear and nonlinear methods for brain-computer interfaces," *IEEE Transactions on Neural Systems and Rehabilitation Engineering*, vol. 11, no. 2, pp. 165–169, 2003.

[210] F. Lotte, M. Congedo, A. Lécuyer, F. Lamarche, and B. Arnaldi, "A review of classification algorithms for EEG-based brain-computer interfaces," *Journal of Neural Engineering*, vol. 4, no. 2, pp. R1–R13, 2007.

[211] R. O. Duda, P. E. Hart, and D. G. Stork, *Pattern Classification*, En Broeck the Statistical Mechanics of Learning Rsity, John Wiley & Sons, 2nd edition, 2000.

[212] G. Baudat and F. Anouar, "Generalized discriminant analysis using a kernel approach," *Neural Computation*, vol. 12, no. 10, pp. 2385–2404, 2000.

[213] W. S. Noble, "What is a support vector machine?" *Nature Biotechnology*, vol. 24, no. 12, pp. 1565–1567, 2006.

[214] C. J. C. Burges, "A tutorial on support vector machines for pattern recognition," *Data Mining & Knowledge Discovery*, vol. 2, no. 2, pp. 121–167, 1998.

[215] I. Rish, "An empirical study of the naive Bayes classifier," *Journal of Universal Computer Science*, vol. 1, no. 2, p. 127, 2001.

[216] R. Boostani and M. H. Moradi, "A new approach in the BCI research based on fractal dimension as feature and Adaboost as classifier," *Journal of Neural Engineering*, vol. 1, no. 4, pp. 212–217, 2004.

[217] J. Qin, Y. Li, and A. Cichocki, "ICA and committee machine-based algorithm for cursor control in a BCI system," in *Advances in Neural Networks—ISNN 2005*, pp. 973–978, Springer, 2005, 2005.

[218] H. Lee and S. Choi, "PCA+HMM+SVM for EEG pattern classification," in *Proceedings of the 7th International Symposium on Signal Processing and Its Applications (ISSPA '03)*, pp. 541–544, July 2003.

[219] F. Galán, M. Nuttin, E. Lew et al., "A brain-actuated wheelchair: asynchronous and non-invasive Brain-computer interfaces for continuous control of robots," *Clinical Neurophysiology*, vol. 119, no. 9, pp. 2159–2169, 2008.

[220] I. Iturrate, J. M. Antelis, A. Kübler, and J. Minguez, "A noninvasive brain-actuated wheelchair based on a P300 neurophysiological protocol and automated navigation," *IEEE Transactions on Robotics*, vol. 25, no. 3, pp. 614–627, 2009.

[221] B. Rebsamen, C. Guan, H. Zhang et al., "A brain controlled wheelchair to navigate in familiar environments," *IEEE Transactions on Neural Systems and Rehabilitation Engineering*, vol. 18, no. 6, pp. 590–598, 2010.

[222] J. Philips, J. D. R. Millán, G. Vanacker et al., "Adaptive shared control of a brain-actuated simulated wheelchair," in *Proceedings of the IEEE 10th International Conference on Rehabilitation Robotics (ICORR '07)*, pp. 408–414, Noordwijk, Netherlands, June 2007.

[223] G. Vanacker, R. Del M J, E. Lew et al., "Context-based filtering for assisted brain-actuated wheelchair driving," *Computational Intelligence & Neuroscience*, vol. 2007, article 3, 2007.

[224] Y. Li, J. Pan, F. Wang, and Z. Yu, "A hybrid BCI system combining P300 and SSVEP and its application to wheelchair control," *IEEE Transactions on Biomedical Engineering*, vol. 60, no. 11, pp. 3156–3166, 2013.

[225] M. Palankar, K. J. De Laurentis, R. Alqasemi et al., "Control of a 9-DoF wheelchair-mounted robotic arm system using a P300 brain computer interface: initial experiments," in *Proceedings of the IEEE International Conference on Robotics and Biomimetics (ROBIO '08)*, pp. 348–353, February 2009.

[226] T. Li, J. Hong, J. Zhang et al., "Brain-machine interface control of a manipulator using small-world neural network and shared control strategy," *Journal of Neuroscience Methods*, vol. 224, no. 6, pp. 26–38, 2014.

[227] E. Iáñez, M. C. Furió, J. Azorín M et al., "Brain-robot interface for controlling a remote robot arm," in *Bioinspired Applications in Artificial and Natural Computation*, pp. 353–361, Springer, Berlin, Germany, 2009.

[228] E. A. Pohlmeyer, B. Mahmoudi, S. Geng, N. Prins, and J. C. Sanchez, "Brain-machine interface control of a robot arm using actor-critic rainforcement learning," in *Proceedings of the 34th Annual International Conference of the IEEE Engineering in Medicine and Biology Society (EMBS '12)*, pp. 4108–4111, September 2012.

[229] C. Wang, B. Xia, J. Li et al., "Motor imagery BCI-based robot arm system," in *Proceedings of the 7th International Conference on Natural Computation (ICNC '11)*, pp. 181–184, July 2011.

[230] D. Elstob and E. L. Secco, "A low cost eeg based BCI prosthetic using motor imagery," *International Journal of Information Technology Convergence and Services*, vol. 6, no. 1, pp. 23–36, 2016.

[231] Y. Chen, S. Chen, I. Zaeni, and C. Wu, "Fuzzy tracking and control algorithm for an SSVEP-based BCI system," *Applied Sciences*, vol. 6, no. 10, article 270, 2016.

[232] N. Kos'Myna, F. Tarpin-Bernard, and B. Rivet, "Bidirectional feedback in motor imagery BCIs: learn to control a drone within 5 minutes," in *Proceedings of the Conference on Human Factors in Computing Systems is the Premier International Conference of Human-Computer Interaction (CHI '14)*, pp. 479–482, Toronto, Canada, May 2014.

[233] A. J. Doud, J. P. Lucas, and B. He, "Continuous 3D control of a virtual helicopter using a motor imagery based BCI," in *Proceedings of the International IEEE/EMBS Conference on Neural Engineering*, pp. 364–367, April-May 2011.

[234] K. Lafleur, K. Cassady, A. Doud, K. Shades, E. Rogin, and B. He, "Quadcopter control in three-dimensional space using a noninvasive motor imagery-based brain-computer interface," *Journal of Neural Engineering*, vol. 10, no. 4, pp. 711–726, 2013.

[235] C. J. Bell, P. Shenoy, R. Chalodhorn, and R. P. N. Rao, "Control of a humanoid robot by a noninvasive brain-computer interface in humans," *Journal of Neural Engineering*, vol. 5, no. 2, pp. 214–220, 2008.

[236] W. Li, C. Jaramillo, and Y. Li, "A brain computer interface based humanoid robot control system," in *Proceedings of the 2nd IASTED International Conference on Robotics (Robo '11)*, pp. 390–396, November 2011.

[237] W. Li, C. Jaramillo, and Y. Li, "Development of mind control system for humanoid robot through a brain computer interface," in *Proceedings of the International Conference on Intelligent System Design and Engineering Application*, pp. 679–682, IEEE Computer Society, 2012.

[238] J. D. R. Millán and J. Mouriño, "Asynchronous BCI and local neural classifiers: an overview of the adaptive brain interface

project," *IEEE Transactions on Neural Systems and Rehabilitation Engineering*, vol. 11, no. 2, pp. 159–161, 2003.

[239] T. Liu, L. Goldberg, S. Gao, and B. Hong, "An online brain-computer interface using non-flashing visual evoked potentials," *Journal of Neural Engineering*, vol. 7, no. 3, Article ID 036003, 2010.

[240] J. Jin, B. Z. Allison, E. W. Sellers et al., "An adaptive P300-based control system," *Journal of Neural Engineering*, vol. 8, no. 3, Article ID 036006, 2011.

[241] D. J. Leamy, R. Collins, and T. E. Ward, "Combining fNIRS and EEG to improve motor cortex activity classification during an imagined movement-based task," in *Proceedings of the International Conference on Foundations of Augmented Cognition: Directing the Future of Adaptive Systems*, pp. 177–185, Springer, 2011.

[242] F. Putze, S. Hesslinger, C.-Y. Tse et al., "Hybrid fNIRS-EEG based classification of auditory and visual perception processes," *Frontiers in Neuroscience*, vol. 8, article 373, 2014.

[243] C. Mulert, L. Jäger, R. Schmitt et al., "Integration of fMRI and simultaneous EEG: towards a comprehensive understanding of localization and time-course of brain activity in target detection," *NeuroImage*, vol. 22, no. 1, pp. 83–94, 2004.

Hindawi
Computational Intelligence and Neuroscience
Volume 2017, Article ID 9528097, 6 pages
https://doi.org/10.1155/2017/9528097

Research Article

An Efficient Framework for EEG Analysis with Application to Hybrid Brain Computer Interfaces Based on Motor Imagery and P300

Jinyi Long,[1,2,3] Jue Wang,[2] and Tianyou Yu[2]

[1]*College of Information Science and Technology, Jinan University, Guangzhou 510632, China*
[2]*School of Automation Science and Engineering, South China University of Technology and Guangzhou Key Laboratory of Brain Computer Interaction and Applications, Guangzhou 510640, China*
[3]*Key Laboratory of Advanced Control and Optimization for Chemical Processes, Ministry of Education, East China University of Science and Technology, Shanghai 200237, China*

Correspondence should be addressed to Jinyi Long; longjinyi@gmail.com

Received 21 August 2016; Revised 8 November 2016; Accepted 12 December 2016; Published 19 February 2017

Academic Editor: Feng Duan

The hybrid brain computer interface (BCI) based on motor imagery (MI) and P300 has been a preferred strategy aiming to improve the detection performance through combining the features of each. However, current methods used for combining these two modalities optimize them separately, which does not result in optimal performance. Here, we present an efficient framework to optimize them together by concatenating the features of MI and P300 in a block diagonal form. Then a linear classifier under a dual spectral norm regularizer is applied to the combined features. Under this framework, the hybrid features of MI and P300 can be learned, selected, and combined together directly. Experimental results on the data set of hybrid BCI based on MI and P300 are provided to illustrate competitive performance of the proposed method against other conventional methods. This provides an evidence that the method used here contributes to the discrimination performance of the brain state in hybrid BCI.

1. Introduction

Hybrid brain computer interfaces (BCIs) based on electroencephalogram (EEG) have attracted a great deal of attention because they can provide higher discriminant performance and more control commands compared to single model BCI [1–4]. In general, many research efforts have been focused on experiment paradigm design based on different BCI modalities to improve the discriminant performance [3–6]. However, in machine learning terms the methodology to analyze different patterns of BCI modalities is also important for discriminant performance improvement.

Signal analysis in BCI aims to predict the brain state of a user out of prescribed options [7, 8]. Many studies have focused on how to improve detection performance under the single modal BCI with different approaches. These approaches for data analysis have been applied in different steps such as feature extraction and selection (e.g., common spatial patter [9, 10]; independent component analysis coupled with heuristic frequency band selection [9]; band weighting [11, 12]) and classification (e.g., linear classifier [13–15], nonlinear classifier [14, 16, 17], and semisupervised learning [18, 19]). Furthermore, some efforts also try to develop a discriminant approach with a unified criterion for classifier coefficient (e.g., spatial filter and temporal filter) optimization from the training data [20–22].

Unlike the single modal BCI, there exist two or more brain patterns in the hybrid BCI (e.g., MI and P300). In machine learning terms, the challenge is that these patterns contain different order information in the signal [3]. For MI based BCI, the second-order information is used, while the first-order information is used for P300-based BCI. This leads to difficulty in the application of conventional statistical analysis to combine and learn brain patterns together. Many

attempts to analyze the signal under the hybrid BCI are carried out though extracting the features from different modalities separately and then concatenating them to feed into some relative simple classifiers [2, 3]. However, these methods combine and learn the features indirectly which would lead to a nonoptimized resolution.

In this paper, we focus on the hybrid BCI paradigm based on our previous work, which includes MI tasks and P300 tasks. This indicates that the brain signal includes first-order and second-order information. To overcome the challenges described above, we propose using a discriminant approach that tries to combine and learn the hybrid features directly. The discriminant approach applied here has been proposed for single modality BCI by Tomioka and Müller [22]. The first-order information of the signal for P300 tasks and the second-order information of the signal for MI tasks are combined in a block diagonal form. These combined features can be selected and learned systematically with a linear classifier under dual spectral regulation. Our experimental results and data analysis demonstrate the efficiency of this discriminant approach.

2. Materials and Methods

2.1. Experiment and EEG Data Collection. A NuAmps device (Neuroscan) is used to measure scalp EEG signals for data acquisition. Each user wears an EEG cap (LT 37) that measures the signals from the electrodes. The EEG signals are referenced to the right ear. Two channels, "HEOG" and "VEOG," representing eye movements are excluded (not shown here). The EEG used for processing is recorded from Ag-AgCl electrodes that are placed at the sites in the frontal, central, parietal, and occipital regions. The following 15 channels are included: "FC3," "FCz," "FC4," "C3," "Cz," "C4," "CP3," "CPz," "CP4," "P3," "Pz," "P4," "O1," "Oz," and "O2." All impedances are kept below 5 kΩ. The EEG signals are amplified, sampled at 250 Hz, and bandpass filtered between 0.5 and 100 Hz.

In this experiment, the data was collected from twelve volunteers (10 males, 2 females) with ages in the range of 22–35 years. The graphic user interface used to combine P300 and MI is the same as described in our previous paper [2] and as shown in Figure 1. There are 8 flashing buttons around the screen. The trial design for data acquisition is shown in Figure 2. In the initial state (0–2.25 s) of each trial, the screen remains blank before a cross appears on the screen from 2.25 to 4 s to attract the subject's visual fixation. From 4 s to 8 s an up or right arrow cue is shown, and the subject is instructed to perform the P300 task or MI task (Table 1). The next trial begins after an interval of 4 s. During this interval the subjects were asked to relax. When the cue (i.e., up/right) appears the 8 buttons begin to alternately flash in a random order. Each button is intensified for 100 ms with a time interval of 120 ms between two consecutive button flashes. Thus, one round of button flashes occurs during a period of 960 ms, and each round is repeated 4 times in each trial. During the P300 task, subjects were instructed to focus on the up center button without any movement imagination, while during MI task, subjects were asked to perform right-hand imagery without any button attention. There are two sessions with each session comprised of 100 total trials (50 trials for each task). The first session is used to generate training data, and test data is derived from the second session.

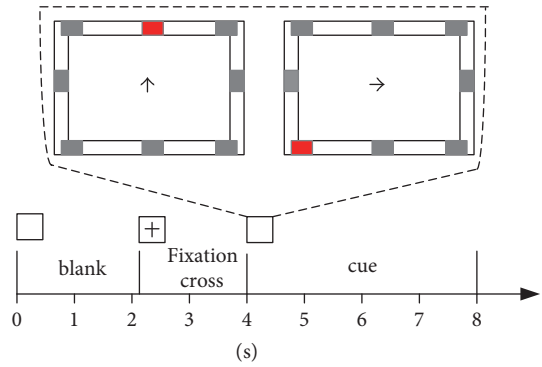

Figure 1: Paradigm for acquisition of data in a trial. At the beginning of the trial (0–2.25 s), the screen is blank. From 2.25 to 4 s a cross is shown onscreen to capture subject's visual attention. From 4 to 8 s, an arrow cue is provided. The subject is instructed to perform a mental task according to the following: right arrows cue right-hand motor imagery and up arrow cues attention to a specific button (center up button in this experiment).

Table 1: Experimental tasks.

Arrow cue	Task
Up	P300 task: focus on the up center button without any MI task
Right	MI task: right-hand imagery without any button attention

2.2. Data Preprocessing and Pattern Extraction. This dataset involved two types of task: one related to P300 and the other corresponded to MI (Table 1). In the P300 task, the categories classified were the up center button attention or not (up or right arrow), while, in the MI task, the categories were the right-hand motor imagery and no motor imagery (up or right arrow). First, we introduce the data preprocessing procedure for these tasks separately below.

For the P300 task, the EEG signal is first bandpass filtered within the range of 0.1–20 Hz and then downsampled to 60 Hz. Next, the signal from a channel is segmented into epochs, each of which is from 0 to 600 ms after a flash of the button, specifically the up center button in this experiment. For each flash of a specific button in the ith trial, an epoch vector can be obtained by concatenating the data vectors derived from the 15 channels and denoted as $X_{\mathrm{P300}}^{(i,l)} \in R^{T\times C}$, where $T = 37$ and $C = 15$ ($l = 1, \ldots, 4$). The feature vector in the ith trial $X_{\mathrm{P300}}^{(i)} \in R^{37\times 15}$ is obtained by averaging four epoch vectors corresponding to four repeats of specific button flashes and is assigned to a target $y \in \{+1, -1\}$. If the trial during training corresponds to attention to the specific button without motor imagery, then the label is set to +1. Otherwise, the label is −1. Then, we apply the spatial and temporal preprocessing matrices P^s and P^t to normalize

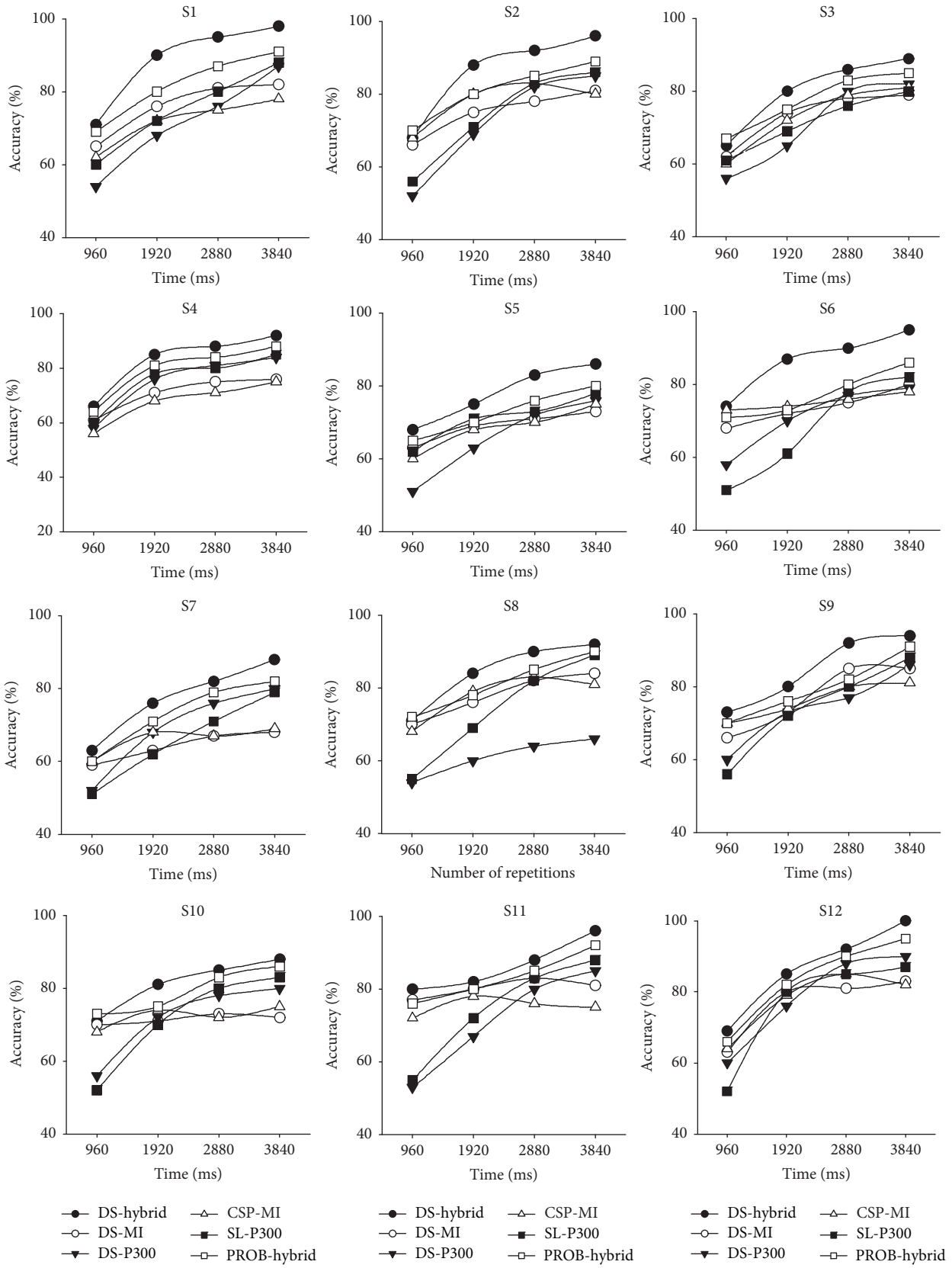

Figure 2: The individual accuracy across time.

each channel and time-point in $X_{\mathrm{P300}}^{(i)}$ to unit variance as $\overline{X}_{\mathrm{P300}}^{(i)} = P^t X_{\mathrm{P300}}^{(i)} P^s$. The P^s and P^t are defined as proposed in [22]. We also choose $P^s = \sum^{s-1/4}$ and $P^t = \sum^{t-1/4}$, where $\sum^s = (1/n)\sum_{i=1}^n \mathrm{cov}(X_{\mathrm{P300}}^{(i)})$ and $\sum^t = (1/n)\sum_{i=1}^n \mathrm{cov}(X_{\mathrm{P300}}^{(i)^T})$ are covariance matrices in the spatial and temporal domain.

For the motor imagery task, EEG data were bandpass filtered within the range of 8–30 Hz and downsampled to 100 Hz. The bandpass filtered signal data $X_{\mathrm{MI}}^{(i)} \in R^{C\times T}$ for the ith trial was started during cue presentation and ended when the cue disappeared, where $C = 15$ and $T = 400$. The target of the ith trial is the same as the P300 task. Here, we used the pattern of the second-order covariance term for the motor imagery task. Similar with the normalization in the P300 task, this pattern is also normalized by applying a spatial whitening matrix $\sum^{s-1/2}$ (i.e., $\Gamma_{\mathrm{MI}}^{(i)} = \sum^{s-1/2} \mathrm{cov}(X_{\mathrm{MI}}^{(i)}) \sum^{s-1/2}$), where $\sum^s = (1/n)\sum_{i=1}^n \mathrm{cov}(X_{\mathrm{MI}}^{(i)})$ is the covariance matrix in the spatial domain [22].

With the above extracted patterns of P300 $\overline{X}_{\mathrm{P300}}^{(i)}$ and motor imagery $\Gamma_{\mathrm{MI}}^{(i)}$ for the ith trial, we can set $X_{\mathrm{P300,MI}}^{(i)}$ as a block diagonal concatenation of both as shown below:

$$X_{\mathrm{P300,MI}}^{(i)} = \begin{bmatrix} \frac{1}{\xi_1}\overline{X}_{\mathrm{P300}}^{(i)} & \\ & \frac{1}{\xi_2}\Gamma_{\mathrm{MI}}^{(i)} \end{bmatrix}, \tag{1}$$

where ξ_1 and ξ_2 are the normalization factors used to standardize each feature to unit variance and defined as the square root of the total variance of each block element [23].

2.3. Linear Classification. The classifier used here is the linear function as shown below:

$$f_\theta\left(X_{\mathrm{P300,MI}}^{(i)}\right) = \left\langle W, X_{\mathrm{P300,MI}}^{(i)} \right\rangle + b, \tag{2}$$

where $\theta \coloneqq (W, b)$, W is a matrix of some appropriate size, and b is a bias term. $\langle W, X_{\mathrm{P300,MI}}^{(i)}\rangle = \sum_{j,k} W(j,k) X_{\mathrm{P300,MI}}^{(i)}(j,k)$ is the inner product between two matrices $X_{\mathrm{P300,MI}}^{(i)}$ and W ($W(j,k)$ denotes the (j,k) element of a matrix W). Denote $W = \sum_{j=1}^J b_j w_j w_j^T$, where w_j is the spatial filter and only the first several spatial filters are enough for good classification performance like a CSP based approach.

Before testing, parameters θ of the above linear classifier by training are obtained. With the training patterns $X_{\mathrm{P300,MI}}^{(i)}$ and their corresponding true targets y_i ($i = 1, \ldots, N$), the parameters can learn by solving the following constrained minimization problem with the dual spectral (DS) norm regularizer [22, 24, 25]:

$$\begin{aligned} \min_{\theta\in\Theta} \quad & \frac{1}{N}\sum_{i=1}^N \log\left(1 + e^{-y_i f_\theta(X_{\mathrm{P300,MI}}^{(i)})}\right) \\ \text{subject to} \quad & \|W\|_* \coloneqq \sum_j^r \delta_j(W) \le C, \end{aligned} \tag{3}$$

where $\delta_j(W)$ is the jth singular value of the weight matrix W and r is the rank of W. C is the hyperparameter that controls the complexity of the model and is selected by cross-validation with the training data set. For each subject, the C value was searched from 0.1 to 10 with a step of 0.2 and was set to the number with the best average performance after cross-validation.

Therefore, with the training parameters, we can predict the target of the pattern $X_{\mathrm{P300,MI}}^{(t)}$ from the test data set as shown below:

$$y_t = \begin{cases} +1 & \text{if } f_\theta\left(X_{\mathrm{P300,MI}}^{(t)}\right) \ge 0, \\ -1 & \text{if } if_\theta\left(X_{\mathrm{P300,MI}}^{(t)}\right) < 0. \end{cases} \tag{4}$$

As described above, we can see that the linear classifier can select and learn the features systematically under dual spectral regulation, in which the features are in a block diagonal form by combing the first-order information of the signal for P300 tasks and the second-order information of the signal for MI tasks. This framework can provide a way to optimize the features of MI and P300 together directly.

2.4. Validation Analysis. For comparison, we also performed the data analysis with the most used methods in BCI community. For the data analysis of MI task, we applied the common spatial patters (CSP) as the MI features and linear discriminant analysis (LDA) as the classifier (CSP-MI). While for the data analysis of P300 task, stepwise LDA was used as the classifier (SL-P300). To further prove the effect of our used method, we performed the classification using the PROB method [26], which we have presented previously [2, 3]. This method is used to combine the features of MI and P300 modalities. Specifically, two linear discriminant analysis (LDA) classifiers are trained using the MI feature vectors obtained by the CSP method and the P300 feature vectors with labels, respectively. Two scores for each trial's MI feature vector and P300 feature vector pair are computed using corresponding classifiers. If the average score is larger than 0, then the label is 1. Otherwise, the label is −1.

3. Results

Before performing the test, the regularization constant C by 10-fold cross-validation for each subject with the best performance was chosen as shown in Table 2. The classification performance obtained by the method proposed above using the chosen regularization constant is shown in Table 2 with an average accuracy of 92.8% (DS-hybrid). We also performed the classification with the MI and P300 separately as shown in Table 2. Their average individual classification accuracies are 79.6% (DS-MI) and 81.4% (DS-P300). The paired t-test showed that combining the MI and P300 resulted in better accuracy than that obtained by only MI ($p < 0.001$) or P300 ($p < 0.001$).

The classification performance with the standard algorithm for the data analysis with MI and P300 paradigms was 79.3% (CSP-MI) and 82.8% (SL-P300) as shown in Table 2 separately. The paired t-test statistical analysis showed that the classification accuracy obtained by DS-hybrid is better than that obtained by both CSP-MI ($p < 0.001$) and SL-P300

Table 2: Classification performance.

	DS-hybrid (%, C)	DS-MI (%, C)	DS-P300 (%, C)	CSP-MI (%)	SL-P300 (%)	PROB-hybrid (%)
S1	98 (0.9)	82 (1.3)	87 (2.3)	78	88	91
S2	96 (1.5)	81 (3.3)	85 (1.5)	85	87	85
S3	89 (5.7)	79 (0.3)	82 (0.9)	75	79	85
S4	92 (0.5)	76 (0.7)	84 (0.7)	80	76	88
S5	86 (2.9)	73 (2.5)	76 (1.3)	72	78	80
S6	95 (6.3)	80 (4.3)	79 (5.75)	81	83	86
S7	88 (4.1)	68 (1.5)	80 (6.3)	68	78	82
S8	92 (1.1)	84 (2.1)	66 (3.7)	82	80	90
S9	94 (2.5)	85 (3.3)	83 (1.7)	86	85	91
S10	88 (1.9)	76 (4.1)	80 (4.3)	74	82	86
S11	96 (0.3)	88 (1.5)	85 (5.7)	86	90	92
S12	100 (1.7)	83 (2.7)	90 (3.1)	85	88	95
Mean ± SD	92.8 ± 4.4	79.6 ± 5.6	81.4 ± 6.2	79.3 ± 5.9	82.8 ± 4.7	87.6 ± 4.3

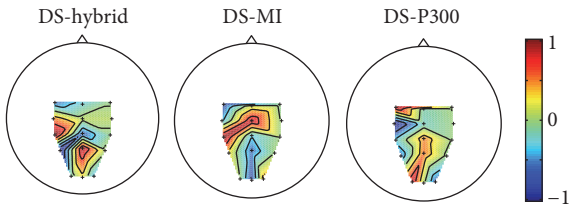

Figure 3: Scalp maps of channel weights for subject 1. All these mapping values are normalized separately to [−1 1].

($p < 0.001$) methods. In addition, the average classification accuracy is 87.6% (PROB-hybrid; Table 2). The paired t-test showed that the classification accuracy obtained by this method is also better than that obtained by the PROB method ($p < 0.001$). This result provides evidence of the efficiency of this method. We also performed 10-fold cross-validation with both sessions of data to replicate the results, providing further evidence of this method's efficiency. We also performed the classification for each repetition in the test set. As shown in Figure 2, classification accuracies after two repeats obtained using our method through combing MI and P300 (DS-hybrid) are more stable and better than that obtained with other methods. This indicates that better performance can be obtained with shorter time using our method.

Figure 3 shows the topographies of the channel weights (i.e., the mean of the first 15 of the first spatial filter for $\overline{X}^{(i)}_{\text{P300}}$ and the last 15 values of the first spatial filter for $\Gamma^{(i)}_{\text{MI}}$ in (1) for DS-hybrid, the first row of CSP transformation matrix for MI paradigm and the classifier weights for P300 paradigm), obtained using the training dataset of S1. We can see that both the left motor cortex and occipital cortex contributed to the discrimination for DS-hybrid, while only left motor cortex for DS-MI and occipital cortex for DS-P300. This pattern of scalp map is consistent in all the subjects.

4. Conclusion

In this study, we propose to use a linear classifier with a dual spectral norm regularizer for multimodalities classification. Relative to the PROB or other conventional methods, this method can perform feature learning, feature selection, and feature combining directly through regularization other than indirect multistep. This method allows us to perform the feature learning jointly with the training of classifier in an optimization framework. Specially, this method can concatenate the features of MI and P300 in a block diagonal manner, allowing us to optimize them together through a more efficient method.

Competing Interests

The authors declare no competing financial interests.

Acknowledgments

This work was supported by the National Key Basic Research Program of China (973 Program) under Grant 2015CB351703; the National High-Tech R&D Program of China (863 Program) under Grant 2012AA011601; the National Natural Science Foundation of China under Grants 91420302, 61403147, and 61573150; and Guangdong Natural Science Foundation under Grants 2014A030312005 and 2014A030313233.

References

[1] B. Z. Allison, C. Brunner, V. Kaiser, G. R. Müller-Putz, C. Neuper, and G. Pfurtscheller, "Toward a hybrid brain–computer interface based on imagined movement and visual attention," *Journal of Neural Engineering*, vol. 7, no. 2, Article ID 026007, 2010.

[2] J. Long, Y. Li, H. Wang, T. Yu, J. Pan, and F. Li, "A hybrid brain computer interface to control the direction and speed of

a simulated or real wheelchair," *IEEE Transactions on Neural Systems and Rehabilitation Engineering*, vol. 20, no. 5, pp. 720–729, 2012.

[3] J. Long, Y. Li, T. Yu, and Z. Gu, "Target selection with hybrid feature for BCI-based 2-D cursor control," *IEEE Transactions on Biomedical Engineering*, vol. 59, no. 1, pp. 132–140, 2012.

[4] G. Pfurtscheller, T. Solis-Escalante, R. Ortner, P. Linortner, and G. R. Muller-Putz, "Self-paced operation of an SSVEP-based orthosis with and without an imagery-based 'brain switch:' a feasibility study towards a hybrid BCI," *IEEE Transactions on Neural Systems and Rehabilitation Engineering*, vol. 18, no. 4, pp. 409–414, 2010.

[5] C. Brunner, B. Z. Allison, D. J. Krusienski et al., "Improved signal processing approaches in an offline simulation of a hybrid brain-computer interface," *Journal of Neuroscience Methods*, vol. 188, no. 1, pp. 165–173, 2010.

[6] Y. Li, J. Pan, F. Wang, and Z. Yu, "A hybrid BCI system combining P300 and SSVEP and its application to wheelchair control," *IEEE Transactions on Biomedical Engineering*, vol. 60, no. 11, pp. 3156–3166, 2013.

[7] G. Pfurtscheller, G. R. Müller-Putz, A. Schlögl et al., "15 Years of BCI research at Graz University of Technology: current projects," *IEEE Transactions on Neural Systems and Rehabilitation Engineering*, vol. 14, no. 2, pp. 205–210, 2006.

[8] J. R. Wolpaw, N. Birbaumer, D. J. McFarland, G. Pfurtscheller, and T. M. Vaughan, "Brain-computer interfaces for communication and control," *Clinical Neurophysiology*, vol. 113, no. 6, pp. 767–791, 2002.

[9] B. Blankertz, R. Tomioka, S. Lemm, M. Kawanabe, and K.-R. Müller, "Optimizing spatial filters for robust EEG single-trial analysis," *IEEE Signal Processing Magazine*, vol. 25, no. 1, pp. 41–56, 2008.

[10] H. Ramoser, J. Müller-Gerking, and G. Pfurtscheller, "Optimal spatial filtering of single trial EEG during imagined hand movement," *IEEE Transactions on Rehabilitation Engineering*, vol. 8, no. 4, pp. 441–446, 2000.

[11] R. Tomioka, G. Dornhege, G. Nolte, K. Aihara, and K.-R. Müller, "Optimizing spectral filters for single trial EEG classification," in *Pattern Recognition*, vol. 4174 of *Lecture Notes in Computer Science*, pp. 414–423, Springer, Berlin, Germany, 2006.

[12] W. Wu, X. Gao, B. Hong, and S. Gao, "Classifying single-trial EEG during motor imagery by iterative spatio-spectral patterns learning (ISSPL)," *IEEE Transactions on Biomedical Engineering*, vol. 55, no. 6, pp. 1733–1743, 2008.

[13] V. Bostanov, "BCI competition 2003-data sets Ib and IIb: feature extraction from event-related brain potentials with the continuous wavelet transform and the t-value scalogram," *IEEE Transactions on Biomedical Engineering*, vol. 51, no. 6, pp. 1057–1061, 2004.

[14] F. Lotte, M. Congedo, A. Lécuyer, F. Lamarche, and B. Arnaldi, "A review of classification algorithms for EEG-based brain-computer interfaces," *Journal of Neural Engineering*, vol. 4, no. 2, 2007.

[15] G. Pfurtscheller and F. Lopes da Silva, *EEG Event-related Desynchronization (ERD) and Event-Related Synchronization (ERS)*, Electroencephalography: Basic Principles, Clinical Applications and Related Fields 958, 1999.

[16] E. Haselsteiner and G. Pfurtscheller, "Using time-dependent neural networks for EEG classification," *IEEE Transactions on Rehabilitation Engineering*, vol. 8, no. 4, pp. 457–463, 2000.

[17] S. Rezaei, K. Tavakolian, A. M. Nasrabadi, and S. K. Setarehdan, "Different classification techniques considering brain computer interface applications," *Journal of Neural Engineering*, vol. 3, no. 2, 2006.

[18] Y. Li and C. Guan, "Joint feature re-extraction and classification using an iterative semi-supervised support vector machine algorithm," *Machine Learning*, vol. 71, no. 1, pp. 33–53, 2008.

[19] Y. Li, C. Guan, H. Li, and Z. Chin, "A self-training semi-supervised SVM algorithm and its application in an EEG-based brain computer interface speller system," *Pattern Recognition Letters*, vol. 29, no. 9, pp. 1285–1294, 2008.

[20] M. Dyrholm, C. Christoforou, and L. C. Parra, "Bilinear discriminant component analysis," *The Journal of Machine Learning Research*, vol. 8, pp. 1097–1111, 2007.

[21] R. Tomioka and K. Aihara, "Classifying matrices with a spectral regularization," in *Proceedings of the 24th International Conference on Machine Learning (ICML '07)*, pp. 895–902, ACM, Corvallis, Ore, USA, June 2007.

[22] R. Tomioka and K.-R. Müller, "A regularized discriminative framework for EEG analysis with application to brain-computer interface," *NeuroImage*, vol. 49, no. 1, pp. 415–432, 2010.

[23] R. Tibshirani, "Regression shrinkage and selection via the lasso: a retrospective," *Journal of the Royal Statistical Society. Series B. Statistical Methodology*, vol. 73, no. 3, pp. 273–282, 2011.

[24] M. Fazel, H. Hindi, and S. P. Boyd, "A rank minimization heuristic with application to minimum order system approximation," in *Proceedings of the American Control Conference*, pp. 4734–4739, Arlington, VA, USA, June 2001.

[25] D. J. MacKay, *Information Theory, Inference, and Learning Algorithms*, vol. 7, Cambridge University Press, 2003.

[26] G. Dornhege, B. Blankertz, G. Curio, and K. R. Müller, "Boosting bit rates in noninvasive EEG single-trial classifications by feature combination and multiclass paradigms," *IEEE Transactions on Biomedical Engineering*, vol. 51, no. 6, pp. 993–1002, 2004.

Hindawi Publishing Corporation
Computational Intelligence and Neuroscience
Volume 2016, Article ID 2637603, 7 pages
http://dx.doi.org/10.1155/2016/2637603

Research Article

Low-Rank Linear Dynamical Systems for Motor Imagery EEG

Wenchang Zhang,[1,2] Fuchun Sun,[1] Chuanqi Tan,[1] and Shaobo Liu[1]

[1] *The State Key Laboratory of Intelligent Technology and Systems, Computer Science and Technology School, Tsinghua University, FIT Building, Beijing 100084, China*
[2] *Institute of Medical Equipment, Wandong Road, Hedong District, Tianjin, China*

Correspondence should be addressed to Fuchun Sun; fcsun@mail.tsinghua.edu.cn

Received 18 September 2016; Revised 14 November 2016; Accepted 16 November 2016

Academic Editor: Feng Duan

The common spatial pattern (CSP) and other spatiospectral feature extraction methods have become the most effective and successful approaches to solve the problem of motor imagery electroencephalography (MI-EEG) pattern recognition from multichannel neural activity in recent years. However, these methods need a lot of preprocessing and postprocessing such as filtering, demean, and spatiospectral feature fusion, which influence the classification accuracy easily. In this paper, we utilize linear dynamical systems (LDSs) for EEG signals feature extraction and classification. LDSs model has lots of advantages such as simultaneous spatial and temporal feature matrix generation, free of preprocessing or postprocessing, and low cost. Furthermore, a low-rank matrix decomposition approach is introduced to get rid of noise and resting state component in order to improve the robustness of the system. Then, we propose a low-rank LDSs algorithm to decompose feature subspace of LDSs on finite Grassmannian and obtain a better performance. Extensive experiments are carried out on public dataset from "BCI Competition III Dataset IVa" and "BCI Competition IV Database 2a." The results show that our proposed three methods yield higher accuracies compared with prevailing approaches such as CSP and CSSP.

1. Introduction

With the development of the simpler brain rhythm sampling technique and powerful low-cost computer equipment over the past two decades, a noninvasive brain-computer interface (BCI) called electroencephalography (EEG) has attracted more and more attention than other BCIs such as magnetoencephalography (MEG), functional magnetic resonance imaging (fMRI), and near infrared spectroscopy (NIRS). Among various EEG signals, certain neurophysiological patterns can be recognized to determine the user's intentions such as visual evoked potentials (VEPs), P300 evoked potentials, slow cortical potentials (SCPs), and sensorimotor rhythms. EEG brings hope to patients with amyotrophic lateral sclerosis, brainstem stroke, and spinal cord injury [1]. Motor imagery (MI), which is known as the mental rehearsal of a motor act without real body movement execution, represents a new approach to access the motor system for rehabilitation at all stages of the stroke recovery. People with severe motor disabilities can use EEG-BCI to realize the communication and control and even to restore their motor disabilities [2, 3]. Therefore, an increasing number of researchers are working on MI-BCI for stroke patient rehabilitation [4, 5].

MI-BCI concentrates on sensorimotor μ- or β-rhythms that has the phenomenon known as event-related synchronization (ERS) or event-related desynchronization (ERD). However, the MI pattern recognition is still a challenge due to the low signal-to-noise ratio, highly subject-specific data, and low processing speed. For these reasons, more and more digital signal processing (DSP) methods and machine learning algorithms are applied to the MI-BCI analysis. Unlike static signals such as images and semantics, the EEG signals are dynamic that lie in a spatiotemporal feature space. Thus a large variety of feature extraction algorithms are proposed, including power spectral density (PSD) values [6, 7], autoregressive (AR) parameters [8, 9], and time-frequency features [10]. For MI-BCI pattern recognition, there are mainly three types of methods: autoregressive components (AR) [11], wavelet transform (WT) [12, 13], and CSP [14, 15]. Because of effectiveness and simplicity in extracting

spatial features, CSP becomes one of the most popular and successful solutions for MI-BCI analysis according to the winners' methods analysis of "BCI Competition III Dataset IVa" [16, 17] and "BCI Competition IV Database 2a" [18, 19]. Therefore, many researchers devote theirselves to improving the original CSP method for better performances, such as common spatiospectral pattern (CSSP) [20], common sparse spectral spatial pattern (CSSSP) [21], subband common spatial pattern (SBCSP) [22], filter bank common spatial pattern (FBCSP) [23], wavelet common spatial pattern (WCSP) [24], and separable common spatiospectral patterns (SCSSP) [25]. Most of these improved CSP methods fuse spectral and spatial characteristics in the spatiospectral feature space and finally achieve success by comparison experiments.

Despite its effectiveness in extracting features of MI-BCI, CSP needs a lot of preprocessing and postprocessing such as filtering, demean, and spatiospectral feature fusion, which influence the classification accuracy easily. In this paper, we utilize linear dynamical systems (LDSs) for processing EEG signals in MI-BCI. Although LDSs succeed in the field of control, to the best of our knowledge, this model has barely been tried in the feature extraction of EEG analysis so far. Compared with CSP method, LDSs have the following advantages: first, LDS can simultaneously generate spatiospectral dual-feature matrix; second, there is no need to preprocess or postprocess signals, and the raw data can be directly fed into the model; third, it is easy to use and of low cost; last, the extracted features from the LDS are much more effective for classification.

Furthermore, we apply low-rank matrix decomposition approaches [26–28] that have the ability to learn representational matrix even in presence of corrupted data. The noise of the data can be get rid of, hence to improve the robustness. However, there are two ways for the EEG low-rank decomposition. One aims at the EEG raw data; the other aims at features extracted from LDSs, which is proposed by us and called low-rank LDSs (LR-LDSs).

This paper mainly has the following contributions. (1) We utilize LDSs for MI-EEG feature extraction to solve the MI pattern recognition problem. (2) Low-rank matrix decomposition method is applied to improve the robustness for the raw data analysis. (3) We propose LR-LDSs on finite Grassmannian feature space. (4) Plenty of comparison experiments demonstrate the effectiveness of these approaches.

The rest of this paper is organized as follows. Section 2 provides LDSs model to realize the feature extraction of EEG signals. Section 3 presents low-rank matrix decomposition method for the EEG raw data analysis. Section 4 introduces LR-LDSs method. Then, the proper classification algorithm is explained in Section 5. Section 6 compares the three proposed methods (LDSs, LR+CSP, and LR-LDSs) with other state-of-the-art algorithms in different databases. Finally, the summary and conclusion are presented in Section 7.

2. LDSs Modeling

LDSs, also known as linear Gaussian state-space models, have been used successfully in modeling and controlling dynamical systems. In recent few years, more and more problems extending to computer vision [29, 30], speech recognition [31], and tactile perception [32] have been solved by LDSs model. EEG signals are sequences of brain electron sampling that have typical dynamic textures. We present the features of EEG dynamic textures by LDSs modeling and apply machine learning (ML) algorithms to capture the essence of dynamic textures for feature extraction and classification.

Let $\{Y(t)\}_{t=1,\ldots,\tau}$, $Y(t) \in R^m$ be a sequence of τ EEG signal sample at each instant of time t. If there is a set of n spatial filters $\varphi_\alpha : R \to R^m$, $\alpha = 1, \ldots, n$, we have $x(t) = \sum_{i=1}^{k} A_i x(t-i) + Bv(t)$ with $A_i \in R^{n\times n}$, $B \in R^{n\times n_v}$, independent and identically distributed realization item $v(t) \in R^{n_v}$ and suppose that sequence of observed variables $Y(t)$ can be represented approximately by function of dimensional hidden state $x(t)$, $y(t) = \varphi(x(t)) + \omega(t)$, where $\omega(t) \in R^m$ is an independent and identically distributed sequence drawn from a known distribution resulting in a positive measured sequence. We redefine the hidden state of $x(t)$ to be $\left[x(t)^T \;\; x(t-1)^T \;\; \cdots \;\; x(t-k)^T\right]^T$ and consider a linear dynamic system as an autoregressive moving average process without firm input distribution:

$$\begin{aligned} x(t+1) &= Ax(t) + Bv(t), \\ y(t) &= \varphi(x(t)) + \omega(t), \\ x(0) &= x_0 \end{aligned} \tag{1}$$

with $v(t)$, $\varphi(x(t))$ distribution unknown, however.

In order to solve the above problem, we can regard it as a white and zero-mean Gaussian noise linear dynamical system and propose a simplified and closed-form solution:

$$\begin{aligned} x(t+1) &= Ax(t) + Bv(t) \quad v(t) \sim N(0, Q), \\ y(t) &= Cx(t) + \omega(t) + \overline{y} \quad \omega(t) \sim N(0, R), \\ x(0) &= x_0, \end{aligned} \tag{2}$$

where $A \in R^{n\times n}$ is the transition matrix that describes the dynamics property, $C \in R^{m\times n}$ is the measurement matrix that describes the spatial appearance, $\overline{y} \in R^m$ is the mean of $y(t)$, and $v(t)$ and $\omega(t)$ are noise components. We should estimate the model parameters A, C, Q, R from the measurements $y(t), \ldots, y(\tau)$ and transform them into the maximum-likelihood solution:

$$\begin{aligned} &\widehat{A}(\tau), \widehat{C}(\tau), \widehat{Q}(\tau), \widehat{R}(\tau) \\ &\quad = \underset{A,C,Q,R}{\operatorname{argmax}}\, p\left(y(1), \ldots, y(\tau)\right), \end{aligned} \tag{3}$$

and, however, optimal solutions of this problem bring computational complexity.

We apply matrix decomposition to simplify the computation by the closed-form solution. The singular value

decomposition (SVD) solution is the best estimate of C in Frobenius function:

$$\begin{aligned} \widehat{C}(\tau), \widehat{X}(\tau) = \underset{C,X}{\operatorname{argmin}} \quad & \|W(\tau)\|_F \\ \text{subject to} \quad & Y(\tau) = CX(\tau) + W(\tau); \\ & C^T C = I. \end{aligned} \tag{4}$$

Let $Y = U\Sigma V^T$, and we get the parameter estimation of $\widehat{C}$, $\widehat{X}$:

$$\begin{aligned} \widehat{C} &= U, \\ \widehat{X} &= \Sigma V^T, \end{aligned} \tag{5}$$

where $\widehat{X} = [X(1), X(2), \ldots, X(\tau)]$. $\widehat{A}$ can be determined by Frobenius:

$$\widehat{A}(\tau) = \underset{A}{\operatorname{argmin}} \left\| X_2(\tau) - AX_1(\tau - 1) \right\|_F, \tag{6}$$

where $X_2(\tau) = [X(2), X(3), \ldots, X(\tau)]$. So the solution is in closed-form using the state estimated

$$\begin{aligned} \widehat{A}(\tau) = & \left[X(:,2) \;\; X(:,3) \;\; \cdots \;\; X(:,\tau) \right] \\ & * \left[X(:,1) \;\; X(:,2) \;\; \cdots \;\; X(:,\tau - 1) \right]^{\dagger}, \end{aligned} \tag{7}$$

where † denotes matrix pseudoinverse.

We can obtain the result $[A, C]$, a couple of spatiotemporal feature matrix. The MATLAB program of LDSs can be found in Supplementary Material algorithm 1 available online at http://dx.doi.org/10.1155/2016/2637603.

3. Low-Rank Matrix Decomposition

EEG signals have poor quality because they are usually recorded by electrodes placed on the scalp in a noninvasive manner that has to cross the scalp, skull, and many other layers. Therefore, they are moreover severely affected by background noise generated either inside the brain or externally over the scalp. Low-rank (LR) matrix decomposition can often capture the global information by reconstructing the top few singular values and the corresponding singular vectors. This method is widely applied in the field of image denoising and face recognition (FR). Concretely, low-rank (LR) matrix recovery seeks to decompose a data matrix X into $A + E$, where A is a low-rank matrix and E is the associated sparse error. Candès et al. [33] propose to relax the original problem into the following tractable formulation:

$$\begin{aligned} \min_{A,E} \quad & \|A\|_* + \alpha \|E\|_1 \\ \text{s.t.} \quad & X = A + E, \end{aligned} \tag{8}$$

where the nuclear norm $\|A\|_*$ (the sum of the singular values) approximates the rank of A and the l_1-norm $\|E\|_1$ is sparse constraint.

Then, Zhang and Li [34] decompose each image into common component, condition component, and a sparse residual. Siyahjani et al. [35] introduce the invariant components to the sparse representation and low-rank matrix decomposition approaches and successfully apply to solve computer vision problems. They add orthogonal constraint to assume that invariant and variant components are linear independent. Therefore, we decompose EEG signals as a combination of three components: resting state component, motor imagery component represented by low-rank matrix, and a sparse residual. However, in practice, it needs some digital signal processing (DSP), that is, wavelet transform or discrete Fourier transform before decomposition. Particularly, raw time-domain signals without any preprocessing are not suitable for low-rank matrix decomposition directly. The training dataset X can be decomposed by $X \coloneqq A + B + E$, where $A \in R^{m \times n}$ is a low-rank matrix and collects event-related EEG signal components, $B \in R^{m \times n}$ approximates invariant and denotes resting state signal components that are sampled by subjects without any motor imagery, and $E \in R^{m \times n}$ is the matrix of sparse noise. Therefore, training dataset can be decomposed as the following formulation:

$$X \coloneqq A + B + E. \tag{9}$$

On ideal condition, each sampling channel of subject's brain EEG signals in resting state is similar. In other words, sum of each different A raw is minimum. B should add common constraint as the following formulation:

$$\sum_{i \neq j} \left\| B_i - B_j \right\|_F^2. \tag{10}$$

We propose optimization problem formulation as

$$\begin{aligned} \min_{A,B,E} \quad & \|A\|_* + \alpha \|E\|_1 + \beta \sum_{i \neq j} \left\| B_i - B_j \right\|_F^2 \\ \text{s.t.} \quad & X = A + B + E. \end{aligned} \tag{11}$$

Then, augmented Lagrange multiplier (ALM) [36] method is utilized to solve the above problem. The augmented Lagrangian function $L(A, B, E, \lambda)$ is given by

$$\begin{aligned} L(A, B, E, \lambda) = & \|A\|_* + \alpha \|E\|_1 + \beta \sum_{i \neq j} \left\| B_i - B_j \right\|_F^2 \\ & + \langle \lambda, X - A - B - E \rangle \\ & + \frac{\mu}{2} \|X - A - B - E\|_F^2, \end{aligned} \tag{12}$$

where μ is a positive scalar and λ is a Lagrange multiplier matrix. We employ an inexact ALM (IALM) method described in Algorithm 1 to solve this problem, where $J(X) = \max(\text{lansvd}(X), \alpha^{-1}\|X\|_F)$ in the initialization $\lambda_0 = X/J(X)$ and lansvd$(\cdot)$ computes the largest singular value.

When low-rank matrix A denoting event-related EEG signal components are generated, we can utilize some feature extraction methods such as CSP and CSSP to classify MI-BCI. In other words, low-rank matrix decomposition method in this section can be considered as a preprocessing part before feature extraction and classification.

Input: Observation matrix X, λ, penalty weights α, β
(1) $\lambda_0 = X/J(X)$; $\mu_0 > 0$; $\rho > 1$; $k = 0$.
(2) while not converged do
(3) // Lines (4)–(12) solve $(A_k, B_k, E_k) = \operatorname{argmin}_{A,B,E} L(A, B, E, \lambda_k, \mu_k)$
(4) $j = 0$; $A_k^0 = A_k$; $B_k^0 = B_k$; $E_k^0 = E_k$
(5) while not converged do
(6) // Line (7)-(8) solves $A_{k+1} = \operatorname{argmin}_A L(A, B_k, E_k, \lambda_k, \mu_k)$
(7) $(U, S, V) = \operatorname{svd}(X - B_{k+1} - E_{k+1} + \lambda_k/\mu_k)$
(8) $A_k^{j+1} = US_{\mu_k^{-1}}[S]V^T$
(9) // Line (10) solves $B_{k+1} = \operatorname{argmin}_B L(A_{k+1}, B, E_k, \lambda_k, \mu_k)$
(10) $E_k^{j+1} = S_{\alpha\mu_k^{-1}}[X - A_k^{j+1} - B_k^j + \lambda_k/\mu_k]$
(11) Update B_k^{j+1} by solving $E_{k+1} = \operatorname{argmin}_E L(A_{k+1}, B_{k+1}, E, \lambda_k, \mu_k)$
(12) $j \leftarrow j + 1$
(13) end while
(14) $A_{k+1} = A_k^{j+1}$, $B_{k+1} = B_k^{j+1}$, $E_{k+1} = E_k^{j+1}$
(15) $\mu_{k+1} = \rho\mu_k$, $\lambda_{k+1} = \lambda_k + \mu_k(X - A_{k+1} - B_{k+1} - E_{k+1})$
(16) $k \leftarrow k + 1$
(17) end while
Output: (A_k, B_k, E_k).

Algorithm 1: Low-rank decomposition via the inexact ALM method.

4. LR-LDSs on Finite Grassmannian

Beginning at an initial state $x1$, the expected observation sequence generated by a time-invariant model $M = (A, C)$ is obtained as $E[y_1, y_2, y_1, \ldots] = [C^T, (CA)^T, (CA^2)^T, \ldots]^T x1$ that lies in the column space of the extended observability matrix given by $O_\infty^T = [C^T, (CA)^T, (CA^2)^T, \ldots]^T \in R^{\infty \times n}$. LDSs can apply the extended observability subspace $\mathcal{O}$ as descriptor, but it is hard to calculate. Turaga et al. [37, 38] approximate the extended observability by taking the L-order observability matrix; that is, $O(n, L) = [C^T, (CA)^T, \ldots, (CA^{L-1})^T]^T$. In this way, an LDS model can be alternately identified as an n-dimensional subspace of R^{Lm}.

Given a database of EEG, we can estimate LDSs model and calculate the finite observability matrix that span subspace as a point on the Riemannian manifold. Then, based on low-rank and sparse matrix decomposition, observability matrix O can be decomposed into $D + E$ as the following formulation:

$$\begin{aligned} \min_{D,E} \quad & \|D\|_* + \alpha \|E\|_1 \\ \text{s.t.} \quad & O = D + E, \end{aligned} \tag{13}$$

where D is a low-rank matrix and E is the associated sparse error.

The inexact ALM method can be also used to solve the optimization problem like Algorithm 1. The output D represents low-rank descriptor for LDSs and can be employed for the classification of EEG trails.

5. Classification Algorithm

We extract features by the above LDSs model and get two feature matrices A and C. Unfortunately, A and C have different modal properties and dimensionalities. So they cannot be represented directly by a feature vector. Riemannian geometry metric for the space of LDSs is hard to determine and needs to satisfy several constraints. Common classifiers such as Nearest Neighbors (NNs), Linear Discriminant Analysis (LDA), and Support Vector Machines (SVM) cannot classify features in matrix form. The feature matrix must be mapped to vector space. We use Martin Distance [39, 40], which is based on the principal angles between two subspaces of the extended observability matrices, as kernel to present distance of different LDS feature matrix. It can be defined as

$$D^2(\Theta_a, \Theta_b) = -2\sum_{i=1}^{n} \log \lambda_i, \tag{14}$$

where $\Theta_a = \{C_a, A_a\}$, $\Theta_b = \{C_b, A_b\}$. λ_i is the eigenvalue solving as the following equation:

$$\begin{bmatrix} 0 & \mathcal{O}_{ab} \\ (\mathcal{O}_{ab})^T & 0 \end{bmatrix} \begin{bmatrix} x \\ y \end{bmatrix} = \lambda \begin{bmatrix} \mathcal{O}_{aa} & 0 \\ 0 & \mathcal{O}_{bb} \end{bmatrix} \begin{bmatrix} x \\ y \end{bmatrix} \quad \text{s.t. } x^T \mathcal{O}_{aa} x = 1,\ y^T \mathcal{O}_{bb} y = 1, \tag{15}$$

where the extended observability matrices $\mathcal{O}_a = [C_a^T, A_a^T C_a^T, \ldots, (A_a^T)^n C_a^T]$, $\mathcal{O}_b = [C_b^T, A_b^T C_b^T, \ldots, (A_b^T)^n C_b^T]$, $\mathcal{O}_{ab} = (\mathcal{O}_a)^T \mathcal{O}_b$. Algorithm 2 in Supplementary Material presents Martin Distance function programed by MATLAB.

We can classify EEG signals by comparing Martin Distance between training data and testing data. Nearest two samples mean that they may be of the same class. So the forecast label and predict accuracy can be calculated. Algorithm 3 in Supplementary Material is the classification method of KNN.

Considering LR-LDSs methods generating A on Finite Grassmannian, unlike two feature matrices (A, C) by LDSs, Euclidean Distance and Mahalanobis Distance can describe

Table 1: Experimental accuracy results (%) obtained from each subject in BCI Competition III Dataset IVa for CSP, CSSP, and our proposed algorithm (LDS).

Subject	aa	al	av	aw	ay	Mean
CSP	71.43	94.64	61.22	89.28	73.02	77.918
CSSP	77.68	96.43	63.27	**90.63**	79.37	81.476
LDSs	78.57	96.43	**64.29**	90.18	79.76	81.846
LR+CSP	77.68	96.43	63.78	90.18	79.76	81.566
LR-LDSs	**79.46**	**98.21**	63.78	90.18	**80.56**	**82.438**

the distance between two feature spaces of EEG trails after LR-LDS. They are simple, efficient, and common for measuring distance between two points. In order to improve the accuracy of classification, we can also employ metric learning methods using the label information to learn a new metric or pseudometric such as neighborhood components analysis and large margin nearest neighbor.

6. Experimental Evaluation

From the above sections, we propose three methods for EEG pattern recognition: LDSs, LR+CSP, and LR-LDSs. Two datasets of motor imagery EEG including BCI Competition III Dataset IVa and BCI Competition IV Database 2a are used to evaluate our three methods compared with other state-of-the-art algorithms such as CSP and CSSP. All experiments are carried out with MATLAB on Intel Core i7, 2.90-GHz CPU with 8 GB RAM.

6.1. BCI Competition III Dataset IVa. Dataset IVa is recorded from five healthy subjects, labeled as "aa," "al," "av," "aw," and "ay," with visual cues indicated for 3.5 s performing right hand and foot motor imagery. The EEG signal has 118 channels and markers that indicate the time points of 280 cues for each subject, band-pass filtered between 0.05 and 200 Hz, and downsampled to 100 Hz.

Before feature extracting for comparison experiment, the raw data needs some preprocessing. Firstly, we extract a time segment located from 0.5 to 3 s and employ FastICA to remove artifacts arising from eye and muscle movements. Secondly, we chose 21 channels over the motor cortex (CP6, CP4, CP2, C6, C4, C2, FC6, FC4, FC2, CPZ, CZ, FCZ, CP1, CP3, CP5, C1, C3, C5, FC1, FC3, and FC5) that related to motor imagery.

In order to improve the performance of CSP and CSSP, we apply Butterworth filter for EEG signals filtering within a specific frequency band between 8 and 30 Hz, which encompasses both the alpha rhythm (8–13 Hz) and the beta rhythm (14–30 Hz) that relate to motor imagery. Then, we program MATLAB code to get spatial filter parameters and feature vectors by variance. Finally, a LDA classifier is used to find a separating hyperplane of the feature vectors.

In LDSs model, the value of a hidden parameter describing dimension of Riemannian feature space is closely related to final accuracy. We chose the highest accuracy performance subject "al" and the lowest accuracy performance subject "av" to show the relationship between hidden parameter and classification accuracy. The result of experiment is presented in Figure 1, which indicates that the accuracy tends to increase when the value of hidden parameter augments approximately and the highest accuracy happens near hidden parameter value of 16.

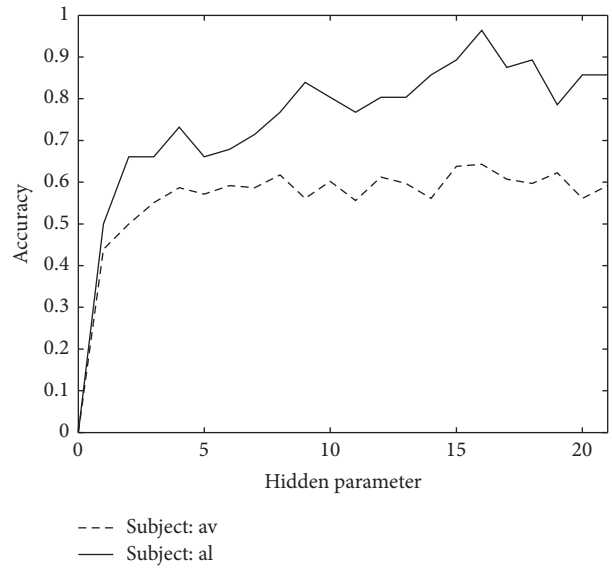

Figure 1: The relationship between hidden parameter and accuracy for LDSs. We choose "al" and "av," which are the highest and lowest accuracy performance, respectively, to show the relationship between hidden parameter and accuracy.

Then five methods including CSP, CSSP, LDSs, LR+CSP, and LR-LDSs are compared with each other. The results are listed in Table 1.

From Table 1, the bold figures present the best performance results. LR-LDSs are in the majority. The last row shows that the mean of LR-LDS classification accuracy is much better than CSP and a little higher than the others. Comparing with CSP and LR+CSP, LR method is very efficient and useful to improve accuracy. LDSs related methods outperform CSP and CSSP due to their both spatial and temporal features extraction.

6.2. BCI Competition IV Database 2a. Database 2a consists of EEG data from 9 subjects. There are four different motor imagery tasks including movement of the left hand, right hand, both feet, and tongue. At the beginning of each trial, a fixation cross and a short acoustic warning tone appear.

Table 2: Experimental accuracy results (%) obtained from each subject in BCI Competition IV Database 2a for CSP, CSSP LDSs, LR+CSP, and LR-LDSs methods.

Subject	A01E	A02E	A03E	A04E	A05E	A06E	A07E	A08E	A09E	Mean
CSP	90.27	53.13	91.67	71.18	61.11	64.24	79.86	91.32	92.36	77.24
CSSP	90.97	56.94	92.01	72.92	61.81	65.28	79.86	93.06	92.71	78.40
LDSs	91.67	55.56	93.06	74.31	62.50	**70.83**	80.56	93.75	93.06	79.48
LR+CSP	92.01	58.68	**95.14**	74.65	61.81	65.28	**81.25**	94.44	**93.40**	79.63
LR-LDSs	**92.01**	**59.02**	94.44	**75.35**	**63.19**	69.44	**81.25**	**95.14**	93.06	**80.32**

After two seconds the subject is cued by an arrow pointing to either the left, right, down, or up that denote the movement of left hand, right hand, foot, or tongue for 1.25 s. Then the subjects carry out the motor imagery task for about 3 s. The BCI signals are sampled by 25 channels including 22 EEG channels and 3 EOG channels with 250 Hz and bandpass-filtered between 0.5 Hz and 100 Hz.

Different from dataset IVa, database 2a is a multiclassification problem. However, LDA is a two-class classifier. Therefore, we choose K-NN algorithms for CSP, CSSP, LDSs, LR+CSP, and LR-LDSs methods uniformly. Table 2 describes the classification accuracies results of five above concerned methods. Similar to the results of BCI Competition III Dataset IVa, the mean accuracies of LDSs, LR+CSP, and LR-LDSs are higher than CSP and CSSP methods. Furthermore, LR-LDSs method abstains the best performance.

7. Conclusion

CSP has gained much success in the past MI-BCI research. However, it is reported that CSP is only a spatial filter and sensitive to frequency band. It needs prior knowledge to choose channels and frequency bands. Without preprocessing, the result of classification accuracy may be poor. LDSs can overcome these problems by extracting both spatial and temporal features simultaneously to improve the classification performance. Furthermore, we utilize a low-rank matrix decomposition approach to get rid of noise and resting state component in order to improve the robustness of the system. Then LR+CSP and LR-LDSs methods are proposed. Comparison experiments are demonstrated on two datasets. The major contribution of our work is realization of LDSs model and LR algorithm for MI-BCI pattern recognition. The proposed LR-LDSs methods achieve a better performance than CSP and CSSP.

Competing Interests

The authors declare that there is no conflict of interests regarding the publication of this paper.

Acknowledgments

This work was supported by the National Natural Science Foundation of China (Grant nos. 91420302 and 91520201).

References

[1] J. R. Wolpaw, N. Birbaumer, D. J. McFarland, G. Pfurtscheller, and T. M. Vaughan, "Brain–computer interfaces for communication and control," *Clinical Neurophysiology*, vol. 113, no. 6, pp. 767–791, 2002.

[2] K. K. Ang and C. Guan, "Brain-computer interface in stroke rehabilitation," *Journal of Computing Science and Engineering*, vol. 7, no. 2, pp. 139–146, 2013.

[3] N. Sharma, V. M. Pomeroy, and J.-C. Baron, "Motor imagery: a backdoor to the motor system after stroke?" *Stroke*, vol. 37, no. 7, pp. 1941–1952, 2006.

[4] S. Silvoni, A. Ramos-Murguialday, M. Cavinato et al., "Brain-computer interface in stroke: a review of progress," *Clinical EEG and Neuroscience*, vol. 42, no. 4, pp. 245–252, 2011.

[5] O. Bai, P. Lin, S. Vorbach, M. K. Floeter, N. Hattori, and M. Hallett, "A high performance sensorimotor beta rhythm-based brain-computer interface associated with human natural motor behavior," *Journal of Neural Engineering*, vol. 5, no. 1, pp. 24–35, 2008.

[6] S. Chiappa and S. Bengio, "HMM and IOHMM modeling of EEG rhythms for asynchronous bci systems," in *Proceedings of the European Symposium on Artificial Neural Networks ESANN*, Bruges, Belgium, April 2004.

[7] J. D. R. Millán and J. Mouriño, "Asynchronous BCI and local neural classifiers: an overview of the adaptive brain interface project," *IEEE Transactions on Neural Systems and Rehabilitation Engineering*, vol. 11, no. 2, pp. 159–161, 2003.

[8] W. D. Penny, S. J. Roberts, E. A. Curran, and M. J. Stokes, "EEG-based communication: a pattern recognition approach," *IEEE Transactions on Rehabilitation Engineering*, vol. 8, no. 2, pp. 214–215, 2000.

[9] G. Pfurtscheller, C. Neuper, A. Schlogl, and K. Lugger, "Separability of EEG signals recorded during right and left motor imagery using adaptive autoregressive parameters," *IEEE Transactions on Rehabilitation Engineering*, vol. 6, no. 3, pp. 316–325, 1998.

[10] T. Wang, J. Deng, and B. He, "Classifying EEG-based motor imagery tasks by means of time-frequency synthesized spatial patterns," *Clinical Neurophysiology*, vol. 115, no. 12, pp. 2744–2753, 2004.

[11] D. J. Krusienski, D. J. McFarland, and J. R. Wolpaw, "An evaluation of autoregressive spectral estimation model order for brain-computer interface applications," in *Proceedings of the 28th Annual International Conference of the IEEE Engineering in Medicine and Biology Society (EMBS '06)*, pp. 1323–1326, IEEE, New York, NY, USA, September 2006.

[12] T. Demiralp, J. Yordanova, V. Kolev, A. Ademoglu, M. Devrim, and V. J. Samar, "Time-frequency analysis of single-sweep

event-related potentials by means of fast wavelet transform," *Brain and Language*, vol. 66, no. 1, pp. 129–145, 1999.

[13] D. Farina, O. F. do Nascimento, M.-F. Lucas, and C. Doncarli, "Optimization of wavelets for classification of movement-related cortical potentials generated by variation of force-related parameters," *Journal of Neuroscience Methods*, vol. 162, no. 1-2, pp. 357–363, 2007.

[14] H. Ramoser, J. Müller-Gerking, and G. Pfurtscheller, "Optimal spatial filtering of single trial EEG during imagined hand movement," *IEEE Transactions on Rehabilitation Engineering*, vol. 8, no. 4, pp. 441–446, 2000.

[15] M. Grosse-Wentrup and M. Buss, "Multiclass common spatial patterns and information theoretic feature extraction," *IEEE Transactions on Biomedical Engineering*, vol. 55, no. 8, article no. 11, pp. 1991–2000, 2008.

[16] B. Blankertz, K.-R. Müller, D. J. Krusienski et al., "The BCI competition III: validating alternative approaches to actual BCI problems," *IEEE Transactions on Neural Systems and Rehabilitation Engineering*, vol. 14, no. 2, pp. 153–159, 2006.

[17] http://www.bbci.de/competition/iii/results/.

[18] M. Tangermann, K. Müller, A. Aertsen et al., "Review of the BCI competition IV," *Frontiers in Neuroscience*, vol. 6, article no. 55, 2012.

[19] http://www.bbci.de/competition/iv/results/.

[20] S. Lemm, B. Blankertz, G. Curio, and K.-R. Müller, "Spatio-spectral filters for improving the classification of single trial EEG," *IEEE Transactions on Biomedical Engineering*, vol. 52, no. 9, pp. 1541–1548, 2005.

[21] G. Dornhege, B. Blankertz, M. Krauledat, F. Losch, G. Curio, and K.-R. Müller, "Combined optimization of spatial and temporal filters for improving brain-computer interfacing," *IEEE Transactions on Biomedical Engineering*, vol. 53, no. 11, pp. 2274–2281, 2006.

[22] Q. Novi, C. Guan, T. H. Dat, and P. Xue, "Sub-band common spatial pattern (SBCSP) for brain-computer interface," in *Proceedings of the 3rd International IEEE/EMBS Conference on Neural Engineering (CNE '07)*, pp. 204–207, IEEE, Kohala Coast, Hawaii, USA, May 2007.

[23] K. K. Ang, Z. Y. Chin, H. Zhang, and C. Guan, "Filter Bank Common Spatial Pattern (FBCSP) in Brain-Computer Interface," in *Proceedings of the International Joint Conference on Neural Networks (IJCNN '08)*, pp. 2390–2397, Hong Kong, China, June 2008.

[24] E. A. Mousavi, J. J. Maller, P. B. Fitzgerald, and B. J. Lithgow, "Wavelet common spatial pattern in asynchronous offline brain computer interfaces," *Biomedical Signal Processing and Control*, vol. 6, no. 2, pp. 121–128, 2011.

[25] A. S. Aghaei, M. S. Mahanta, and K. N. Plataniotis, "Separable common spatio-spectral patterns for motor imagery BCI systems," *IEEE Transactions on Biomedical Engineering*, vol. 63, no. 1, pp. 15–29, 2016.

[26] E. J. Candès, X. Li, Y. Ma, and J. Wright, "Robust principal component analysis?" *Journal of the ACM*, vol. 58, no. 3, article 11, 2011.

[27] C.-F. Chen, C.-P. Wei, and Y.-C. F. Wang, "Low-rank matrix recovery with structural incoherence for robust face recognition," in *Proceedings of the IEEE Conference on Computer Vision and Pattern Recognition (CVPR '12)*, pp. 2618–2625, June 2012.

[28] R. Vidal and P. Favaro, "Low rank subspace clustering (LRSC)," *Pattern Recognition Letters*, vol. 43, no. 1, pp. 47–61, 2014.

[29] P. Saisan, G. Doretto, Y. N. Wu, and S. Soatto, "Dynamic texture recognition," in *Proceedings of the IEEE Computer Society Conference on Computer Vision and Pattern Recognition (CVPR '01)*, pp. II-58–II-63, Kauai, Hawaii, USA, December 2001.

[30] G. Doretto, A. Chiuso, Y. N. Wu, and S. Soatto, "Dynamic textures," *International Journal of Computer Vision*, vol. 51, no. 2, pp. 91–109, 2003.

[31] B. Mesot and D. Barber, "Switching linear dynamical systems for noise robust speech recognition," *IEEE Transactions on Audio, Speech and Language Processing*, vol. 15, no. 6, pp. 1850–1858, 2007.

[32] R. Ma, H. Liu, F. Sun, Q. Yang, and M. Gao, "Linear dynamic system method for tactile object classification," *Science China: Information Sciences*, vol. 57, no. 12, pp. 1–11, 2014.

[33] E. J. Candès, X. Li, Y. Ma, and J. Wright, "Robust principal component analysis?" *Journal of the ACM*, vol. 58, no. 3, 2011.

[34] Q. Zhang and B. Li, "Mining discriminative components with low-rank and sparsity constraints for face recognition," in *Proceedings of the 18th ACM SIGKDD International Conference on Knowledge Discovery and Data Mining (KDD '12)*, pp. 1469–1477, ACM, August 2012.

[35] F. Siyahjani, R. Almohsen, S. Sabri, and G. Doretto, "A supervised low-rank method for learning invariant subspaces," in *Proceedings of the IEEE International Conference on Computer Vision (ICCV '15)*, pp. 4220–4228, Santiago, Chile, December 2015.

[36] Z. Lin, M. Chen, and Y. Ma, "The Augmented Lagrange Multiplier Method for Exact Recovery of Corrupted Low-Rank Matrices," 2010.

[37] P. Turaga, A. Veeraraghavan, A. Srivastava, and R. Chellappa, "Statistical computations on grassmann and stiefel manifolds for image and video-based recognition," *IEEE Transactions on Pattern Analysis and Machine Intelligence*, vol. 33, no. 11, pp. 2273–2286, 2011.

[38] M. Harandi, R. Hartley, C. Shen, B. Lovell, and C. Sanderson, "Extrinsic methods for coding and dictionary learning on Grassmann manifolds," *International Journal of Computer Vision*, vol. 114, no. 2-3, pp. 113–136, 2015.

[39] R. J. Martin, "A metric for ARMA processes," *IEEE Transactions on Signal Processing*, vol. 48, no. 4, pp. 1164–1170, 2000.

[40] A. B. Chan and N. Vasconcelos, "Classifying video with kernel dynamic textures," in *Proceedings of the IEEE Computer Society Conference on Computer Vision and Pattern Recognition (CVPR '07)*, 6, 1 pages, June 2007.